

People's Democratic Republic of Algeria
Ministry Of Higher Education And Scientific Research
University of Ghardaia



Faculty of Natural Sciences, Life and Earth Sciences

Department of Biology

**Dissertation submitted in partial fulfilment of the requirements for
Academic Master Degree**

In: Biological Sciences

Speciality: Applied biochemistry

Submitted by: Sarra HADDAD

**Molecular docking assessment of sesquiterpene lactones
from *Saussurea lappa* as potential anti-melanoma agents**

Defended publicly on: 11/06/2024

Board of examiners:

Mme. Z. KEBILI	MAA	University of Ghardaia	Chairwoman
Mr. Z. BENBEKHTI	MAA	University of Ghardaia	Supervisor
Mr. M. BAKLI	MCA	University of Ghardaia	Examiner

Academic year: 2023-2024

Acknowledgements

First and foremost, I want to thank Allah, the Almighty, for giving me the knowledge, strength, and persistence to finish this study project successfully.

*I want to express my deep appreciation to my respected supervisor, **Mr. Zineddine BENBEKHTI**, Assistant Professor, for all the help, support, and instructions he gave me during this study. His wise views and extensive knowledge were critical in shaping this project.*

*Thank you very much to the respected board of examiners: the chairwoman, **Mme. Zohra KEBILI**, Assistant Professor, and the examiner, **Mr. Mahfoud BAKLI**, Lecturer, for reading my dissertation and giving me such helpful feedback and suggestions. The helpful comments and ideas they provided allowed me to refine and improve the quality of this contribution study.*

I really want to thank my Biology Department teachers for all the great information they have given me. They were committed to teaching and academic excellence, which helped me build a good base for starting my research.

Thank you very much for your contributions to the growth of knowledge and the pursuit of academic success.

*I am extremely grateful to **Nada Rayhan Aribi**, my English professor, for providing me with the confidence and encouragement to write this thesis.*

To my family, thank you for all the days and nights of support and prayers.

May Allah greatly bless you all.

Dedication

This work
is dedicated to
the brave and honourable
people of
GAZA.

Abbreviations & Symbols

2D: Two- Dimensional

3D: Three-Dimensional

8XE: ERK2 reference ligand

Å: Angstrom

Å²: Square Angstrom

Å³: Cubic Angstrom

ACS: American Cancer Society

ADME: Absorption, Distribution,
Metabolism, and Excretion

Akt: Protein kinase B

ALDH1A1: Aldehyde Dehydrogenase 1
Family Member A1

ALM: Acral Lentiginous Melanomas

ARAF: A-Rapidly Accelerated
Fibrosarcoma

ATP: Adenosine triphosphate

BBB: Blood-Brain Barrier

BRAF: B-Rapidly Accelerated
Fibrosarcoma

CCND1: Cyclin D1

CDK4: Cyclin-Dependent Kinase 4

CDKN2A: Cyclin-Dependent Kinase
Inhibitor 2A

CRAF: C-Rapidly Accelerated
Fibrosarcoma

CYP: Cytochrome P450

ETCM: Encyclopaedia of Traditional
Chinese Medicine

ERK: Extracellular Signal-Regulated
Kinase

ERK2: Extracellular Signal-Regulated
Kinase 2

g/mol: Gram per mole

GDP: Guanosine Diphosphate

GNP: Phosphoaminophosphonic acid
guanylate ester

GRB2: Growth factor receptor-bound
protein 2

GTP: Guanosine Triphosphate

HeLa: Human cervical epithelioid
carcinoma (cells were taken from
Henrietta Lacks)

HepG2: Hepatoma G2 (Human
hepatocellular carcinoma G2)

HIA: Human Intestinal Absorption

HRAS: Harvey Rat Sarcoma Viral Oncogene Homolog.

HSP90: Heat Shock Protein 90

ID: Identification

IKK: Inhibitor of Nuclear Factor kappa B Kinase

iLog P : in-house Log P (a physics-based approach to predict the n-octanol/water partition coefficient)

kcal/mol: Kilocalorie per mole

KIT: Proto-Oncogene Receptor Tyrosine Kinase

KRAS: K-Ras Proto-Oncogene (Kirsten rat sarcoma virus protein)

LMM: Lentigo Maligna Melanoma

MAPK: Mitogen-Activated Protein Kinase

Mcl-1: Myeloid Cell Leukaemia 1

MEK: Mitogen-Activated Protein Kinase/Extracellular Signal-Regulated Kinase Kinase

MITF: Melanocyte Inducing Transcription Factor

MW: Molecular weight

MOPAC: Molecular Orbital Package

NF- κ B: Nuclear Factor kappa B

NM: Nodular Melanoma

NRAS: Neuroblastoma RAS Oncogene

OVCAR-3: Human ovarian adenocarcinoma

PDB: Protein Data Bank

PDB REDO: Protein Data Bank REDO

P-gp: P-glycoprotein (multidrug Resistance Protein)

PI3K: Phosphoinositide 3-Kinase

PM7: Parameterization Method 7

RAF: Rapidly Accelerated Fibrosarcoma

RAS: Rat sarcoma virus (proto-oncogene)

RAS-GAPs: RAS-GTPase-Activating Proteins

RAS-GEFs: RAS-Guanine Nucleotide Exchange Factors

RTK: Receptor Tyrosine Kinase

SLs: Sesquiterpene Lactones

SMILES: Simplified Molecular Input Line Entry System

SOS: Son of Sevenless (a RAS guanine nucleotide exchange factor)

SSM: Superficial Spreading Melanoma

TERT: Telomerase Reverse Transcriptase

TP53: Tumour Protein 53

TPSA: Topological Polar Surface Area

UV: Ultraviolet

V1Y: BRAF reference ligand

WLOGP: predictive model of lipophilicity.

المخلص

الميلانوما، نوع من أنواع سرطان الجلد القاتل والأكثر شيوعًا في جميع أنحاء العالم ، والذي ينتج عن طفرات في الجينات المشفرة لبروتينات BRAF و NRAS المتضمنة في مسار MAPK، وهو مسار ناقل للإشارة الخلوية، رئيسي في تطور ونمو هذا النوع من السرطان بخلايا الميلانوسيت.

على الرغم من أن العلاجات الكيميائية التي تستهدف تثبيط هذا المسار واعدة، إلا أن المقاومة لها غالبًا ما تتطور، مما يستلزم استكشاف عوامل جديدة.

استُخدمت طرق نمذجة تعتمد على الالتحام الجزيئي وتوقع خصائص ADME لدراسة تسع مركبات طبيعية، وهي لاكتونات سيسكيتيربينية، مشتقة من نبات سوسوريا لوبا (*Saussurea lappa*)، لتحديد إمكاناتها كمثبطات لبروتينات NRAS و BRAF و ERK2 بمسار MAPK.

أظهر لاباديلكتون أعلى ألفة ارتباط بطاقة ارتباط مساوية لـ -9.5 kcal/mol مع بروتين ERK2، متجاوزًا بذلك الجزيء المرجعي 8XE، ومشكلًا تفاعلات استقرار وارتباط من نوع الرابطة الهيدروجينية والكارهة للماء في حين أظهر ديهيدروكوستوس لكتون ارتباطًا أفضل ببروتين BRAF و ERK2 بطاقة ارتباط مساوية لـ -8.9 kcal/mol و -8.5 kcal/mol على الترتيب.

أظهرت نتائج توقعات ADME أن جميع المركبات التي تمت دراستها لها خصائص فيزيوكيميائية مواتية، معتدلة الألفة للدهون وامتصاصًا معويًا عاليًا.

خلصت النتائج مجتمعةً إلى أن لاكتونات سيسكيتيربين من سوسوريا لوبا، ولا سيما لاباديلكتون ولاكتون ديهيدروكوستوس لاكتون، تمثل مثبطات طبيعية واعدة لمسار MAPK التي يمكن أن تشكل علاجات مستهدفة جديدة للميلانوما.

الكلمات الدالة: الميلانوما، مسار MAPK، الإلتحام الجزيئي، ADME، لكتونات السسكيتيربين، سوسوريا لوبا.

Abstract

Melanoma, a deadly skin cancer, is increasing in global incidence. The MAPK pathway, frequently mutated in BRAF and NRAS genes, plays a central role in melanoma progression.

Although targeted therapies against this pathway have shown promise, resistance often emerges, which necessitates the exploration of novel agents.

The *in silico* molecular docking method and ADME prediction were used to test nine natural compounds, sesquiterpene lactones, from the medicinal plant *Saussurea lappa* for their potential as melanoma key pathway inhibitors (NRAS, BRAF, and ERK2).

Lappadilactone had the strongest binding affinity, especially to ERK2 equal to **-9.5 kcal/mol**, outperforming the reference ligand 8XE in binding energy. It formed stabilising interactions within the active site, such as hydrogen bonds and hydrophobic contacts. Dehydrocostus lactone demonstrated significant binding to both BRAF and ERK2 with binding energy of **-8.9 kcal/mol** and **-8.5 kcal/mol**, respectively.

ADME predictions showed that the compounds had favourable physicochemical properties, moderate lipophilicity, and high predicted gastrointestinal absorption.

These findings suggest that sesquiterpene lactones from *Saussurea lappa*, particularly Lappadilactone and Dehydrocostus lactone, represent promising natural-based MAPK pathway inhibitors with the potential to be novel targeted therapies against metastatic melanoma.

Keywords: melanoma, MAPK pathway, molecular docking, ADME, sesquiterpene lactones, *Saussurea lappa*.

Résumé

Le mélanome, un cancer de la peau mortel, est de plus en plus répandu dans le monde. La voie MAPK, fréquemment affectée par des mutations dans les gènes codant pour les protéines BRAF et NRAS, joue un rôle central dans la progression du mélanome.

Bien que les thérapies ciblant cette voie soient prometteuses, une résistance se développe souvent, nécessitant l'exploration de nouveaux agents.

Les méthodes *in silico* basées sur l'amarrage moléculaire et l'ADME ont été utilisées pour étudier neuf composés naturels, des lactones sesquiterpéniques, dérivés de la plante médicinale *Saussurea lappa*, afin de déterminer leur potentiel en tant qu'inhibiteurs des protéines NRAS, BRAF et ERK2, de la voie MAPK, une voie métabolique clé dans le mélanome.

Les résultats de Docking moléculaire obtenus ont montré que : parmi les molécules étudiées la Lappadilactone présentait l'affinité de liaison la plus élevée, en particulier avec la protéine ERK2 avec une énergie de liaison égale à **-9.5 kcal/mol**, surpassant le ligand de référence 8XE et formant des interactions stabilisantes de type liaison hydrogène et hydrophobe, alors que la Dehydrocostus lactone a montré une meilleure liaison vis-à-vis BRAF et ERK2 avec une énergie de liaison égale à **-8.9 kcal/mol** et **-8.5 kcal/mol**, respectivement.

ADME ont montré que tous les composés étudiés avaient des propriétés physicochimiques favorables, une lipophilie modérée et une absorption gastro-intestinale prédite élevée.

L'ensemble des résultats permet de conclure que les lactones sesquiterpéniques de *Saussurea lappa*, en particulier la Lappadilactone et la lactone Dehydrocostus, représentent des inhibiteurs naturels prometteurs de la voie MAPK qui pourraient constituer de nouvelles thérapies ciblées pour le mélanome métastatique.

Mots-clés : mélanome, voie MAPK, Docking moléculaire, ADME, lactones sesquiterpéniques, *Saussurea lappa*.

Table of Contents

Acknowledgements	i
Dedication	ii
Abbreviations & Symbols	iii
المخلص	vi
Abstract	vii
Résumé	viii
Table of Figures	xi
Tables list.....	xiii
Introduction	1
Materials & Methods.....	7
1. Ligand structure preparation and activities prediction	7
2. Target selection and preparation.....	11
3. Molecular docking.....	14
3.1 Docking parameters.....	15
3.2 Visualization and analysis of docking results.....	15
4. ADME predictions.....	17
Results and Discussion.....	18
1. Molecular docking results	18
1.1 Interaction mode between SLs and NRAS.....	18
1.2 Interaction mode between SLs and BRAF	41

1.3 Interaction mode between SLs and ERK2	64
2. ADME analysis.....	86
2.1 Physicochemical Properties.....	86
2.2 Pharmacokinetic Properties	86
2.3 Drug-likeness.....	87
3. General Discussion.....	90
Conclusion.....	92
Bibliographical References	94
Annexes	i

Table of Figures

Figure 1. MAPK signalling pathway	3
Figure 2. Indian <i>Saussurea lappa</i> roots	5
Figure 3. PASS online resource website interface	10
Figure 4. Open Targets Platform website interface	11
Figure 5. CB-DOCK2 website interface	14
Figure 6. Workflow diagram of in silico study process.....	16
Figure 7. Interaction mode of GNP and NRAS	20
Figure 8. Interaction mode of Lappadilactone and NRAS	22
Figure 9. Interaction mode of Dehydrocostus lactone and NRAS	24
Figure 10. Interaction mode of Isozaluzanin C and NRAS.....	26
Figure 11. Interaction mode of Zaluzanin C and NRAS	28
Figure 12. Interaction mode of Costunolide and NRAS	30
Figure 13. Interaction mode of Arbusculin A and NRAS.....	32
Figure 14. Interaction mode of Reynosin and NRAS.....	34
Figure 15. Interaction mode of Santamarin and NRAS	36
Figure 16. Interaction mode of α -cyclocostunolide and NRAS	38
Figure 17. Binding energy of SLs-NRAS complexes	40
Figure 18. Interaction mode of VIY and BRAF	43
Figure 19. Interaction mode of Lappadilactone and BRAF	45
Figure 20. Interaction mode of Dehydrocostus lactone and BRAF	47

Figure 21. Interaction mode of Isozaluzanin C and BRAF	49
Figure 22. Interaction mode of Zaluzanin C and BRAF	51
Figure 23. Interaction mode of Costunolide and BRAF.....	53
Figure 24. Interaction mode of Arbusculin A and BRAF	55
Figure 25. Interaction mode of Reynosin and BRAF	57
Figure 26. Interaction mode of Santamarin and BRAF.....	59
Figure 27. Interaction mode of α -cyclocostunolide and BRAF	61
Figure 28. Binding energy of SLs-BRAF complexes.....	63
Figure 29. Interaction mode of 8XE and ERK2	65
Figure 30. Interaction mode of Lappadilactone and ERK2.....	67
Figure 31. Interaction mode of Dehydrocostus lactone and ERK2.....	69
Figure 32. Interaction mode of Isozaluzanin C and ERK2.....	71
Figure 33. Interaction mode of Zaluzanin C and ERK2.....	73
Figure 34. Interaction mode of Costunolide and ERK2	75
Figure 35. Interaction mode of Arbusculin A and ERK2	77
Figure 36. Interaction mode of Reynosin and ERK2	79
Figure 37. Interaction mode of Santamarin and ERK2	81
Figure 38. Interaction mode of α -cyclocostunolide and ERK2.....	83
Figure 39. Binding energy of SLs-ERK2 complexes	85
Figure 40. SwissADME BIOLED-Egg model for selected <i>Saussurea lappa</i> SLs within ADME parameters.....	89

Tables list

Table 1. <i>Saussurea lappa</i> 's sesquiterpene lactone ligand names, IDs and 2D structures.....	8
Table 2. Structures of reference ligands.....	13
Table 3. <i>In silico</i> physicochemical properties of selected sesquiterpene lactones.....	86
Table 4. <i>In silico</i> pharmacokinetic properties of selected sesquiterpene lactones.....	87
Table 5. <i>In silico</i> drug-likeness properties of selected sesquiterpene lactones.....	88

Introduction

Introduction

Skin cancers are the most widely diagnosed type of cancer globally, with more than 1.5 million new cases estimated in 2020 (Arnold *et al.*, 2022). Melanoma is one of the three primary varieties of skin cancer; the other two are squamous cell carcinoma and basal cell carcinoma. Although it only accounts for approximately 5% of cases, it is still the deadliest severe range and the fastest growing cancers worldwide (Liu & Sheikh, 2014).

Epidemiological studies have provided valuable insights into the causes of melanoma. Ultraviolet (UV) radiation exposure has been identified as a significant risk factor for the development of melanoma (Liu & Sheikh, 2014). According to projections by the American Cancer Society (ACS), it is estimated that in 2024, there will be approximately 100,640 new cases of melanoma diagnosed, with a higher incidence among men (59,170 cases) than women (41,470 cases). Furthermore, the ACS anticipates that melanoma will claim the lives of around 8,290 patients, with a higher mortality rate among men (5,430 deaths) compared to women (2,860 deaths) (Melanoma Skin Cancer Statistics, 2023).

Cutaneous melanoma is a malignant tumour of melanocytes, which synthesises the melanin pigment in the basal layer of the epidermis that determines skin colour. Wallace Clark, described four histological variants of melanoma: (i) superficial spreading melanoma (SSM), (ii) nodular melanoma (NM), (iii) lentigo maligna melanoma (LMM), and (iv) Acral lentiginous melanomas (ALM) (Fristiohady *et al.*, 2022; Davis *et al.*, 2019). Of these, the superficial spreading form remains the most common especially in fair-skinned people and accounts for about 70% of melanomas followed by nodular form that represents about 15–30% of melanoma cases. The lentigo maligna and acral lentiginous forms represent less than 10% of melanoma cases (Liu & Sheikh, 2014). While these figures illustrate the significant prevalence of melanoma, understanding the molecular pathways that drive melanoma development and progression is crucial for developing effective therapies.

The 2018 classification of melanocytic tumours by the World Health Organisation identifies nine pathways to melanoma, seven of which are primary cutaneous, including the mitogen-activated protein kinase (MAPK) pathway, the protein kinase B (PI3K /AKT) pathway, the cell-cycle regulation pathway, the pigmentation-related pathway, the p53 pathway, the epigenetic factors, and some other pathways (Guo *et al.*, 2021). Both gene amplifications in

KIT, CCND1, CDK4, MITF, and TERT, as well as gene deletion/loss-of-function in TP53 and CDKN2A, are present (Cazzato, 2023; Ferrara & Argenziano, 2021).

The IKK complex, a regulator of NF- κ B signalling involved in cell proliferation and apoptosis, has also been proposed as a potential therapeutic target for melanoma (Yang *et al.*, 2010). Similarly, the Mcl-1 protein has been identified as an important target in melanoma treatment, with inhibitors showing the ability to induce apoptosis and sensitize melanoma cells to treatment (Respondek *et al.*, 2020). Moreover, in the context of melanoma metastasis, the role of specific genes like HSP90 and ALDH1A1 has been highlighted as potential targets to impede tumour growth and metastasis (Mielczarek-Lewandowska *et al.*, 2020). However, several signalling pathways contribute to melanoma development, activation of the mitogen-activated protein kinase (MAPK) pathway is the most common driver and the key player in melanoma (Mielczarek-Lewandowska *et al.*, 2020; Amaral *et al.*, 2017b; Shain *et al.*, 2015; Evans *et al.*, 2013). Overall, targeting specific proteins and signalling pathways in melanoma presents a promising approach for developing effective therapeutic strategies against this aggressive form of skin cancer.

The activation of the MAPK pathway (Figure 1) occurs under physiological conditions through extracellular binding of growth factors to receptor tyrosine kinases (RTKs). Through a series of phosphorylation events, the MAPK pathway transmits extracellular signals from the cell membrane to the nucleus (Evans *et al.*, 2013). In normal cell, interaction between an RTK and its ligand is necessary to activate the MAPK pathway, triggering a cascade of intracellular events that leads to cellular growth, increased survival and inhibition of apoptosis. The switch on/off key of this pathway is RAS proteins (HRAS, KRAS and NRAS) which are monomeric GTP-binding proteins. The activation status of RAS proteins is determined by their binding state, when bound to GTP, they are active and can engage downstream target enzymes, but when bound to GDP, they are inactive and cannot interact with these effectors (Downward, 2003), this cycle involving the action of RAS-guanine nucleotide exchange factors (RAS-GEFs) and RAS-GTPase-activating proteins (RAS-GAPs), respectively (Punekar *et al.*, 2022). When RAS is activated, Rapidly Accelerated Fibrosarcoma (RAF) protein and its components (ARAF, BRAF and CRAF) are activated by phosphorylation. Thus, BRAF and CRAF serine/threonine kinases can act as downstream mediators. Activated RAF interact with and phosphorylate mitogen-activated extracellular signal-regulated kinase kinase (MEK) that further phosphorylates and activates mitogen-activated extracellular-signal regulated kinase

(ERK). ERK activation has an important role in oncogenesis, promoting cellular growth and differentiation. Activated ERK is also responsible for the upstream negative feedback, which occurs at different levels of the MAPK pathway (Amaral *et al.*, 2017b).

MAPK; Mitogen-Activated Protein Kinase, RTK; Receptor Tyrosine Kinase, GRB2; Growth factor receptor-bound protein 2, SOS; Son of Sevenless a RAS guanine nucleotide exchange factor, GTP; Guanosine

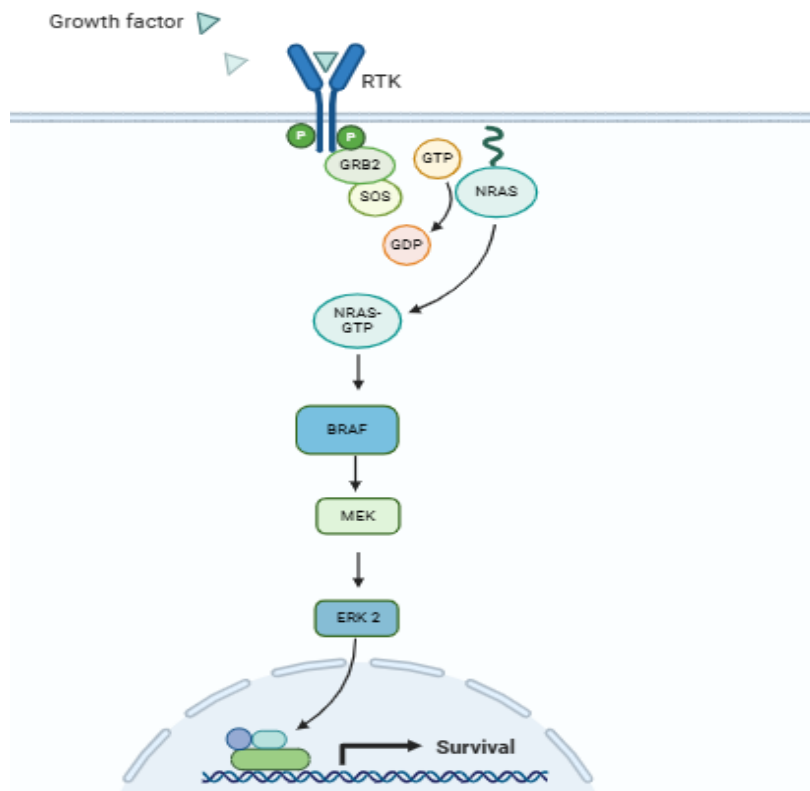


Figure 1. MAPK signalling pathway

Triphosphate, GDP; Guanosine Diphosphate, NRAS; Neuroblastoma RAS, BRAF; B-Rapidly Accelerated Fibrosarcoma, MEK; Extracellular Signal-Regulated Kinase Kinase, ERK2; Extracellular Signal-Regulated Kinase.

In melanoma cells, the MAPK pathway is dysregulated. The BRAF mutation (BRAFV600) is identified in about 45-60% of the patients (Amaral *et al.*, 2017a). A proto-oncogene, BRAF is a member of the RAS-RAF-MEK-ERK kinase pathway and encodes a serine/threonine protein kinase. Normally, in response to growth signals, BRAF engages in homo- or heterodimerization with another RAF kinase. Nevertheless, BRAF acts as a self-sufficient, persistently activated monomer when an activating mutation occurs. This causes uncontrolled cell proliferation and could contribute to the growth and development of tumours. The most prevalent BRAF alteration is the mutation V600E, which converts valine to glutamic acid. It is responsible for about 90% of BRAF-activating mutations and 50% of all metastatic

melanomas. Additionally, activating mutations in the NRAS gene, another component of the MAPK pathway, especially in codons 12, 13, and 61 (Downward, 2003), have also been implicated in the development of melanoma, further emphasizing the importance of this signalling cascade in the disease pathogenesis. The NRAS GTPase or neuroblastoma RAS oncogene occurs in 15–20% of melanoma patients (Liu & Sheikh, 2014).

Surgical intervention alone can successfully operate on melanoma during its initial phases, leading to high survival rates. However, after metastasis occurs, surgery and traditional treatments such as radiation and chemotherapy become less effective, leading to a significant decrease in survival rates (Davis *et al.*, 2019). Targeted therapies aimed at inhibiting the dysregulated MAPK pathway which has been proven to be effective (Whipple *et al.*, 2016), particularly BRAF and MEK inhibitors, have shown promise in treating melanoma. However, resistance mechanisms often emerge, necessitating the exploration of novel therapeutic approaches (Amaral *et al.*, 2017b).

Natural products have long been a rich source of bioactive compounds with diverse chemical structures and pharmacological properties (Newman & Cragg, 2020). They are generally safe, non-toxic, easily accessible, and cost-effective (Fristiohady *et al.*, 2022; Khan *et al.*, 2019). They can exert their anticancer effects by inhibiting proliferation, inducing apoptosis, and blocking migration, and invasion in human melanoma. Natural products and their synthetic analogues represent a source of new drugs; approximately 80% of approved chemotherapy drugs such as Taxol, epothilones, and vinca alkaloids are derived from bioactive natural products. Besides, more than half of all drugs are based on bioactive natural products, which has become a current trend to minimize the side effects and resistance associated with chemotherapy due to their ability to induce apoptosis more selectively in cancer cells than in normal cells. Fristiohady *et al.* (2022) evaluated 40 medicinal plants for potential anticancer compounds against melanoma skin cancer, using *in vitro* and *in vivo* experiments.

Saussurea lappa, a perennial, aromatic and medicinal plant from the *Asteraceae* family, is one of the best-known species of its genus (Figure 2). Native to India and Pakistan and cultivated in southwestern China, the dried roots of *Saussurea lappa* are used in traditional medicine to treat various diseases such as asthma, bronchitis, typhoid fever, cholera, coughs, cold, ulcers, gastric disorders, and chronic skin diseases in Asia (Alotaibi *et al.*, 2021; Zahara *et al.*, 2014).

The roots of *Saussurea lappa* are exceptionally rich in sesquiterpene lactones (SLs) which contribute to the plant's remarkable therapeutic potential and makes it an attractive source for the discovery of novel bioactive compounds, particularly due to its anticancer properties (Alotaibi *et al.*, 2021).



Figure 2. Indian *Saussurea lappa* roots (Sharma, 2020)

Sesquiterpene lactones, a class of terpenoids have garnered significant interest due to their wide range of biological activities, including cytotoxic, anti-inflammatory, and anticancer effects (Chadwick *et al.*, 2013). These compounds, have demonstrated potential in inhibiting melanoma cell growth and inducing apoptosis through various mechanisms, such as induction of oxidative stress, and interference with cell cycle progression (Fristiohady *et al.*, 2022). Sesquiterpene lactones represent one of the largest classes of secondary metabolites, with over 6000 structures reported (Brás *et al.*, 2023). These fifteen-carbon compounds are formed through the condensation of three isoprene units, followed by cyclization and oxidative transformation to create a cis or trans-fused lactone ring. A significant characteristic of sesquiterpene lactones is the presence of a γ -lactone ring, often accompanied by an α -methylene group. The structural diversity of sesquiterpene lactones may present hydroxyls, esterified hydroxyls, epoxide groups, glycosylated forms, and occasional halogen or sulphur atoms. Their bitter, colourless, and lipophilic character exhibit a wide range of structural arrangements (Ivanescu *et al.*, 2015), which can be broadly divided into three groups based on

their carbocyclic skeletons: (i) guaiane, (ii) eudesmane, and (iii) germacrene (Hassan & Masoodi, 2020).

In addition to the intriguing possibilities for therapeutic applications of sesquiterpene lactones, Sun *et al.* (2003), isolated and identified eight sesquiterpene lactones from *Saussurea lappa*. These compounds were found to be active against HepG2, HeLa, and OVCAR-3 cell Lines. Moreover, we selected another SL from the Vijayalakshmi *et al.* (2022) study, bringing the total number of sesquiterpene lactones evaluated in this study to nine.

The previous findings indicate the possibility of sesquiterpene lactones for further research into their mode of action against melanoma, highlighting the importance of finding novel, safe, and efficient anti-melanoma agents due to the emergence of multi-drug resistance in current chemotherapies (Chinembiri *et al.*, 2014).

The aim of the current study is to gain a deeper understanding of the molecular interactions between the sesquiterpene lactones from *Saussurea lappa* and their key melanoma-related proteins, such as NRAS, BRAF, and ERK2, in order to evaluate them as potential anti-melanoma agents and to understand their relationship with putative MAPK pathway.

We executed a computational molecular docking simulation, a computer method used in drug discovery (Danao *et al.*, 2022), to predict how the sesquiterpene lactones from *Saussurea lappa* would bind to target proteins. Researchers widely use this structure-based *in silico* approach for virtual screening, identifying potential therapeutic compounds by predicting ligand-target interactions at the molecular level (Manimegalai *et al.*, 2024; Velasquez-López *et al.*, 2022; Pinzi & Rastelli, 2019). Based on the predicted conformational space and binding energy (the best is the least), it calculates the interactions and forces, such as electrostatic, hydrogen bonds, hydrophobic, and van der Waals forces (Nirmalraj *et al.*, 2021; Batool *et al.*, 2019; Kapetanovic, 2008). Followed by prediction of some physicochemical and pharmacokinetic properties by using *in silico* ADME study.

Materials & Methods

Materials & Methods

In order to evaluate the potential anti-melanoma effects of sesquiterpene lactones derived from the roots of *Saussurea lappa*, an *in silico* study was performed. This investigation included the selection and preparation of ligands, the selection and preparation of targets, molecular docking simulations and visual analyses of resulting modelled complex, followed by absorption, distribution, metabolism, and excretion (ADME) predictions.

1. Ligand structure preparation and activities prediction

Nine sesquiterpene lactones were selected from previous studies by Sun *et al.* (2003) and Vijayalakshmi *et al.* (2022) based on their proven experimental anti-cancer activities (Table 1), and retrieved from PubChem, ChemSpider, and ETCM (Encyclopaedia of Traditional Chinese Medicine) databases in SMILES (Simplified Molecular Input Line Entry System) format then submitted to ChemMOP (MOPAC) (scbdd.com) website for generating the 3D configuration and optimisation by the PM7 parameterization method to obtain energetically stable conformations in mol2 file format suitable for molecular docking with CB-Dock2.

The PASS Online web resource (<http://www.way2drug.com/passonline/>) from the Way 2 Drug: Understanding Chemical-Biological Interaction web site was used to predict the potential biological and antitumor activities for the selected compounds based on their structure formulas (Filimonov *et al.*, 2014) (Figure 3). The prediction results were collected and analysed.

Table 1. *Saussurea lappa*'s sesquiterpene lactone ligand names, IDs and 2D structures

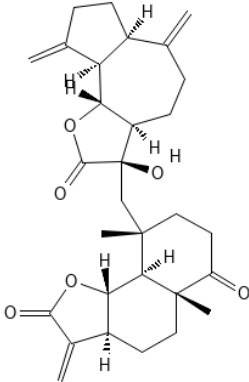
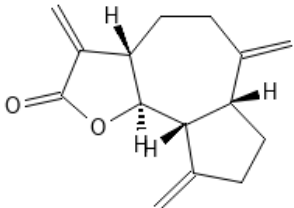
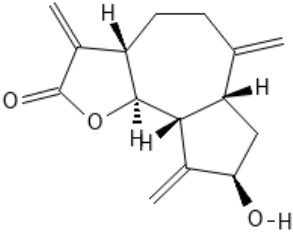
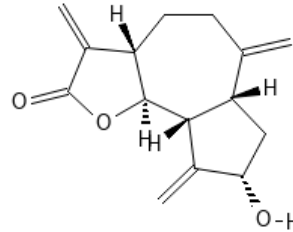
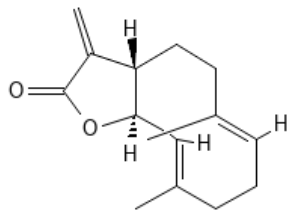
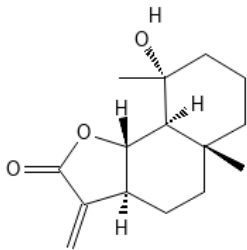
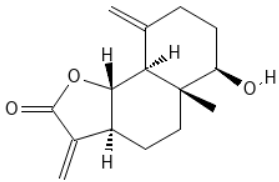
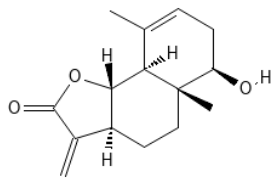
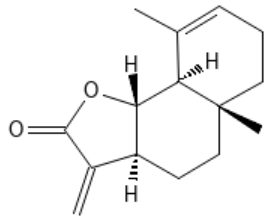
No. compound	Compound 1	Compound 2	Compound 3	Compound 4
Compound Name	Lappadilactone	Dehydrocostus lactone	Isozaluzanin C	Zaluzanin C
PubChem ID	11081540	73174	470970	72646
2D Structure	 The structure of Lappadilactone is a complex sesquiterpene lactone. It features a central bicyclic core with a five-membered lactone ring fused to a six-membered ring. The structure is highly substituted with multiple methyl groups, some shown with wedges and dashes to indicate stereochemistry. There are also several exocyclic double bonds (methylidenes) attached to the ring system.	 Dehydrocostus lactone is a sesquiterpene lactone with a bicyclic core similar to Lappadilactone. It has a five-membered lactone ring fused to a six-membered ring. The structure is substituted with methyl groups and exocyclic double bonds, with different stereochemistry compared to Lappadilactone.	 Isozaluzanin C is a sesquiterpene lactone with a bicyclic core. It features a five-membered lactone ring fused to a six-membered ring. The structure is substituted with methyl groups and exocyclic double bonds, and includes a hydroxyl group (-OH) on one of the rings.	 Zaluzanin C is a sesquiterpene lactone with a bicyclic core. It features a five-membered lactone ring fused to a six-membered ring. The structure is substituted with methyl groups and exocyclic double bonds, and includes a hydroxyl group (-OH) on one of the rings.

Table 1. continued

No. compound	Compound 5	Compound 6	Compound 7	Compound8	Compound 9
Compound Name	Costunolide	Arbusculin A	Reynosin	Santamarin	α -cyclocostunolide
PubChem ID	5281437	160153	482788	188297	442191
2D Structure					

PASSonline sarra hadd (Log out) Go

» Home | » Definitions | » Products | » Services | » FAQ | » Contacts

Predict new compound View old results View/change profile

SMILES MOL file Marvin JS

C=C1CC[C@H]2C(=C)CC[C@@H]3[C

Get prediction

0,654	0,008	Chemopreventive
0,665	0,021	Phosphatase inhibitor
0,691	0,053	CYP2J substrate
0,645	0,010	Ovulation inhibitor
0,641	0,025	Oxidoreductase inhibitor
0,617	0,005	Transcription factor inhibitor
0,633	0,025	Antiinflammatory
0,619	0,013	Cardiovascular analeptic
0,610	0,008	Transcription factor NF kappa B stimulant
0,610	0,008	Transcription factor stimulant
0,603	0,003	Aromatase inhibitor
0,576	0,005	Antineoplastic (melanoma)

Figure 3. PASS online resource website interface

2. Target selection and preparation

Based on the findings obtained from previous studies and *in silico* predictions using the Open Targets Platform (<https://platform.opentargets.org/>) an open-source resource that systematically assists drug target selection and prioritisation using publicly available data (Ochoa *et al.*, 2023) was used to predict the targets with the best association score related to melanoma disease as a strength step adding to the experimental findings (Figure 4).

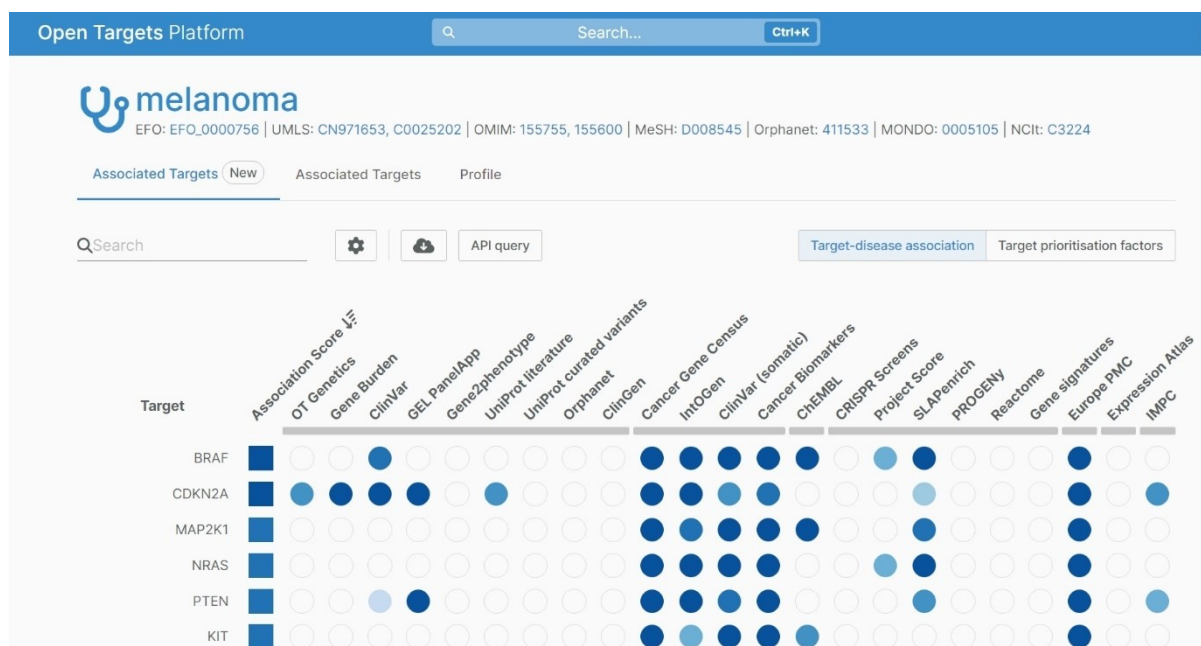


Figure 4. Open Targets Platform website interface

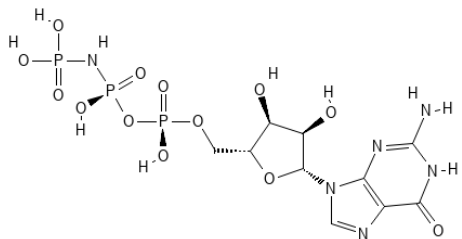
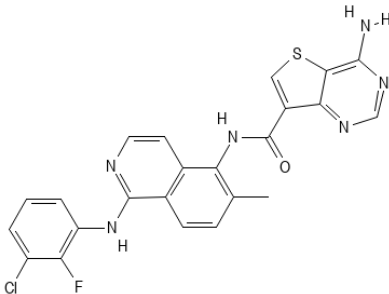
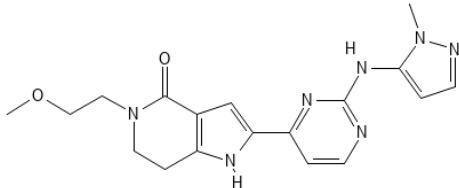
The protein structures of the MAPK signalling pathway and their binding ligands, NRAS (PDB ID: 5UHV) in complex with its ligand GNP, BRAF (PDB ID: 6XFP) in complex with its ligand V1Y and ERK2 (PDB ID: 5NHJ) in complex with its ligand 8XE were downloaded from the Protein Data Bank (PDB) (Fermi *et al.*, 1984) and PDB REDO (server used to retrieve updated and optimised versions of PDB entries) (van Beusekom *et al.*, 2018) in PDB format and mol2 file format, respectively. Table 2 shows the names and structures of the reference ligands.

The selection criteria for these proteins included the following:

- The source organism is *Homo sapiens* (human proteins);
- Completed structures with no missing amino acid residues;
- The proteins are in complexes with their respective ligands providing the experimental binding data.

Although the MEK protein is an important component of the MAPK signalling pathway, it was excluded from this study because there are no complete structures available in the PDB database that meet the selection criteria.

Table 2. Structures of reference ligands

Target Name	NRAS	BRAF	ERK2
Reference ligand	GNP	V1Y	8XE
PubChem ID	135403657	89655386	126480562
2D Structure			

3. Molecular docking

CB-Dock2 (Figure 5), one of the blind docking tool servers ([CB-Dock2: An accurate protein-ligand blind docking tool \(labshare.cn\)](#)), was used to improve docking accuracy by predicting protein binding regions, calculating centres and sizes, and performing docking using Autodock Vina software (Liu *et al.*, 2022).

The nine sesquiterpene lactone ligands were docked to the three targets individually in 20 CB-Dock2 predicted cavities. Data related to the best pose, such as Vina scores, cavity sizes, and cavity centre cartesian coordinate locations, were reported. Additionally, the protein-ligand complexes were downloaded in PDB format. Furthermore, the reference ligands were redocked with their own targets, following the same approach.

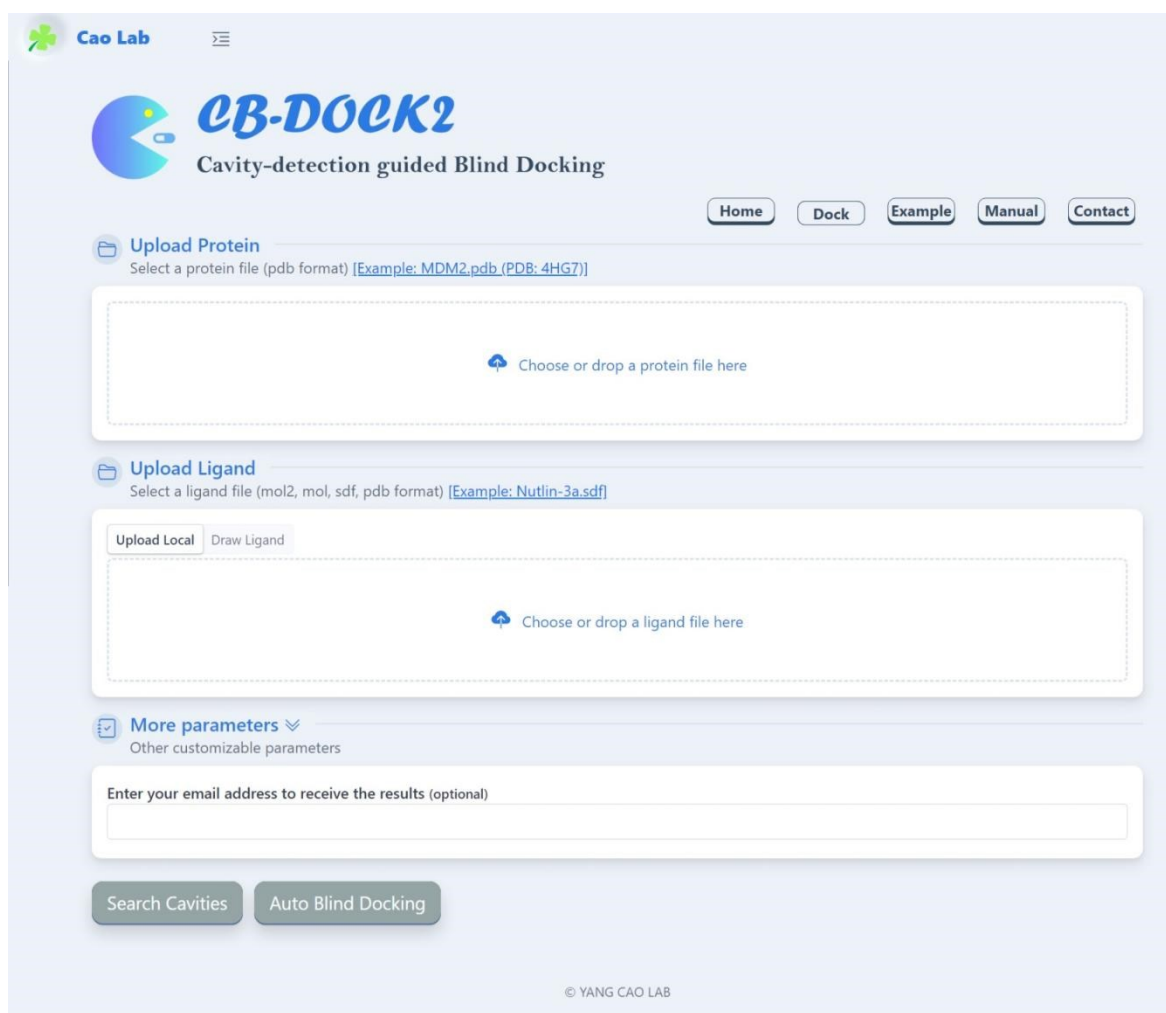


Figure 5. CB-DOCK2 website interface

3.1 Docking parameters

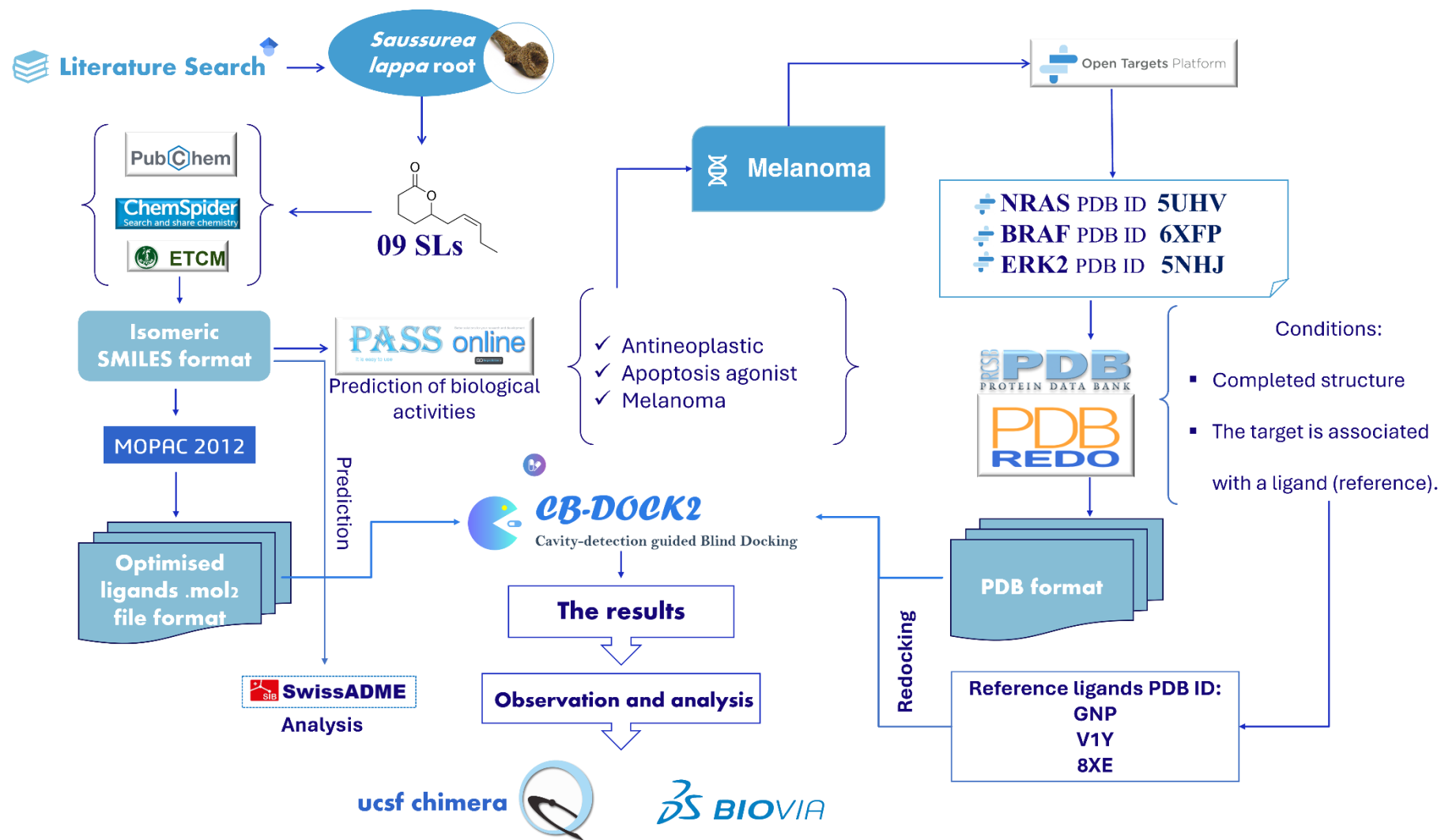
Search algorithms: CB-Dock2 integrates cavity detection, docking, and homologous template fitting algorithms to enhance binding site identification and binding pose prediction accuracy in protein-ligand blind docking (Liu *et al.*, 2022).

Scoring functions: Scoring functions are used to predict affinities in receptor-ligand complexes. CB-Dock2's scoring functions include an empirical scoring function (Liu *et al.*, 2022).

3.2 Visualization and analysis of docking results

Visualization: Discovery Studio (BIOVIA Discovery Studio 2024 v24.1.0.23298) was used for the computational visualisation of receptor-ligand interaction binding types in 2D diagrams. whereas UCSF Chimera 1.17.3 was used for 3D visualization.

Analyses were executed from the best poses and included the evaluation and comparison of binding energy (kcal/mol) and interaction mode of the modelled complexes of the study with the redocked experienced complexes. The workflow of our *in silico* experiment is illustrated in Figure 6.

Figure 6. Workflow diagram of *in silico* study process

4. ADME predictions

“Although the published confirmation to date supports the safety and perhaps the efficiency of *Saussurea lappa*, the quality of the evidence is limited” (Zahara *et al.*, 2014). To assess the drug-likeness and potential pharmacokinetic properties of the selected sesquiterpene lactone ligands, ADME (Absorption, Distribution, Metabolism, and Excretion) predictions were performed using the SwissADME web tool (<http://www.swissadme.ch/>) (Daina *et al.*, 2017) and the following parameters were evaluated for each ligand:

- Physicochemical properties such as molecular weight, lipophilicity (iLog P), and topological polar surface area (TPSA).
- Pharmacokinetic properties include gastrointestinal absorption, blood-brain barrier permeability, and whether the substance is a P-glycoprotein substrate or non-substrate. In addition, whether or not the sesquiterpenes are CYP1A2, CYP2C19, CYP2C9, CYP2D6 and CYP3A4 inhibitors.
- Drug-likeness by examining Lipinski's Rule of Five, bioavailability score, and synthetic accessibility.

Results & Discussion

Results and Discussion

Both *in vitro* and *in vivo* research has demonstrated promising anti-melanoma effects of various natural products derived from plants, such as pristimerin, picropodophyllin, oridonin, zeaxanthin, withaferin, and polyphenols, by impacting essential pathways involved in cell proliferation, apoptosis, and metastasis (Isacescu *et al.*, 2023; Fristiohady *et al.*, 2022).

Multiple other *In silico* studies have highlighted the potential effectiveness of different natural compounds in targeting melanoma. For instance, research indicates that compounds from microalgae, like phycocyanin and phycocyanobilin, that target BRAF V600E, could potentially serve as new drugs for melanoma treatment (Prasetiya *et al.*, 2023). Our study, in the same context, assessed the potential anti-melanoma activities of SLs from *Saussurea lappa* roots at molecular level.

1. Molecular docking results

1.1 Interaction mode between SLs and NRAS

1.1.1 Study of the GNP interactions with the protein NRAS (Redocking the reference)

The reference ligand Phosphoaminophosphonic acid guanylate ester GNP in complex with NRAS protein (Figure 7) reveal the best binding mode exposes a predicted binding energy of **-12 kcal/mol**.

The binding pocket of the GNP-NRAS complex with calculated cavity volume of 10 Å³, and predicted location centred at 13, 27, and 23 in terms of x, y and z coordinates respectively. include of the following residues: GLY10, ALA11, GLY12, **GLY13**, **VAL14**, **GLY15**, **LYS16**, **SER17**, **ALA18**, **PHE28**, VAL29, ASP30, GLU31, TYR32, ASP33, PRO34, **THR35**, ASP57, THR58, ALA59, **GLY60**, GLN61, **ASN116**, **LYS117**, ASP119, LEU120, SER145, **ALA146** and **LYS147**.

The binding of GNP to the NRAS protein involves an extensive network of interactions, including electrostatic, hydrogen bonding, hydrophobic, and unfavourable contacts.

Several electrostatic attractive charge interactions are observed between the NZ atom of **LYS16** and the O2B (3.97 Å), N3B (3.38 Å), O1G (4.77 Å), and O2G (5.09 Å) atoms of GNP.

Additionally, an attractive charge interaction is established between the PG atom of GNP and the O1A atom of GNP itself, with a distance of 5.51 Å.

A total of fourteen conventional hydrogen bonds are formed between GNP and various residues of NRAS, including **GLY13**, **VAL14**, **GLY15**, **LYS16**, **SER17**, **ALA18**, **THR35**, **GLY60**, **ASN116**, **ALA146**, and **LYS147**, with distances ranging from 2.83 Å to 3.30 Å. Furthermore, three carbon-hydrogen bonds are observed, involving the C3', C5', and C8 atoms of GNP, with distances ranging from 3.54 Å to 3.73 Å. Several hydrophobic interactions are also present, including a pi-cation interaction between the NZ atom of **LYS117** and the aromatic ring of GNP (4.30 Å), two pi-pi T-shaped interactions with the **PHE28** residue (4.57 Å and 4.95 Å), and six pi-alkyl interactions involving **ALA18**, **LYS117**, **ALA146**, and **LYS147**, with distances ranging from 3.93 Å to 5.41 Å.

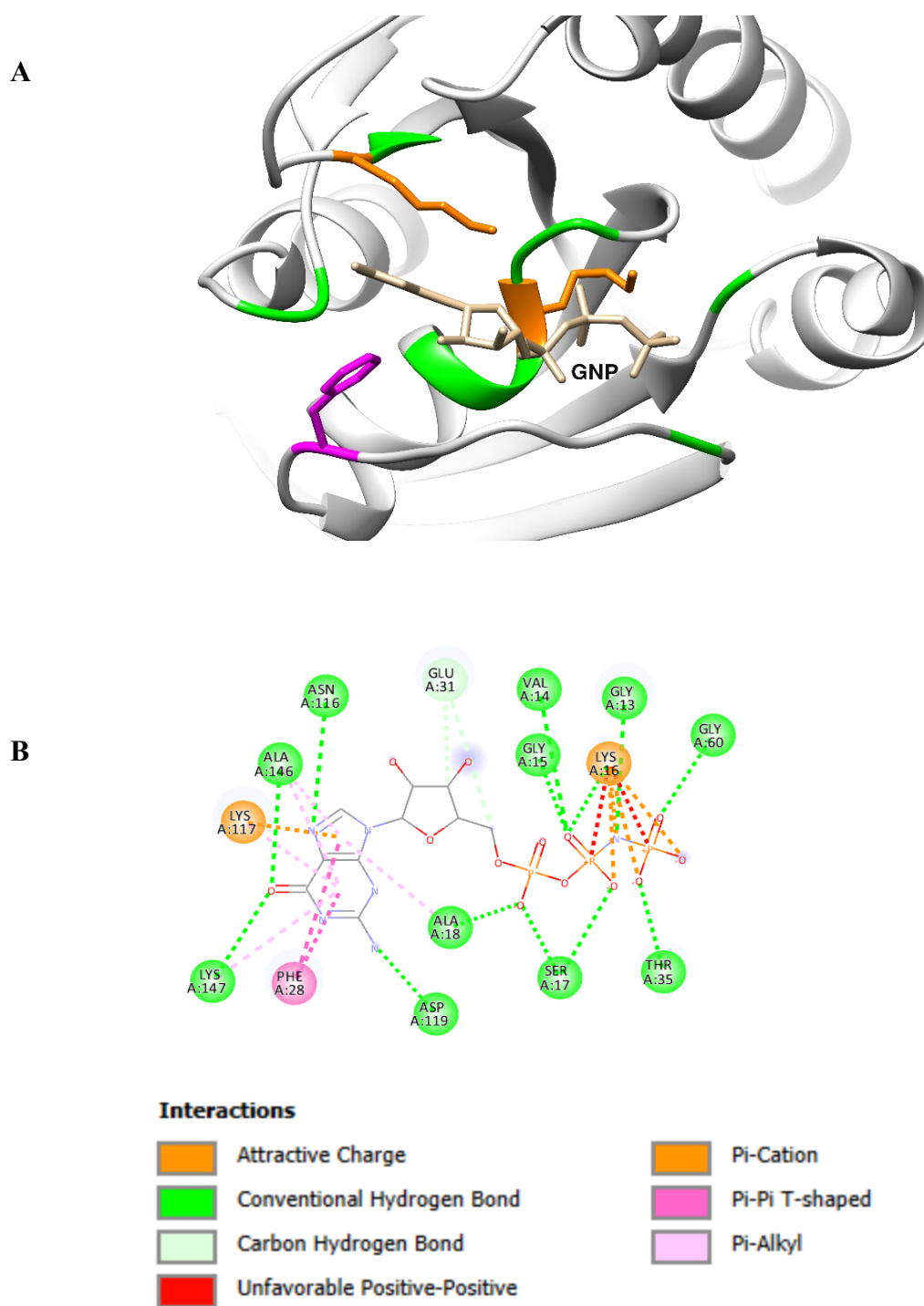


Figure 7. Interaction mode of GNP and NRAS

A) Three-dimensional model; B) Two-dimensional model

1.1.2 Study of Lappadilactone interactions with NRAS

The conformer of Lappadilactone binds to NRAS (PDB: 5UHV) with the best predicted binding energy equal to **-10.1 kcal/mol**.

The pose interacts with the protein in a position surrounded by the following amino acid residues: GLY12, GLY13, VAL14, GLY15, LYS16, **SER17**, **ALA18**, PHE28, VAL29, ASP30, GLU31, TYR32, ASP33, **PRO34**, THR35, THR58, ALA59, GLY60, GLN61, ASN85, ASN116, LYS117, ASP119, LEU120, SER145, ALA146 and LYS147, in a cavity characterised by a volume of 1013 Å³ and centre coordinates (x, y, z): 9, 34, 20.

The complex (Figure 8) displays two conventional hydrogen bonds between Lappadilactone and NRAS protein, the first is formed between the nitrogen atom (N) in **SER17** and the oxygen atom (O) of Lappadilactone at a distance of 3.15 Å. The second bond is involving the nitrogen atom (N) of **ALA18** and the oxygen atom (O) of Lappadilactone, with a distance of 2.77 Å.

In addition to the hydrogen bonding interactions, one hydrophobic alkyl interaction with a distance of 4.63 Å tightens the binding with the contribution of **PRO34** residue.

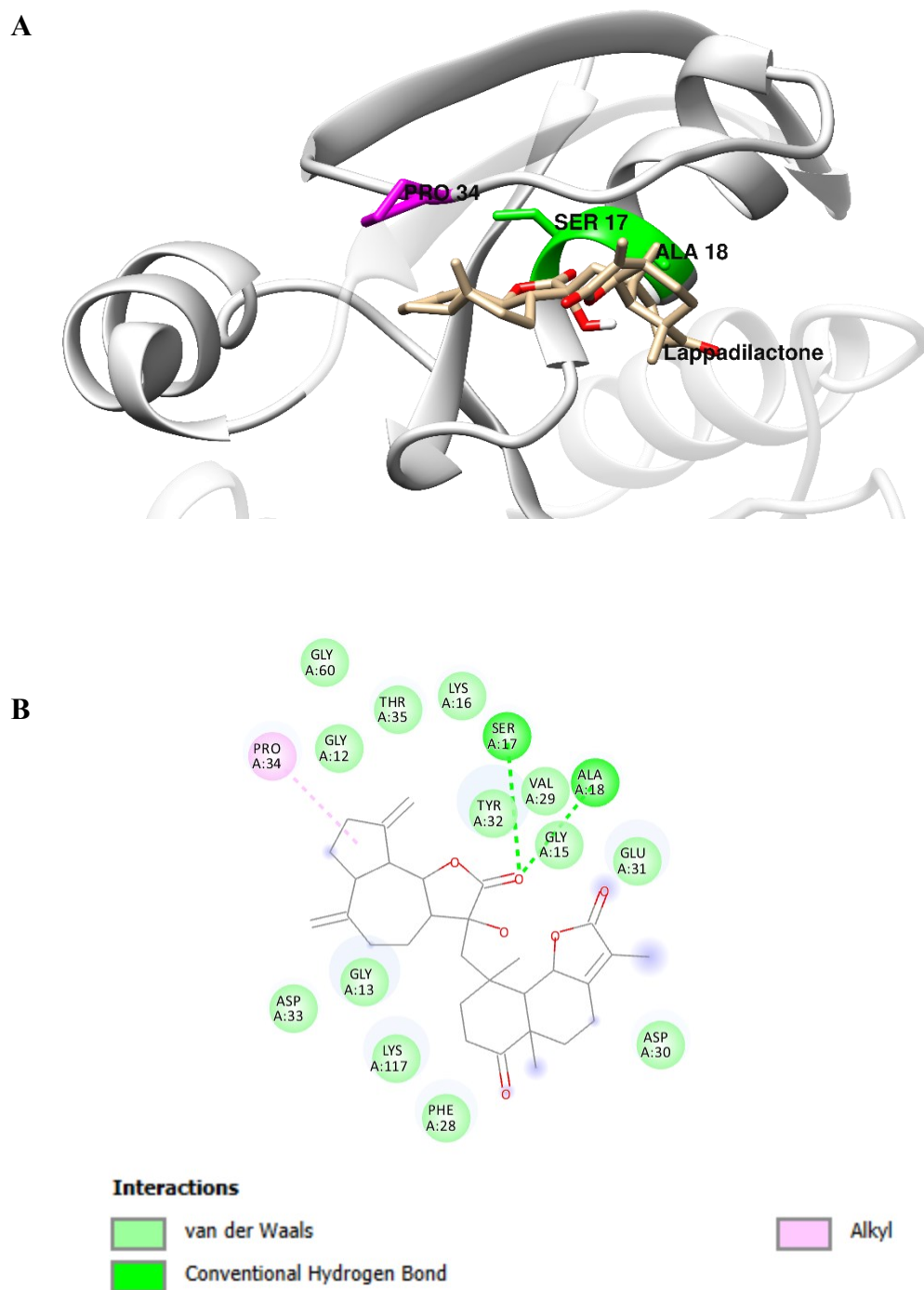


Figure 8. Interaction mode of Lappadilactone and NRAS

A) Three-dimensional model; B) Two-dimensional model

1.1.3 Study of Dehydrocostus lactone interactions with NRAS

The top-ranked binding mode of Dehydrocostus lactone with NRAS protein (PDB: 5UHV), shows a predicted binding energy of **-7.9 kcal/mol**.

According to the molecular docking study and visual analysis, The Dehydrocostus lactone binds to a pocket formed by the following residues: ALA11, GLY12, GLY13, **VAL14**, GLY15, **LYS16**, SER17, **ALA18**, LEU19, ILE21, **PHE28**, VAL29, ASP30, GLU31, TYR32, ASP33, PRO34, THR35, ASP57, THR58, ALA59, GLY60, GLN61, ASN116, LYS117, ASP119, LEU120, SER145, ALA146 and LYS147 in a space of 1013 Å³ and a centre at coordinates (x, y, z): 9,34,20.

Dehydrocostus lactone resides in a cavity within the NRAS protein, forming two conventional hydrogen bonds. The nitrogen atom (N) of **VAL14** forms the first hydrogen bond with the O2 atom of Dehydrocostus lactone at a distance of 3.09 Å. The second conventional hydrogen bond connects the NZ atom of **LYS16** to the same O2 atom at a distance of 3.10 Å.

In addition to the hydrogen bonding interactions, several hydrophobic contacts contribute to the binding. Two alkyl interactions are observed between Dehydrocostus lactone and the **ALA18** residue at distances of 4.83 Å and 3.58 Å. Furthermore, a pi-alkyl interaction is present between the aromatic ring of **PHE28** and Dehydrocostus lactone at a distance of 5.47 Å (Figure 9).

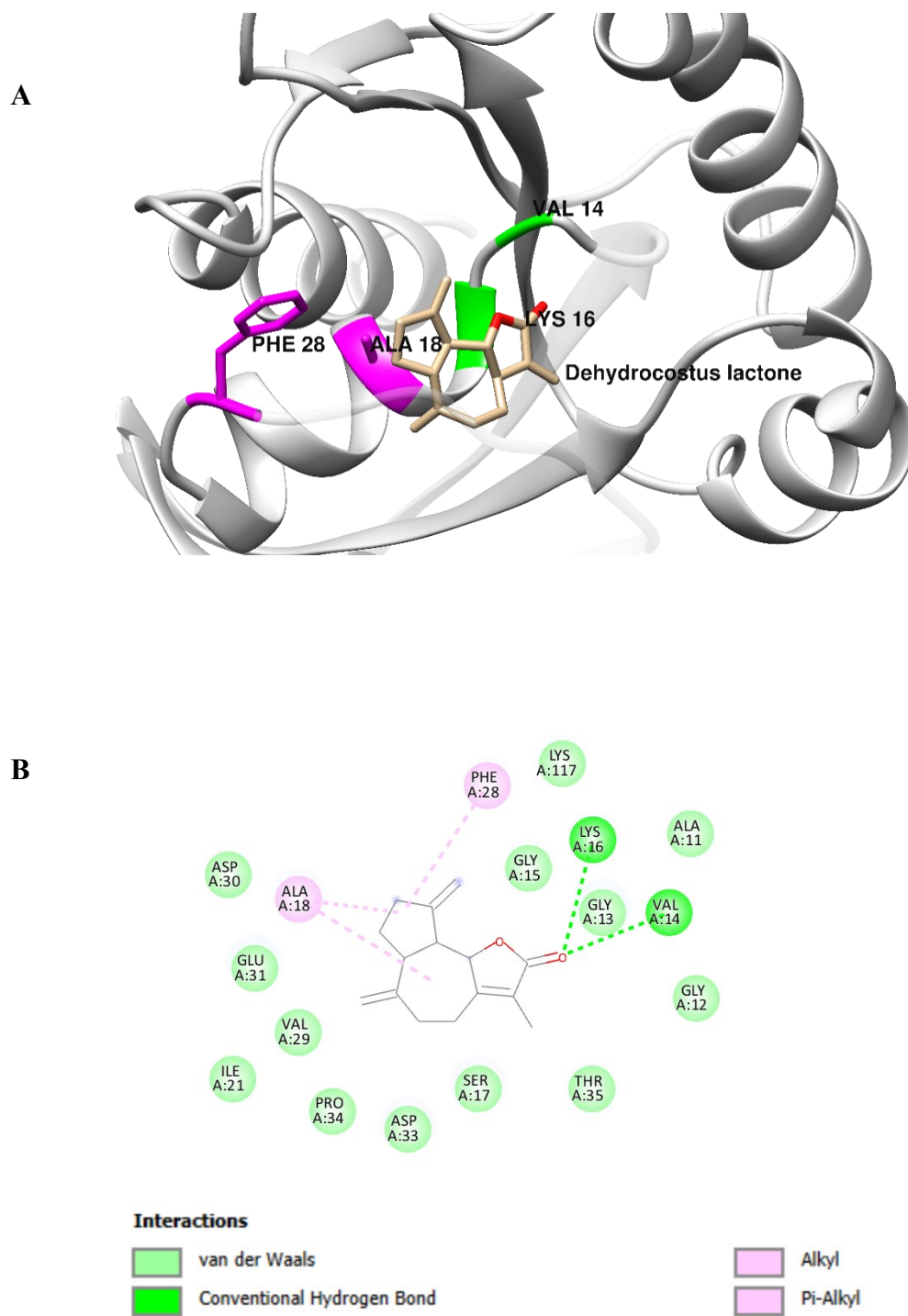


Figure 9. Interaction mode of Dehydrocostus lactone and NRAS

A) Three-dimensional model; B) Two-dimensional model

1.1.4 Study of Isozaluzanin C interactions with NRAS

The predicted binding energy associated with the most favourable binding pose emerges as **-8.2 kcal/mol**, for the Isozaluzanin C-NRAS complex.

Isozaluzanin C resides within the binding pocket of the NRAS protein composed of ALA11, GLY12, GLY13, VAL14, **GLY15**, **LYS16**, SER17, ALA18, ILE21, PHE28, VAL29, ASP30, GLU31, TYR32, ASP33, **PRO34**, **THR35**, ILE36, ASP57, THR58, ALA59, **GLY60**, **GLN61**, TYR64, ASN116, LYS117, ASP119, LEU120, ALA146 and LYS147. The calculated cavity volume is 1013 Å³, with the predicted centre located at (9, 34, 20).

The conformer exhibits five conventional hydrogen bond interactions (Figure 10), the nitrogen atom (N) for each of **GLY15**, **LYS16**, **THR35**, **GLY60** and **GLN61** residues act as hydrogen bonds donor to the O1, O1, O2, O3 and O3 atoms of Isozaluzanin C at distances of 3.02 Å, 3.30 Å, 3.37Å, 3.14 Å and 3.08 Å, respectively.

In addition to the hydrogen bonding interactions, a hydrophobic alkyl interaction is observed between Isozaluzanin C and the **PRO34** residue at a distance of 4.52 Å.

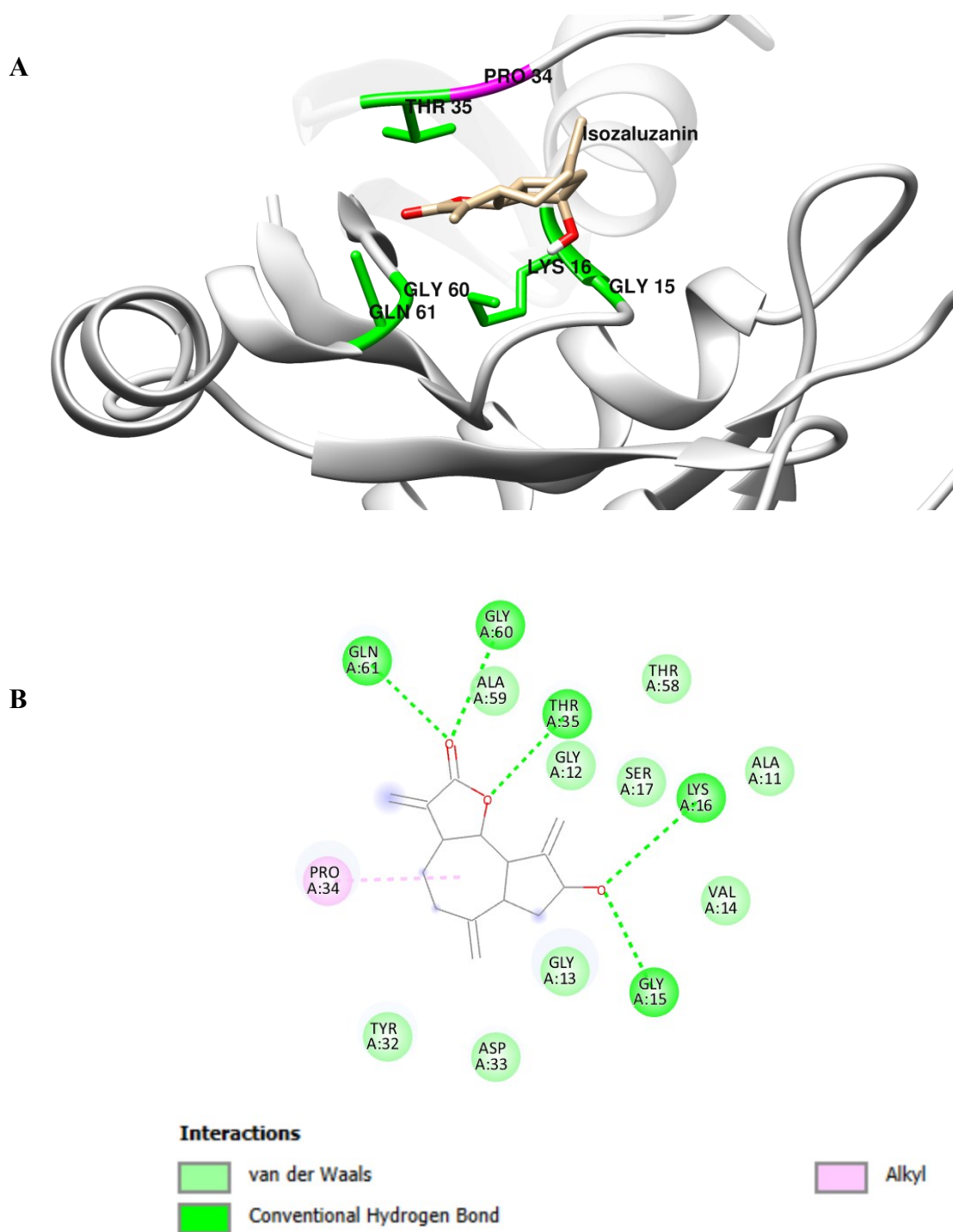


Figure 10. Interaction mode of Isozaluzanin C and NRAS

A) Three-dimensional model; B) Two-dimensional model

1.1.5 Study of Zaluzanin C interactions with NRAS

The Zaluzanin C-NRAS complex analysis reveals a predicted binding energy value equal to **-8.2 kcal/mol** for a favourable binding pose.

Zaluzanin C resides within the first binding pocket of the NRAS protein composed of ALA11, GLY12, GLY13, VAL14, GLY15, **LYS16**, SER17, ALA18, PHE28, VAL29, ASP30, GLU31, TYR32, ASP33, **PRO34**, **THR35**, ASP57, THR58, ALA59, **GLY60**, **GLN61**, TYR64, ASN116, LYS117, ASP119, LEU120, SER145, ALA146 and LYS147. The calculated pocket volume is 1013 Å³, with the predicted binding pocket centre located at (9, 34, 20).

In the binding pocket (Figure 11), Zaluzanin C forms four conventional hydrogen bonds. The nitrogen atom (N) for each of **LYS16**, **THR35**, **GLY60**, and **GLN61** residues act as hydrogen bonds donor to the O1, O2, O3 and O3 atoms of Zaluzanin C at distances of 3.27 Å, 3.37 Å, 3.16 Å and 3.09 Å, respectively.

This complex also exhibits one hydrophobic alkyl interaction between Zaluzanin C and the **PRO34** at a distance of 4.54 Å.

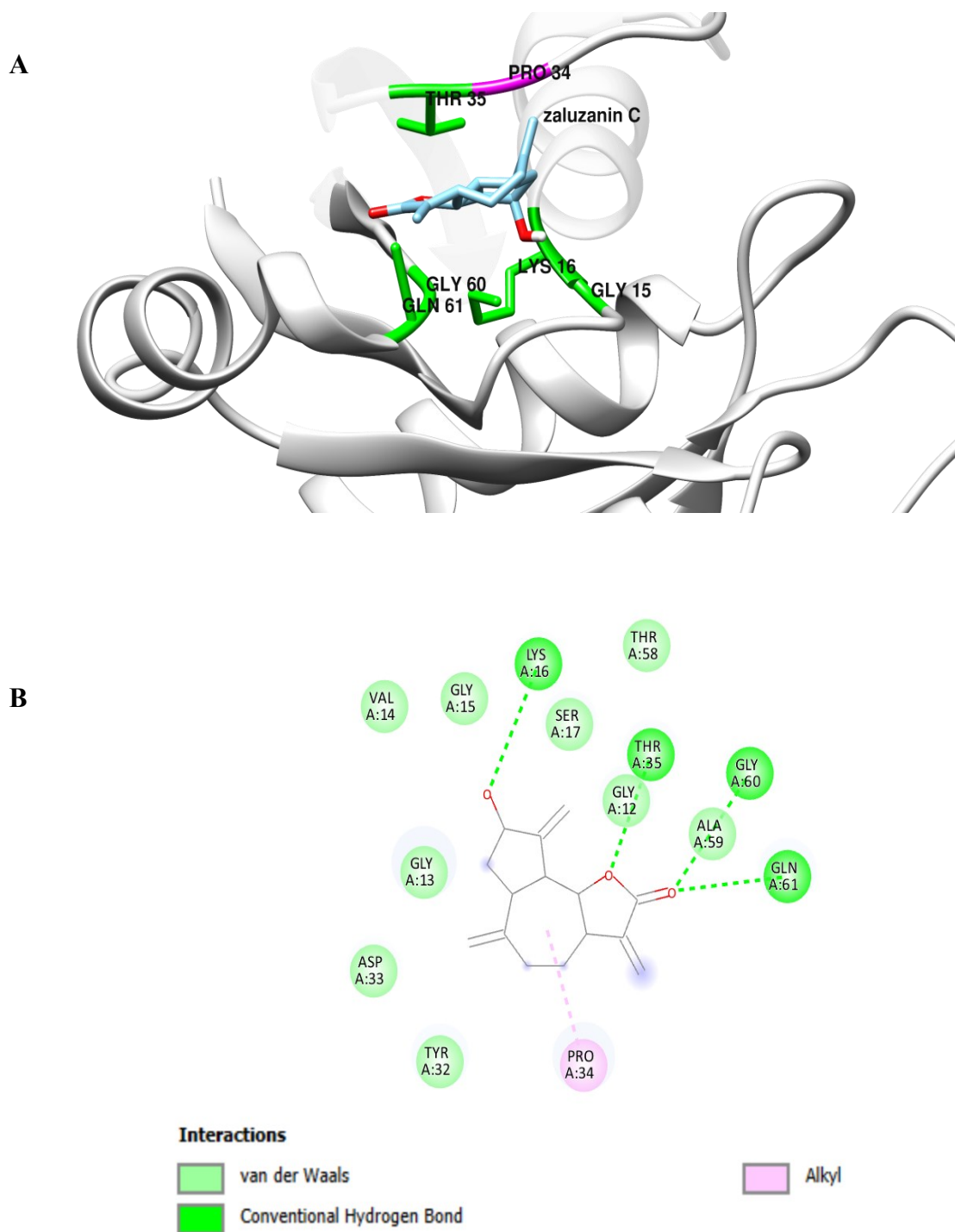


Figure 11. Interaction mode of Zaluzanin C and NRAS

A) Three-dimensional model; B) Two-dimensional model

1.1.6 Study of Costunolide interactions with NRAS

The Costunolide -NRAS complex analysis reveals a predicted binding energy value equalling **-7.0 kcal/mol**, for favourable binding pose.

Costunolide binds in the NRAS pocket (Figure 12), surrounded by the amino acids GLY12, GLY13, VAL14, GLY15, **LYS16**, **SER17**, **ALA18**, PHE28, **VAL29**, ASP30, GLU31, **TYR32**, ASP33, PRO34, THR35, ASP57, THR58, ASN116, LYS117, ASP119, LEU120, SER145, ALA146 and LYS147. The calculated pocket volume is 1013 Å³, with the predicted centre located at (9, 34, 20).

The binding of Costunolide to NRAS involves a network of hydrogen bonding and hydrophobic interactions. Four conventional hydrogen bonds are observed between Costunolide and the NRAS protein. The nitrogen atom (N) of **LYS16** forms a hydrogen bond with the O2 atom of Costunolide at a distance of 3.03 Å. The nitrogen atom (N) of **SER17** participates in two hydrogen bonds with the O1 and O2 atoms of Costunolide, with distances of 3.24 Å and 3.04 Å, respectively. Additionally, the OG atom of **SER17** acts as a hydrogen bond donor to the O1 atom of Costunolide, with a distance of 2.86 Å.

In addition to the hydrogen bonding interactions, several hydrophobic contacts are observed. Two alkyl interactions are predicted between Costunolide and the **ALA18** residue at distances of 5.33 Å and 3.95 Å. Another alkyl interaction is formed between the C15 atom of Costunolide and the **VAL29** residue at a distance of 4.05 Å. Furthermore, a pi-alkyl interaction is evident between the aromatic ring of **TYR32** and the C1 atom of Costunolide at a distance of 4.71 Å.

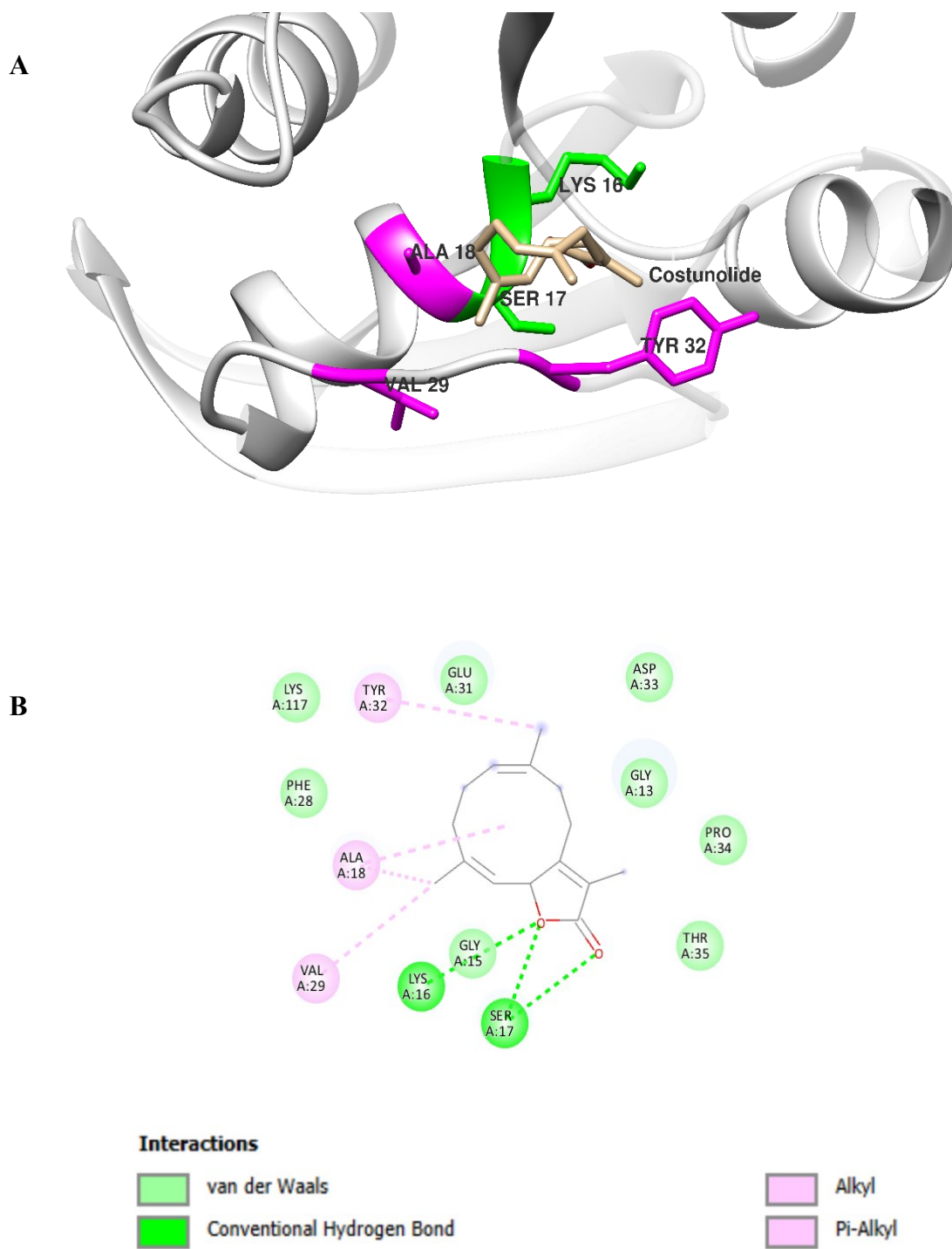


Figure 12. Interaction mode of Costunolide and NRAS

A) Three-dimensional model; B) Two-dimensional model

1.1.7 Study of Arbusculin A interactions with NRAS

The most favourable binding mode of Arbusculin A-NRAS complex exhibits a predicted binding energy value **-7.0 kcal/mol**.

Arbusculin A docks into a cavity with a calculated volume of 1013 Å³ and coordinates (x, y, z): 09,34,20, surrounded by the following residues: GLY12, GLY13, VAL14, GLY15, LYS16, SER17, **ALA18**, ILE21, **PHE28**, **VAL29**, ASP30, GLU31, TYR32, ASP33, PRO34, **THR35**, ASP57, THR58, GLY60, ASN116, LYS117, ASP119, LEU120 and LYS147.

The binding of Arbusculin A to the NRAS protein involves hydrogen bonding and hydrophobic interactions. Two conventional hydrogen bonds are observed. The O1 atom of Arbusculin A acts as a hydrogen bond acceptor, forming conventional hydrogen bonds with the nitrogen (N) and the OG1 atom of **THR35** at distances of 2.95 Å and 2.96 Å, respectively (Figure 13).

Several hydrophobic interactions contribute to the binding. Three alkyl interactions are present, involving the **ALA18** residue with distances of 4.64 Å and 4.09 Å, and the **VAL29** residue with a distance of 4.85 Å. Furthermore, a pi-alkyl interaction is possible between the aromatic ring of **PHE28** and Arbusculin A, with a distance of 5.41 Å.

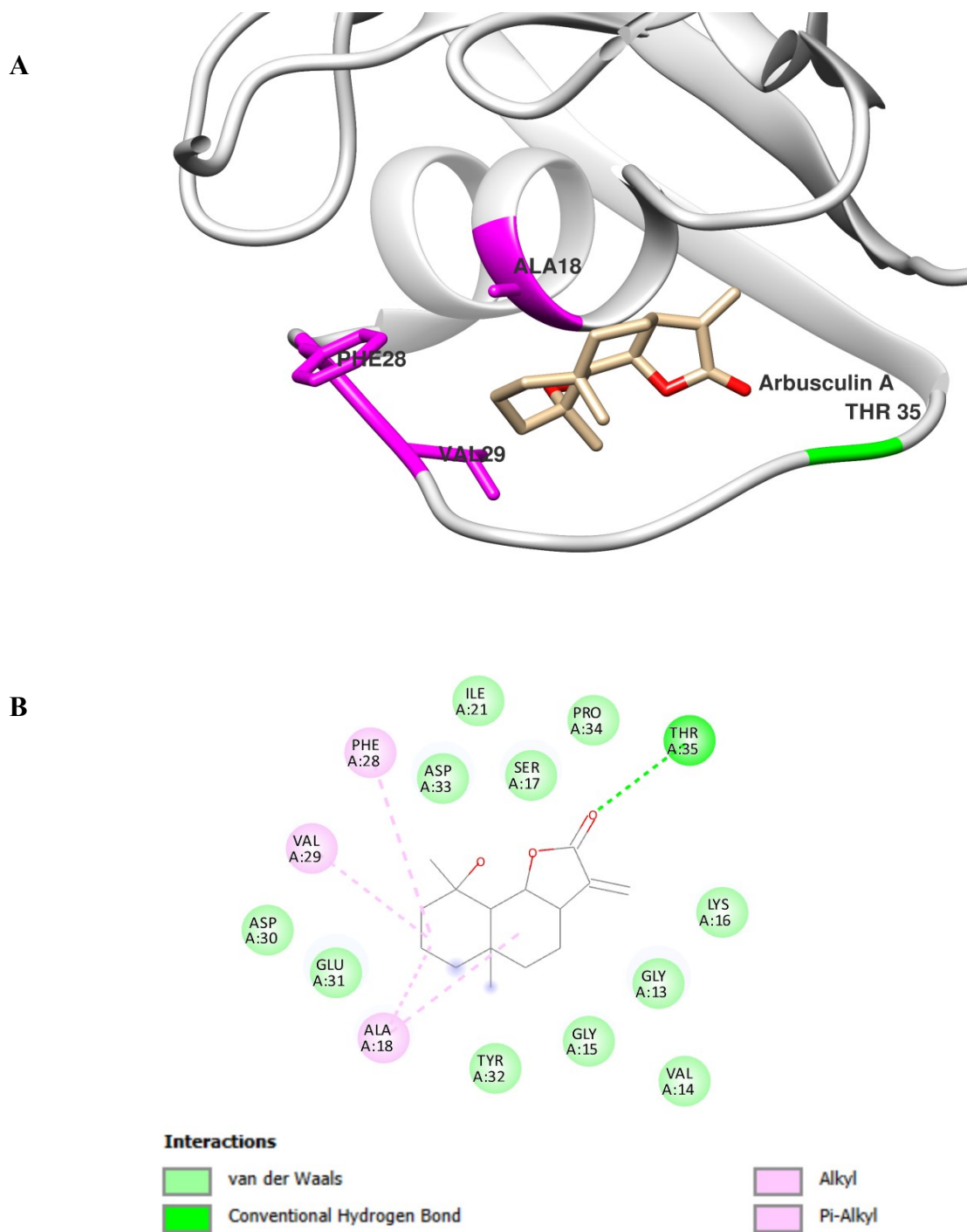


Figure 13. Interaction mode of Arbusculin A and NRAS

A) Three-dimensional model; B) Two-dimensional model

1.1.8 Study of Reynosin interactions with NRAS

The top-ranked binding mode of Reynosin binds to NRAS with a predicted binding energy of **-6.7 kcal/mol**.

The Reynosin occupies a binding pocket with a volume of 1013 Å³ with the predicted binding pocket centre located at (9, 34, 20). Including the subsequent amino acids: GLY12, **GLY13**, VAL14, GLY15, LYS16, SER17, **ALA18**, PHE28, VAL29, ASP30, GLU31, TYR32, ASP33, PRO34, THR35, ASN85, ASN116, LYS117, ASP119, LEU120, ALA146 and LYS147.

The binding of Reynosin to the NRAS protein involves two key interactions. A conventional hydrogen bond is formed between the nitrogen atom (N) of **GLY13** and the O3 atom of Reynosin, with a distance of 3.05 Å. Additionally, a hydrophobic alkyl interaction is observed between ligand and the **ALA18** residue, with a distance of 4.93 Å (Figure 14).

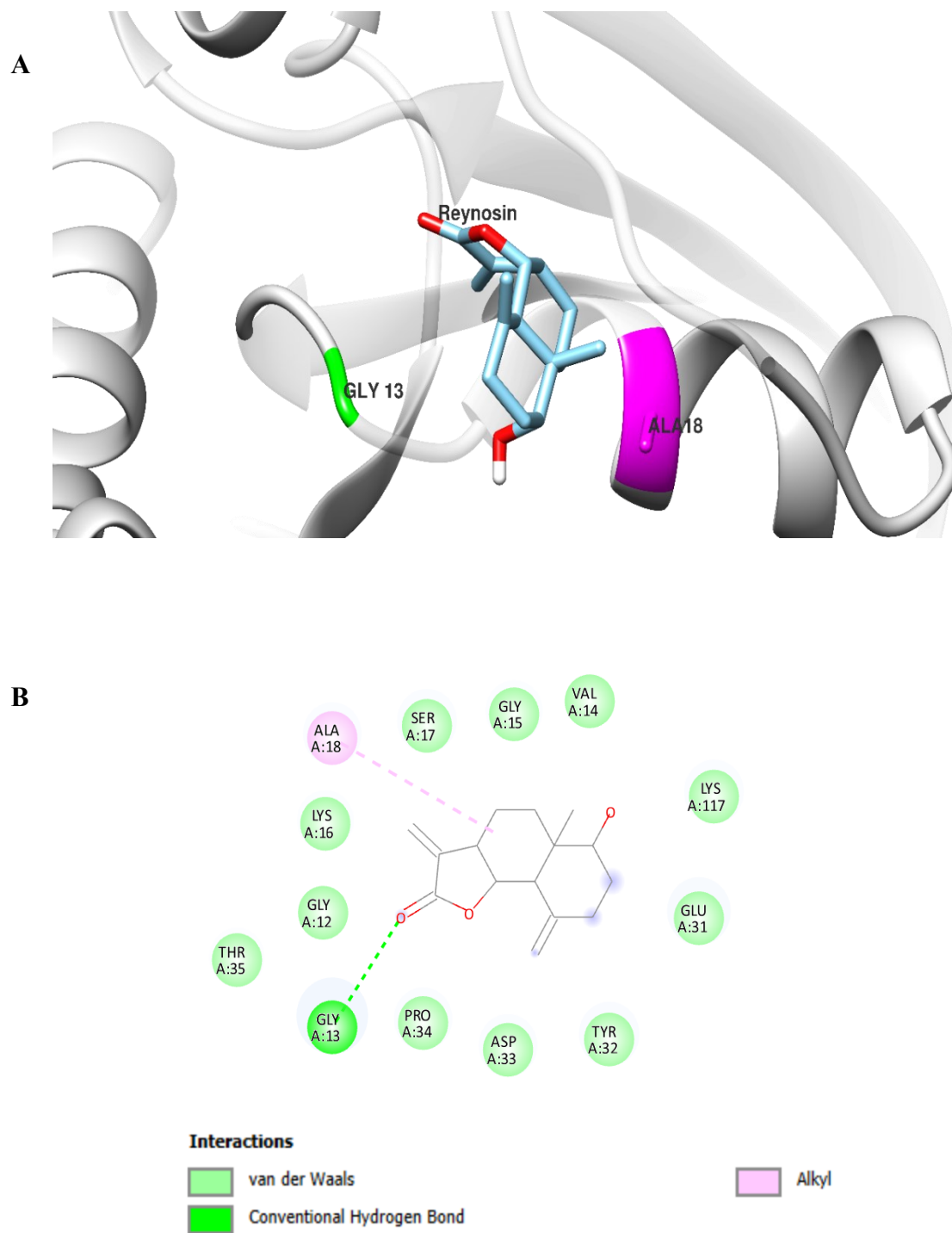


Figure 14. Interaction mode of Reynosin and NRAS

A) Three-dimensional model; B) Two-dimensional model

1.1.9 Study of Santamarin interactions with NRAS

The Santamarin-NRAS complex exposes a predicted binding energy of **-7.1 kcal/mol** in the best pose.

The binding pocket is composed of the following residues: ALA11, GLY12, GLY13, VAL14, GLY15, LYS16, SER17, **ALA18**, **PHE28**, VAL29, ASP30, GLU31, TYR32, ASP33, PRO34, THR35, ASN116, **LYS117**, ASP119, LEU120, SER145, ALA146 and LYS147. The calculated cavity volume is 1013 Å³, with a predicted centre located at coordinates (9, 34, 20).

Regarding the hydrophobic interactions, an alkyl interaction is identified between the **ALA18** residue and the Santamarin ligand, with a distance of 4.85 Å. Another alkyl interaction is observed between the **LYS117** residue and the Santamarin ligand, with a distance of 4.66 Å. Additionally, **PHE28** residue contribute to the establishment of a pi-alkyl interaction with a distance of 4.99Å (Figure 15).

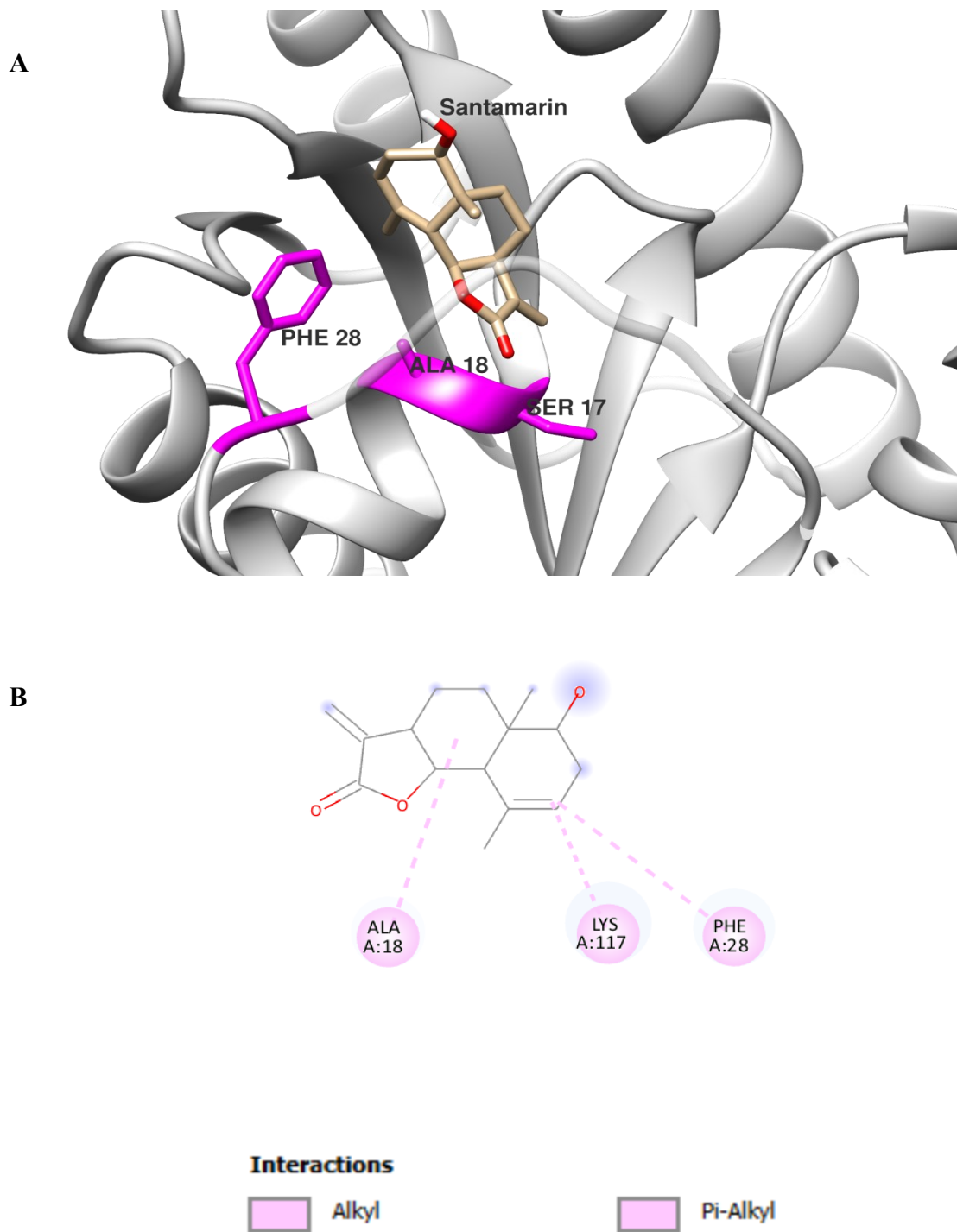


Figure 15. Interaction mode of Santamarin and NRAS

A) Three-dimensional model; B) Two-dimensional model

1.1.10 Study of α -cyclocostunolide interactions with NRAS

The α -cyclocostunolide-NRAS complex analysis displays a predicted binding energy of **-7.3 kcal/mol** for the best binding mode.

Alpha-cyclocostunolide resides within a binding pocket composed of ALA11, GLY12, GLY13, VAL14, GLY15, LYS16, **SER17**, **ALA18**, ILE21, PHE28, **VAL29**, ASP30, GLU31, TYR32, ASP33, PRO34, **THR35**, ASN85, ASN116, LYS117, ASP119, LEU120, SER145, ALA146 and LYS147. The calculated cavity volume is 1013 Å³, with the predicted centre located at coordinates (9, 34, 20).

The binding of α -cyclocostunolide to the NRAS protein (Figure 16) involves the formation of several hydrogen bonding and hydrophobic interactions. Three conventional hydrogen bonds are observed. The OG atom of **SER17** acts as a hydrogen bond donor to the O1 atom of α -cyclocostunolide at a distance of 3.21 Å. The nitrogen (N) and the OG1 atoms of **THR35** form hydrogen bonds with the O1 atom of α -cyclocostunolide at distances of 3.23 Å and 2.70 Å, respectively.

Furthermore, two hydrophobic alkyl interactions contribute to stabilising the binding. One interaction is present between α -cyclocostunolide and the **ALA18** residue, with a distance of 3.97 Å. Another alkyl interaction is observed between α -cyclocostunolide and the **VAL29** residue at a distance of 4.62 Å.

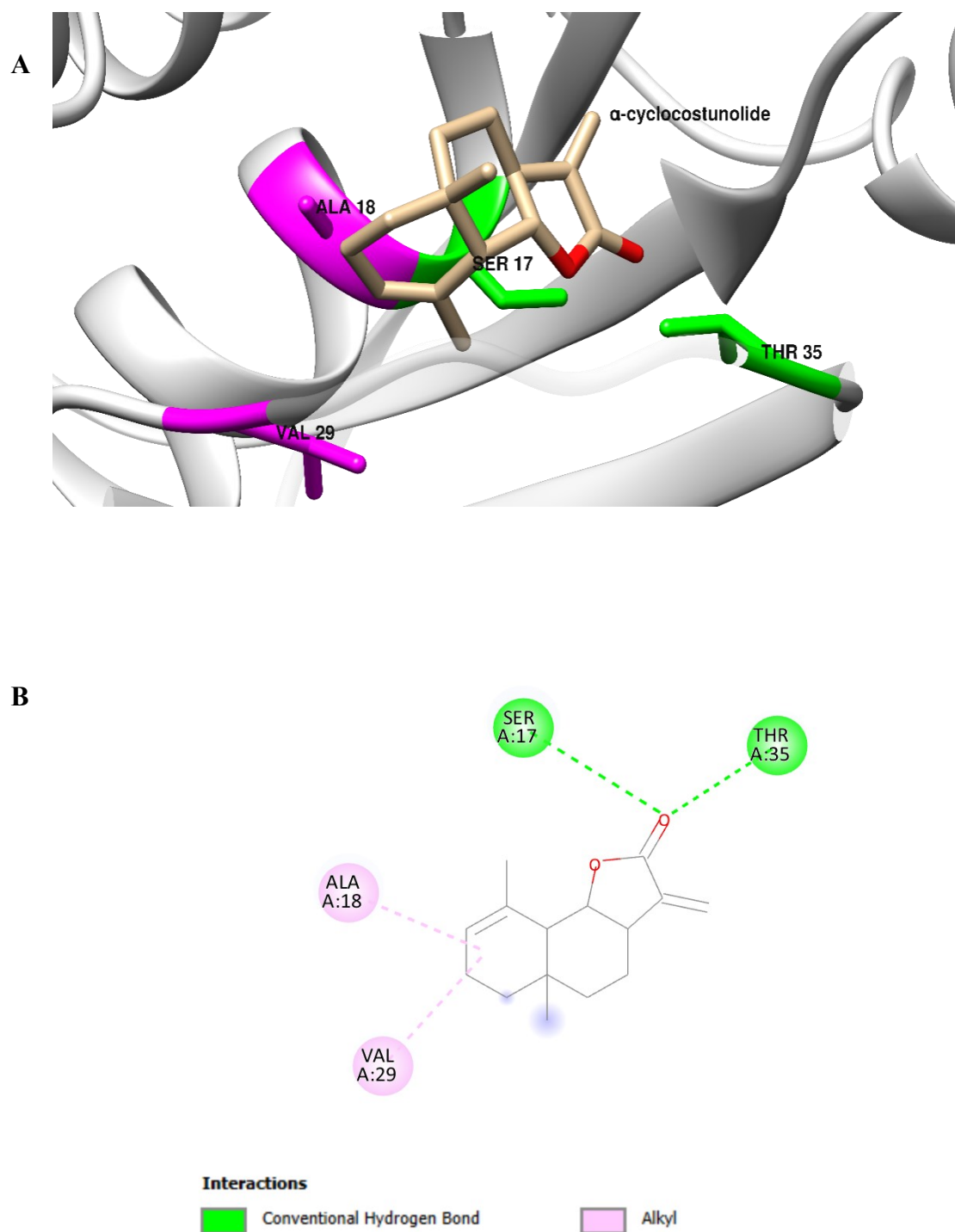


Figure 16. Interaction mode of α -cyclocostunolide and NRAS

A) Three-dimensional model; B) Two-dimensional model

Molecular docking and visual analysis of SLs in association with the NRAS protein have identified these plant-derived molecules as potential inhibitors of this oncogenic GTPase.

The reference ligand, Phosphoaminophosphonic acid guanylate ester (GNP), is the non-hydrolysable analogue of GTP, exhibited a high binding energy of **-12.0 kcal/mol**, forming an extensive network of interactions, including 14 conventional hydrogen bonds, 3 carbon-hydrogen bonds, and various hydrophobic contacts such as pi-cation, pi-pi T-shaped, and pi-alkyl interactions with key residues like GLY13, VAL14, **GLY15**, **LYS16**, SER17, ALA18, **THR35**, **GLY60**, ASN116, LYS117, ALA146, LYS147 and PHE28.

Lappadilactone (compound 1), Isozaluzanin C (compound 3), and Zaluzanin C (compound 4) seemed to be the most promising candidates among the assessed SLs, displaying binding energies of **-10.1 kcal/mol**, **-8.2 kcal/mol** and **-8.2 kcal/mol**, respectively. Lappadilactone formed two conventional hydrogen bonds with SER17 and ALA18, as well as a hydrophobic alkyl interaction with PRO34. Isozaluzanin C exhibited the highest number of conventional hydrogen bonds among the SLs, forming five bonds with residues such as **GLY15**, **LYS16**, **THR35**, **GLY60** and GLN61, as well as a hydrophobic alkyl interaction with PRO34. Compared to Zaluzanin C, Isozaluzanin C outperformed by forming an additional conventional hydrogen bond facilitated by the hydroxyl group in the planar conformation. Conversely, the hydroxyl group perpendicular to the plane in Zaluzanin C did not contribute to another hydrogen bond formation. Although both showed similar binding energy values.

The other SLs: Dehydrocostus lactone, Costunolide, Arbusculin A, Reynosin, Santamarin, and α -cyclocostunolide, showed varying degrees of binding affinity (Figure 17) and interactions. While some compounds formed fewer or no hydrogen bonds, they exhibited a number of hydrophobic interactions, particularly alkyl and pi-alkyl interactions, which contributed to the overall stability of the complexes.

With minor variations, SLs and the reference ligand GNP generally share the same binding pocket and key interacting residues on NRAS. Similar cavity volumes and binding pocket centres suggest a common NRAS binding site.

Overall, the molecular docking studies and interaction analyses indicate that lappadilactone, Isozaluzanin C and Zaluzanin C are the most promising sesquiterpene lactone compounds for

targeting NRAS based on their favourable binding energies and significant number of favourable interactions.

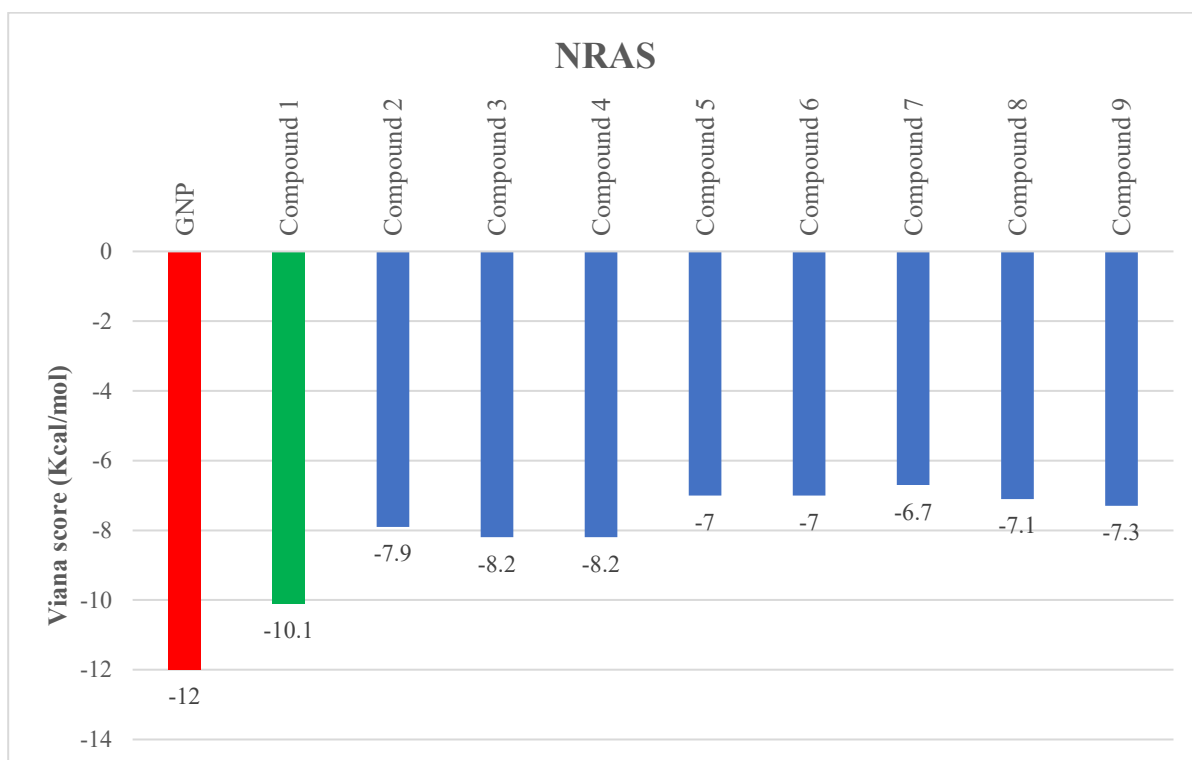


Figure 17. Binding energy of SLs-NRAS complexes

1.2 Interaction mode between SLs and BRAF

1.2.1 Study of the V1Y interactions with the protein BRAF (Redocking the reference)

The reference ligand Belvarafenib (V1Y) in complex with Serine–threonine protein kinase BRAF protein reveal the best binding mode exposes a predicted binding energy equal to **-12.8 kcal/mol**.

The binding pocket of the V1Y-BRAF complex, with a calculated cavity volume of 2727 Å³ and predicted location centred at -2, 13, and 12 in terms of x, y and z coordinates, respectively, includes the following residues: ILE463, GLY464, SER465, **VAL471**, **ALA481**, VAL482, **LYS483**, **GLU501**, VAL504, **LEU505**, **ILE513**, **LEU514**, ILE527, VAL528, **THR529**, GLN530, **TRP531**, **CYS532**, SER535, SER536, LYS539, LEU567, HIS574, ASN580, PHE583, ILE592, GLY593, **ASP594**, **PHE595**, GLY596, LEU597, THR599 and VAL600.

The binding of V1Y to BRAF (Figure 18) is characterized by an extensive network of interactions; a total of four conventional hydrogen bonds are observed. The nitrogen atom of **CYS532** acts as a hydrogen bond donor to the N18 atom of V1Y at a distance of 3.35 Å. The nitrogen atom of **ASP594** forms a hydrogen bond with the N23 atom of V1Y at a distance of 2.95Å.

In addition, the N20 atom of V1Y forms a hydrogen bond with the oxygen atom of **CYS532** at a distance of 3.22 Å, while the N25 atom of V1Y forms a hydrogen bond with the OE2 atom of **GLU501** at a distance of 3.09 Å.

A halogen interaction is also observed, with the N23 atom of V1Y interacting with the F32 atom of V1Y at a distance of 3.05 Å. Furthermore, the NZ atom of **LYS483** forms a pi cation interaction with the aromatic ring of V1Y at a distance of 4.14 Å, coupled with a pi donor hydrogen bond between the N20 atom of V1Y and the aromatic ring of **TRP531** at a distance of 3.85 Å.

Multiple hydrophobic interactions contribute to binding, there is a pi-sigma interaction between the CG2 atom of **THR529** and V1Y at a distance of 3.75 Å. Pi-sulphur interaction is observed between the S13 atom of V1Y and the aromatic ring of **PHE595** at a distance of 5.64 Å.

In addition, three sets of pi-pi stacking interactions are evident involving the aromatic rings of V1Y and **TRP531** with distances between 4.37 Å and 5.58 Å. There are also two pi-pi-T-shaped interactions with distances of 4.79 Å and 5.47 Å between the aromatic rings of V1Y and **PHE595**.

Furthermore, the complex exhibits several hydrophobic alkyl and pi-alkyl interactions. The CL33 atom of V1Y forms an alkyl interaction with **ILE513** at a distance of 4.76 Å, pi-alkyl interactions are observed between V1Y and residues **VAL471**, **ALA481** (two interactions), **LYS483**, **LEU505**, **LEU514**, and **CYS532**, with distances ranging from 4.39 Å to 5.41 Å.

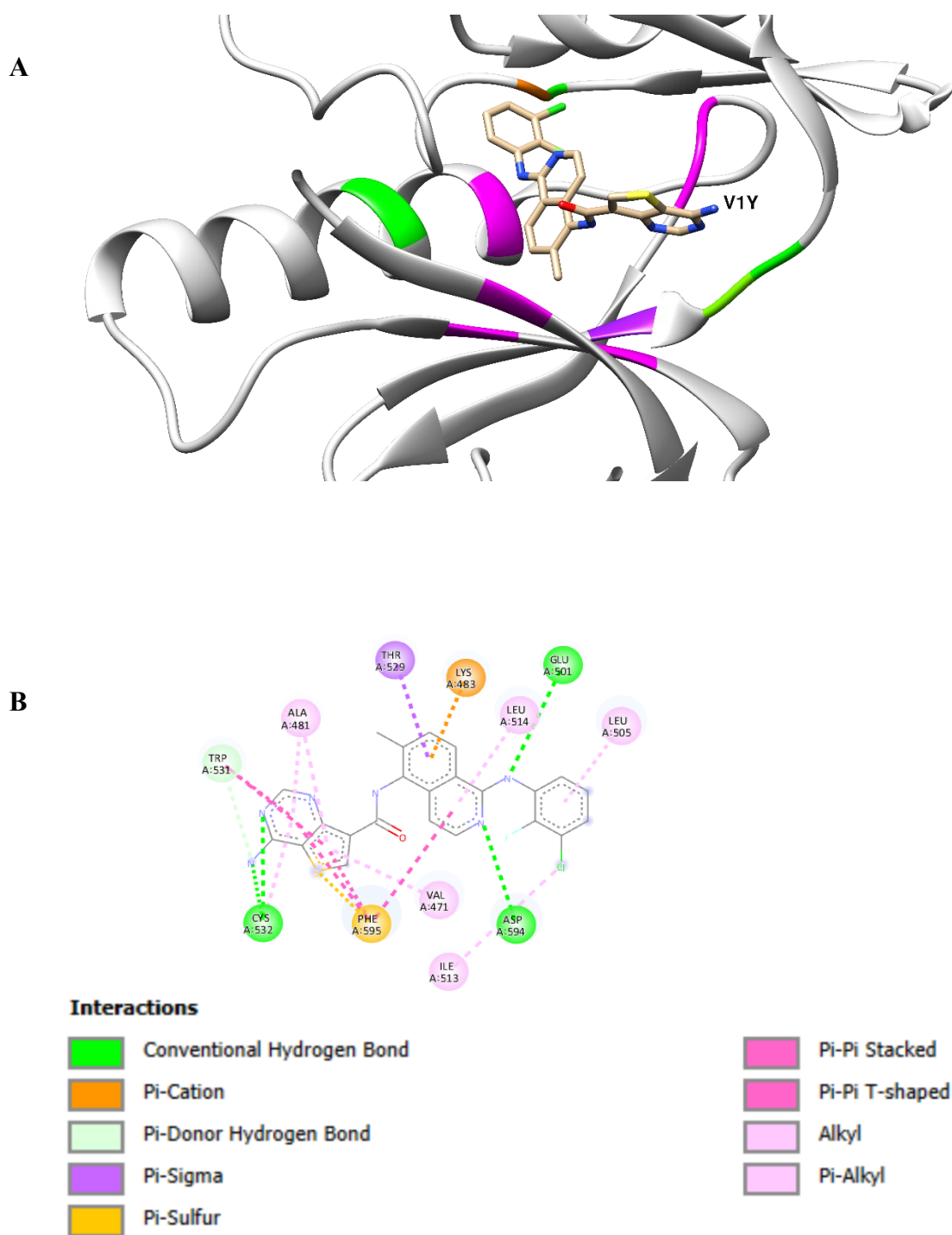


Figure 18. Interaction mode of V1Y and BRAF

A) Three-dimensional model; B) Two-dimensional model

1.2.2 Study of lappadilactone interactions with BRAF

The results of molecular docking and visual analysis show that the conformer of Lappadilactone binds to Serine–threonine protein kinase BRAF (PDB: 6XFP) with the best predicted binding energy equal to **-9.1 kcal/mol**.

The pose interacts with the protein in a position surrounded by the following residues: ILE463, GLY464, SER465, **VAL471**, **ALA481**, LEU514, THR529, GLN530, **TRP531**, CYS532, GLY534, SER535, SER536, LYS539, LYS578, ASN580, ASN581, PHE583, PHE595, **GLY596**, **THR599**, VAL600, LYS601 and SER614, in a cavity characterised by a volume of 2727 Å³ and centre coordinates (x, y, z): -2, 13, 12.

The complex (Figure 19) displays one conventional hydrogen bonds between Lappadilactone and 6XFP: the **THR599** residue forms a connection between its OG1 atom and the oxygen atom (O) of Lappadilactone at a distance of 2.73 Å. the **GLY596** amino acid residue forms a carbon hydrogen bond between its CA atom and the oxygen atom of Lappadilactone at a distance of 3.55 Å.

In addition to hydrogen bonds, the formation of four hydrophobic bonds of alkyl and pi-alkyl interactions type, including **VAL471**, **ALA481**, **TRP531**, and **PHE595** with distances ranging from 4.33 to 5.25 Å, increases the stability of the binary complex between lappadilactone and BRAF.

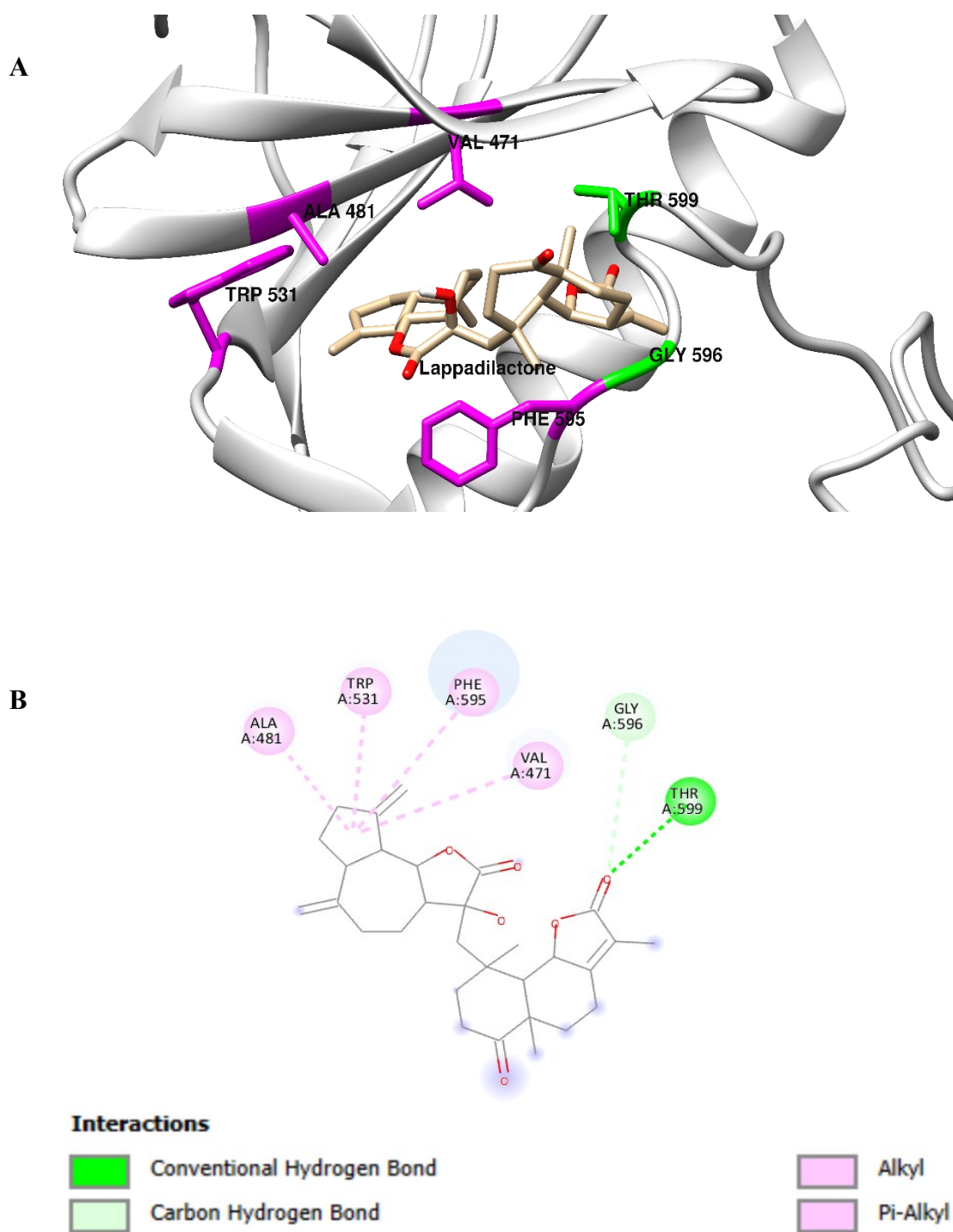


Figure 19. Interaction mode of Lappadilactone and BRAF

A) Three-dimensional model; B) Two-dimensional model

1.2.3 Study of Dehydrocostus lactone interactions with BRAF

The top-ranked binding mode of Dehydrocostus lactone with Serine–threonine protein kinase BRAF (PDB: 6XFP), shows a predicted binding energy of **-8.9 kcal/mol**.

According to the molecular docking study and visual analysis, The Dehydrocostus lactone binds to a pocket formed by the following residues: ILE463, GLY464, **VAL471**, **ALA481**, LYS483, ALA497, ASN500, GLU501, VAL504, LEU505, THR508, ILE513, LEU514, **THR529**, GLN530, **TRP531**, **CYS532**, LEU567, SER571, ILE572, ILE573, HIS574, ARG575, **PHE583**, ILE592, GLY593, ASP594, **PHE595**, LEU597, THR599, ARG603, TRP604 and SER605 in a space of 2727 Å³ and a centre at coordinates (x, y, z): 18, 27, 18.

Dehydrocostus lactone resides in a cavity within the BRAF protein (Figure 20), forming one conventional hydrogen bond with the OG1 atom of the **THR529** residue and the oxygen atom of the ligand at a distance of 3.25 Å.

Four alkyl and four Pi-Alkyl hydrophobic interactions involve **VAL471**, **ALA481**, **CYS532**, **TRP531**, **PHE583** and **PHE595** residues acting as donors to alkyl and pi-alkyl moieties, with distances ranging from 4.11 Å to 5.33 Å.

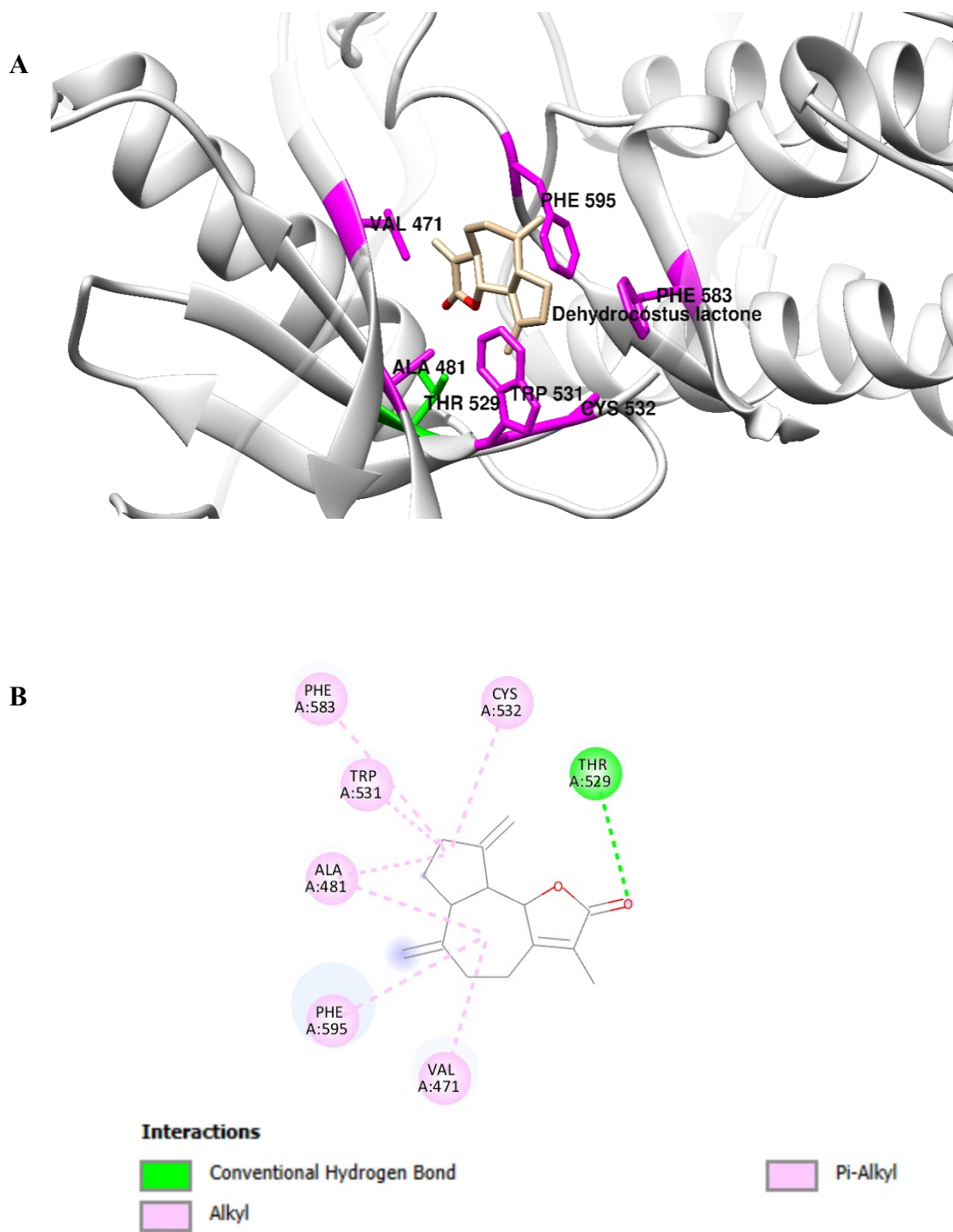


Figure 20. Interaction mode of Dehydrocostus lactone and BRAF

A) Three-dimensional model; B) Two-dimensional model

1.2.4 Study of Isozaluzanin C interactions with BRAF

The Isozaluzanin C-BRAF complex analysis reveals a predicted binding energy equal to **-8.3 kcal/mol**, for favourable binding pose.

Isozaluzanin C resides within the binding pocket of the BRAF protein composed of GLY464, **VAL471**, ALA481, LYS483, ALA497, ASN500, GLU501, VAL504, LEU505, THR508, ILE513, LEU514, THR529, GLN530, **TRP531**, **CYS532**, LEU567, SER571, ILE572, ILE573, HIS574, ARG575, PHE583, ILE592, GLY593, **ASP594**, **PHE595**, LEU597, THR599, ARG603, TRP604 and SER605. The calculated cavity volume is 2727 Å³, with the predicted centre located at (-2, 13, 12).

The complex (Figure 21) exhibits three hydrogen bond interactions, two of them are conventional hydrogen bond, **CYS532** acts as a hydrogen bond donor to Isozaluzanin C at a distance of 3.17 Å. While, **ASP594** acts as a hydrogen bond receptor from H16 Isozaluzanin C atom at a distance of 2.42 Å. The third interaction is a carbon hydrogen bond connect between the CA of **TRP531** atom and the O3 atom of the ligand Isozaluzanin C.

Furthermore, the complex demonstrates two alkyl and pi-alkyl hydrophobic interactions contributing to its stability: contacts with **VAL471**, and **PHE595** residues at distances of 4.82Å and 4.67 Å, respectively.

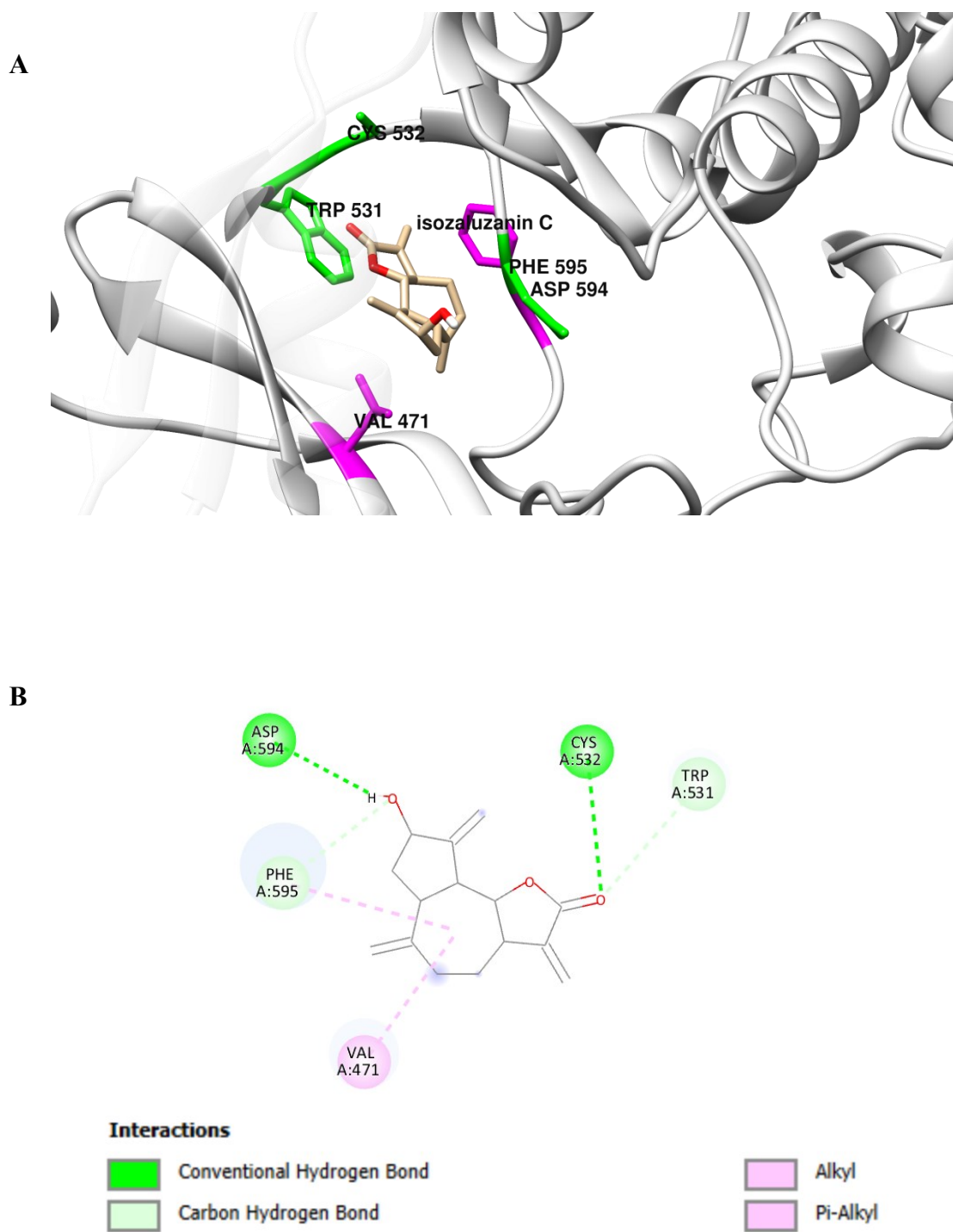


Figure 21. Interaction mode of Isozaluzanin C and BRAF

A) Three-dimensional model; B) Two-dimensional model

1.2.5 Study of Zaluzanin C interactions with BRAF

The Zaluzanin C-BRAF complex analysis reveals a binding energy estimated to **-8.3 kcal/mol**, for a favourable binding pose.

Zaluzanin C resides within the binding pocket of BRAF protein composed of ILE463, GLY464, VAL471, TYR472, ALA481, VAL482, LYS483, ALA497, ASN500, GLU501, VAL504, LEU505, THR508, ILE513, LEU514, ILE527, THR529, GLN530, **TRP531**, **CYS532**, GLU533, GLY534, SER535, SER536, LYS539, LEU567, ILE572, ILE573, HIS574, ARG575, PHE583, ILE592, GLY593, **ASP594**, PHE595, GLY596, LEU597, THR599, ARG603 and TRP604. The calculated pocket volume is 2727 Å³ with the predicted centre located at (-2, 13, 12).

In binding pocket, Zaluzanin C forms two conventional hydrogen bonds. One is between the nitrogen atom of the **CYS532** residue and the O3 atom of Zaluzanin C, with a distance of 3.17 Å. The other is between the H16 atom of the ligand and the oxygen atom of the **ASP594** residue at a distance of 2.47 Å. Additionally, a carbon-hydrogen bond is observed between the CA atom of **TRP531** and the O3 atom of Zaluzanin C, at a distance of 3.45 Å.

This complex also exhibits two hydrophobic interactions: an alkyl interaction between Zaluzanin C and the side chain of **VAL471** at a distance of 4.80 Å, and a pi-alkyl interaction between Zaluzanin C and the aromatic ring of **PHE595** at a distance of 4.71 Å (Figure 22).

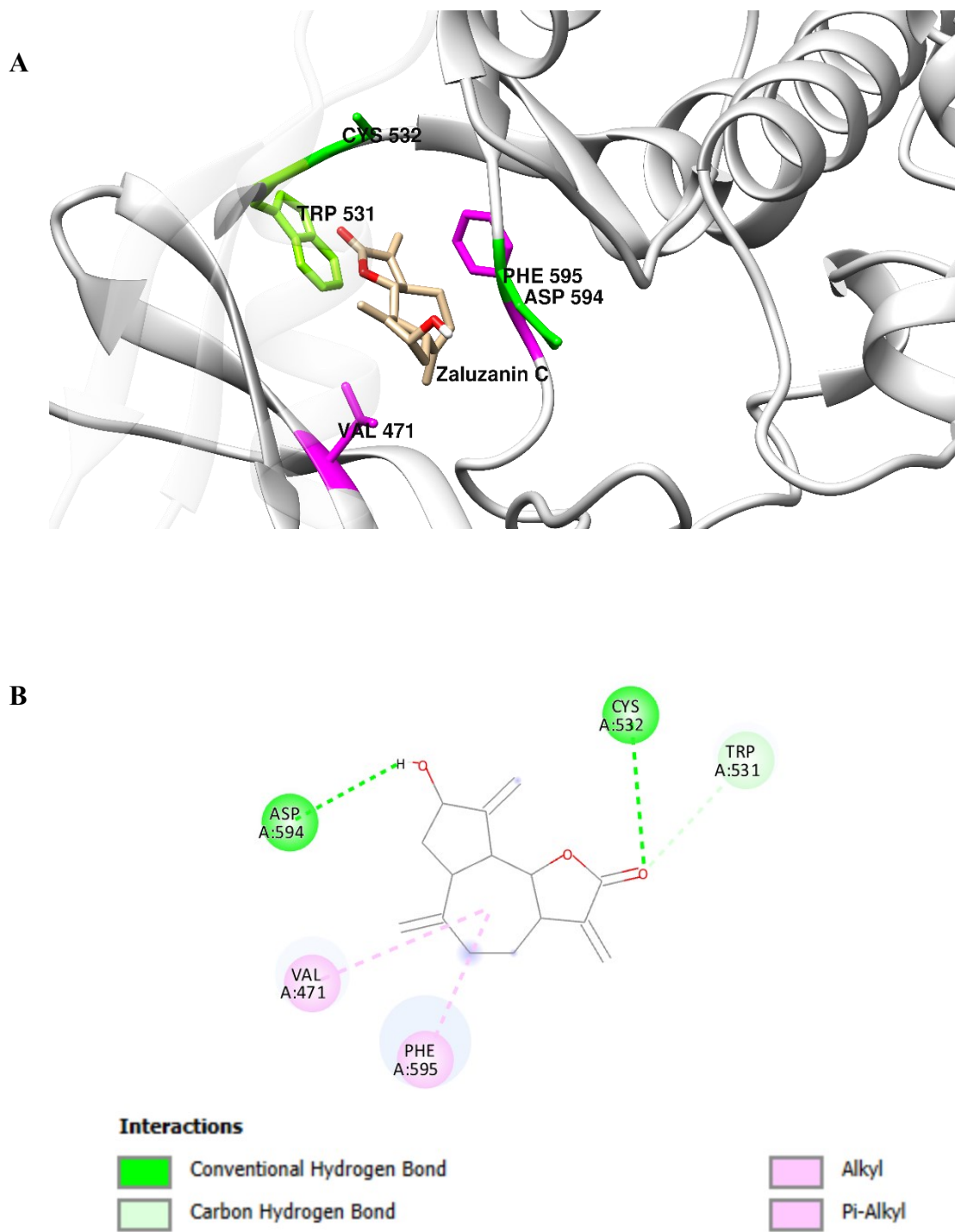


Figure 22. Interaction mode of Zaluzanin C and BRAF

A) Three-dimensional model; B) Two-dimensional model

1.2.6 Study of Costunolide interactions with BRAF

The Costunolide-BRAF complex analysis reveals a predicted binding energy value equalling **-8.2 kcal/mol**, for favourable binding pose.

Costunolide binds in the BRAF pocket, surrounded by the residues ILE463, GLY464, **VAL471**, ALA481, LYS483, ALA497, ASN500, GLU501, VAL504, LEU505, THR508, ILE513, LEU514, THR529, GLN530, TRP531, CYS532, GLY534, SER535, SER536, LYS539, LEU567, SER571, ILE572, ILE573, HIS574, ARG575, ASP576, ASN580, PHE583, ILE592, GLY593, ASP594, **PHE595**, GLY596, LEU597, THR599, VAL600, ARG603 and TRP604. The calculated pocket volume is 2727 Å³, with the predicted centre located at (-2, 13, 12).

The binding of Costunolide to BRAF forms four hydrophobic interactions, one hydrophobic alkyl interaction with the **VAL471** residue at a distance of 4.63 Å. Furthermore, three hydrophobic pi-alkyl interactions are formed by the **PHE595**, with the C1, C15 atoms, and the Costunolide moiety at distances of 4.24 Å, 5.12 Å, and 4.72 Å, respectively (Figure 23).

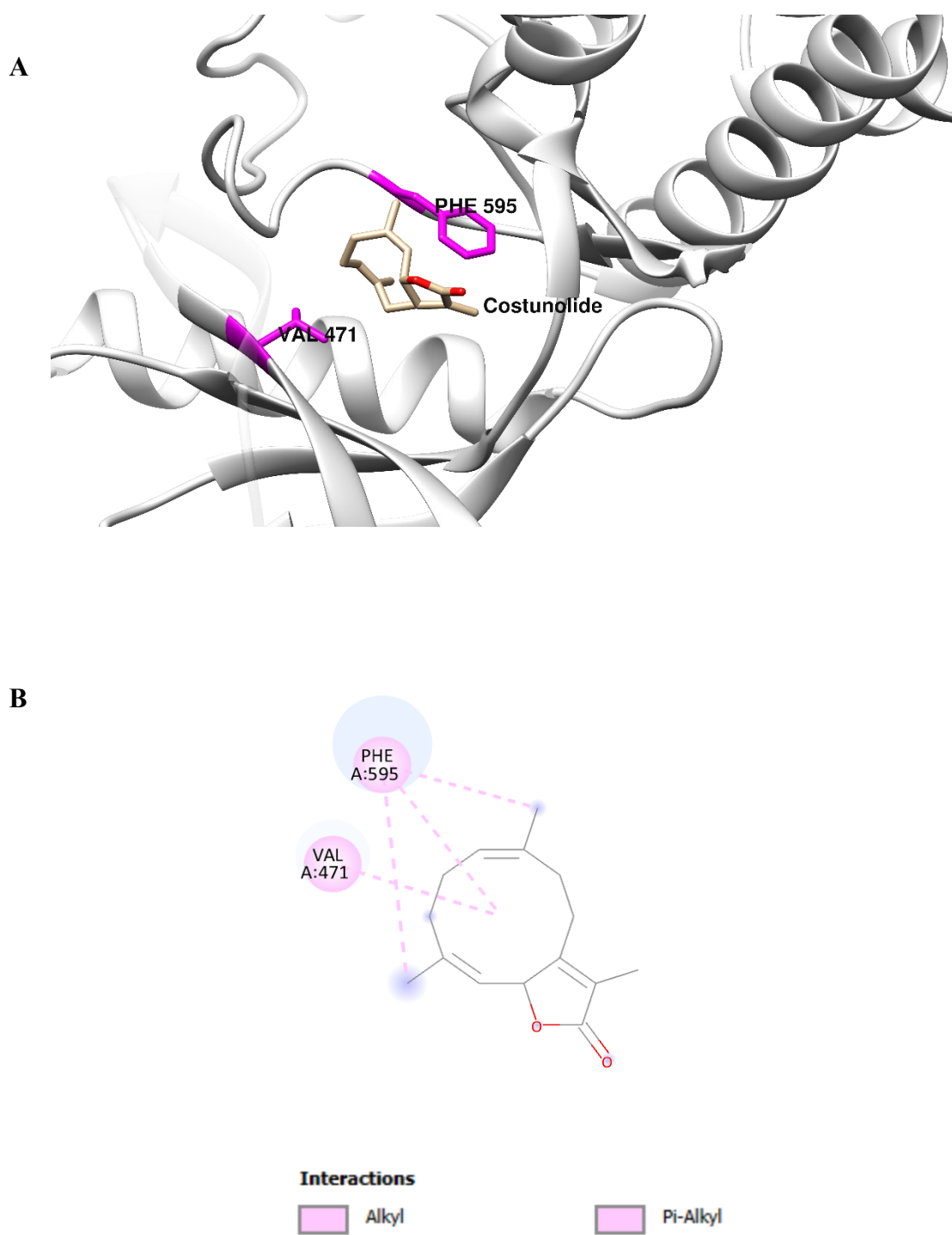


Figure 23. Interaction mode of Costunolide and BRAF

A) Three-dimensional model; B) Two-dimensional model

1.2.7 Study of Arbusculin A interactions with BRAF

the most favourable binding pose of Arbusculin A-BRAF complex exhibits a predicted binding energy value **-7.4 kcal/mol**.

Arbusculin A docks into a cavity with a calculated volume of 1334 Å³ and coordinates (x, y, z): -12, 14, 41, surrounded by the following residues: SER467, PHE468, LEU485, THR491, GLN493, GLN494, LEU495, ALA497, PHE498, ALA598, LYS601, SER602, **ARG603**, TRP604, **SER605**, HIS608 and **PHE610**.

A hydrogen bonding network of three conventional hydrogen bonds is observed between the Arbusculin A and the BRAF protein, involving: the **ARG603** interact with its NH1 atom with O1 atom of Arbusculin A at a distance of 3.03 Å. The oxygen atom of the side chain (OG) of **SER605** forms a hydrogen bond with the third oxygen atom (O3) of Arbusculin A at a distance of 2.65 Å. The H21 atom of Arbusculin A acts as a hydrogen bond donor to the backbone oxygen of **ARG603**, with a distance of 2.27 Å. Additionally, there is a carbon-hydrogen bond formed between the CD atom of **ARG603** and the O1 atom of Arbusculin A, with a distance of 3.19 Å.

Furthermore, two hydrophobic pi-alkyl interactions are present. One is between Arbusculin A and the aromatic ring of **PHE468** at a distance of 4.97 Å. The other is between the ligand and the aromatic ring of **PHE610** at a distance of 5.32 Å (Figure 24).

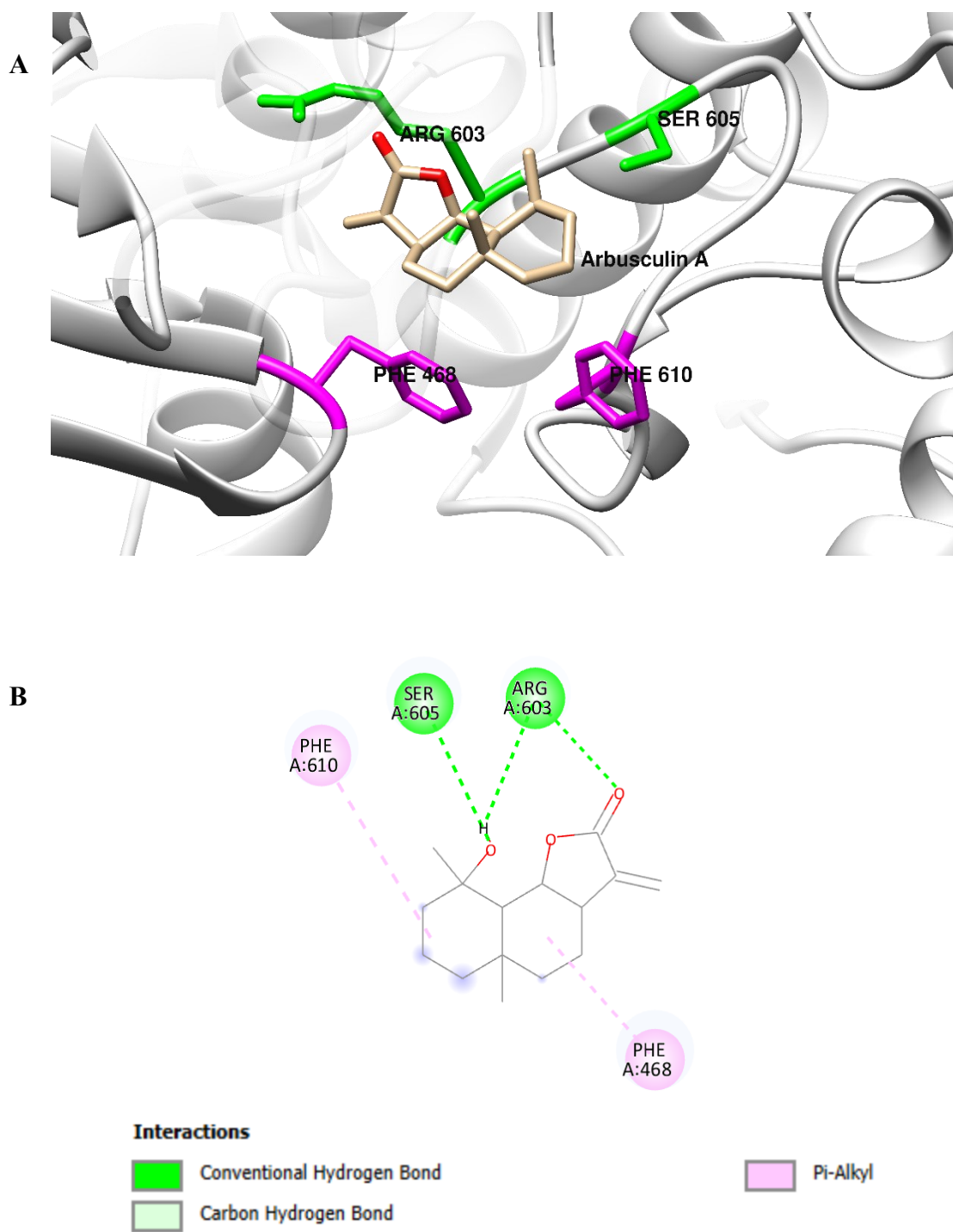


Figure 24. Interaction mode of Arbusculin A and BRAF

A) Three-dimensional model; B) Two-dimensional model

1.2.8 Study of Reynosin interactions with BRAF

The top-ranked binding mode of Reynosin binds to Serine–threonine protein kinase BRAF displays a predicted binding energy of **-6.6 kcal/mol**.

Reynosin occupies a binding pocket with a volume of 474 Å³ and the predicted binding pocket centre located at coordinates (-8, 4, 2). Including the subsequent amino acids: SER467, PHE468, LEU485, **THR491**, **GLN493**, **GLN494**, LEU495, **ALA497**, LYS601, SER602, **ARG603**, TRP604, **SER605**, HIS608 and PHE610.

The binding of Reynosin to BRAF protein involves four hydrogen bonds. Three of them are conventional hydrogen bonds. The oxygen atom OG1 of **THR491** side chain acts as a hydrogen bond donor to the O3 atom of Reynosin at a distance of 2.89 Å. The NE2 atom of **GLN494** forms a hydrogen bond with the O2 atom of Reynosin at a distance of 3.27 Å. The H18 atom of Reynosin acts as a hydrogen bond donor to the backbone oxygen of **GLN493** at a distance of 2.92 Å. Additionally, there is a carbon-hydrogen bond formed between the C12 atom of Reynosin and the oxygen atom OG1 of **SER605** at a distance of 3.71 Å.

Furthermore, two hydrophobic alkyl interactions are apparent between Reynosin and the BRAF protein residues. One is with the **ALA497** residue at a distance of 4.26 Å, and the other is with the **ARG603** residue at a distance of 4.82 Å (Figure 25).

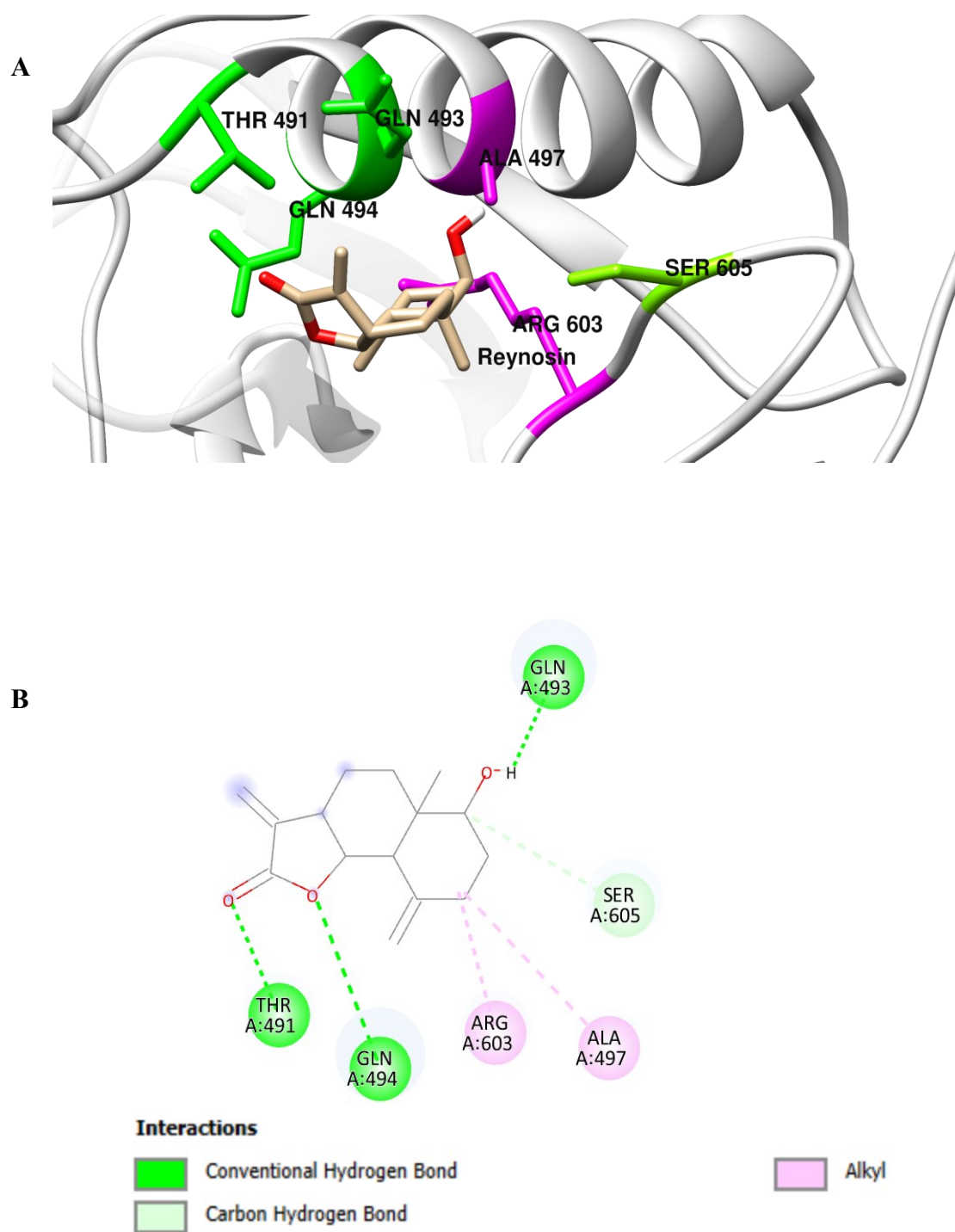


Figure 25. Interaction mode of Reynosin and BRAF

A) Three-dimensional model; B) Two-dimensional model

1.2.9 Study of Santamarin interactions with BRAF

The Santamarin-BRAF complex exposes a predicted binding energy of **-8.0 kcal/mol** in the best pose.

The binding pocket is composed of the following residues: ILE463, GLY464, VAL471, ALA481, VAL482, LYS483, ALA497, ASN500, GLU501, VAL504, LEU505, THR508, ILE513, **LEU514**, ILE527, VAL528, THR529, GLN530, TRP531, CYS532, GLY534, SER535, SER536, LYS539, LEU567, ILE572, ILE573, HIS574, ARG575, ASN580, PHE583, ILE592, GLY593, ASP594, **PHE595**, GLY596, LEU597, THR599, ARG603, TRP604 and GLY606. The calculated cavity volume is 2727 Å³, with the predicted centre located at coordinates (-2, 13, 12).

There are two hydrophobic interactions present into the complex Santamarin-BRAF, a pi-sigma interaction is identified between the C7 atom of the Santamarin ligand and the **PHE595** residue of the BRAF protein, with a distance of 3.46 Å. Additionally, an alkyl hydrophobic interaction is observed between the **LEU514** residue and the ligand, at a distance of 4.98 Å (Figure 26).

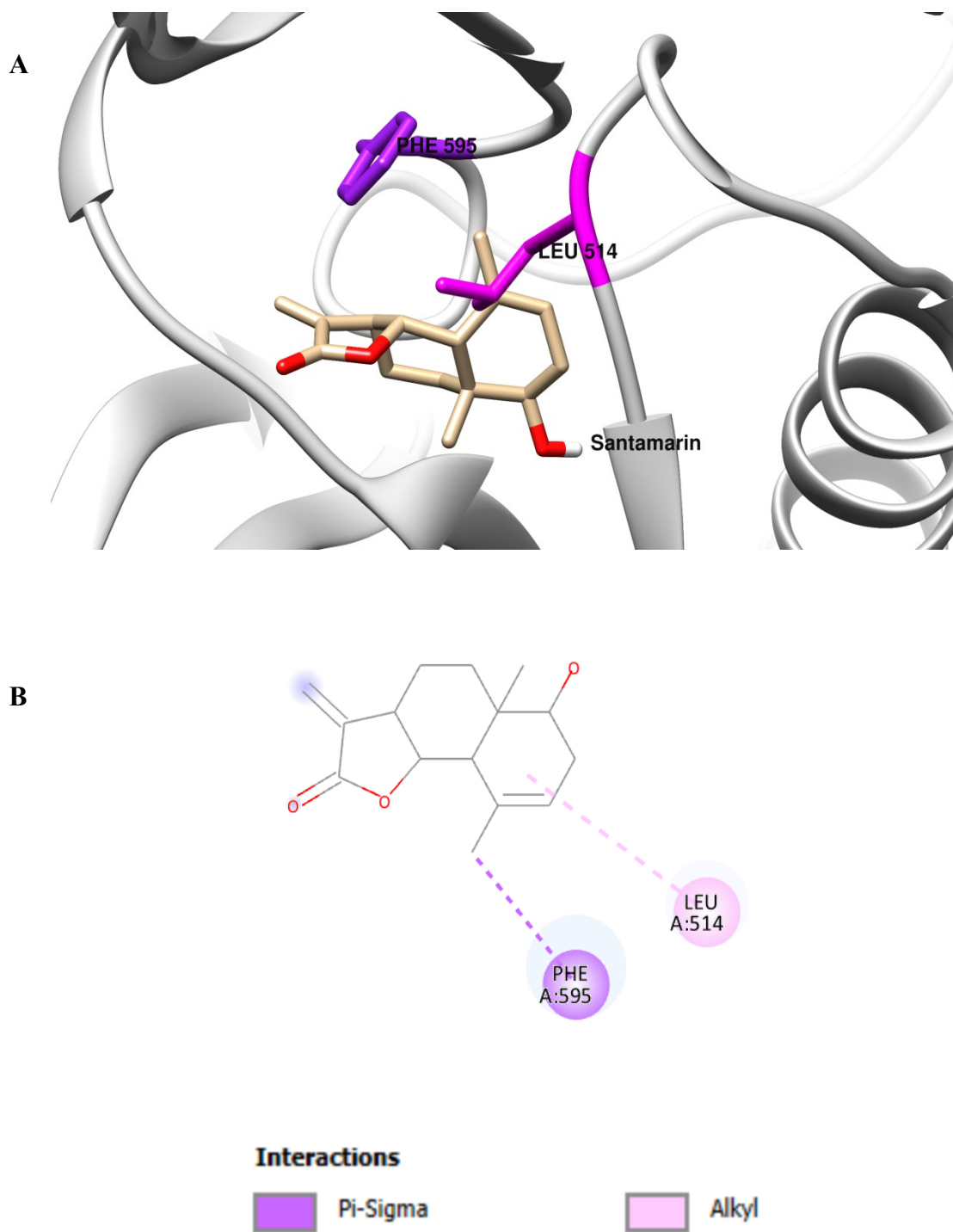


Figure 26. Interaction mode of Santamarin and BRAF

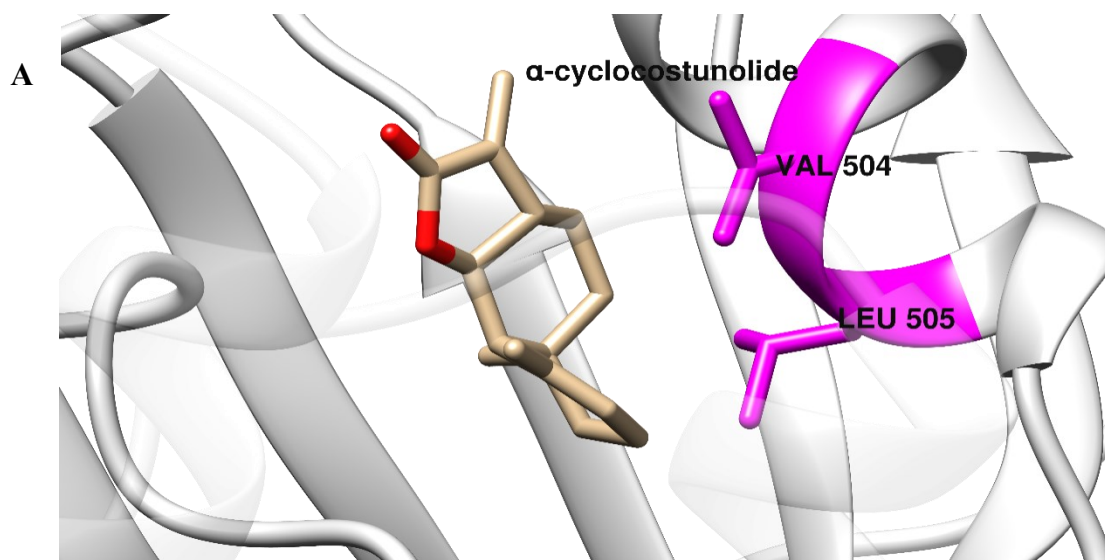
A) Three-dimensional model; B) Two-dimensional model

1.2.10 Study of α -cyclocostunolide interactions with BRAF

The α -cyclocostunolide-BRAF complex analysis displays a predicted binding energy of **-8.4 kcal/mol** for the best binding mode.

Alpha-cyclocostunolide resides within a binding pocket composed of ILE463, GLY464, SER465, VAL471, TYR472, ALA481, LYS483, ASN500, GLU501, **VAL504**, **LEU505**, ILE513, LEU514, THR529, GLN530, TRP531, CYS532, GLY534, SER535, SER536, LYS539, LEU567, ILE572, ILE573, HIS574, ARG575, ASN580, PHE583, ILE592, GLY593, ASP594, PHE595, GLY596, LEU597, THR599 and TRP604. The calculated cavity volume is 2727 Å³, with the predicted centre located at (-2, 13, 12).

The complex demonstrates four alkyl hydrophobic interactions contributing to its stability: contacts with **VAL504** residue at distances of 4.36 Å and 5.21 Å, and with **LEU505** residue at distances of 5.48 Å and 5.27 Å (Figure 27).



B

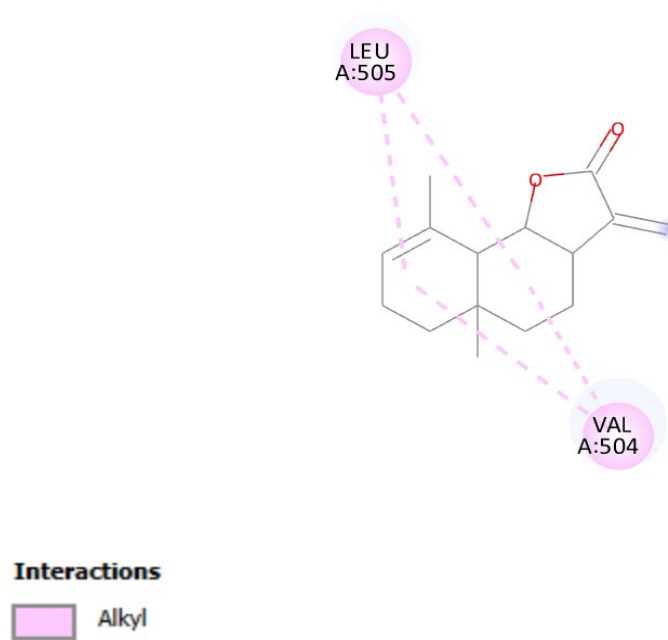


Figure 27. Interaction mode of α -cyclocostunolide and BRAF

A) Three-dimensional model; B) Two-dimensional model

Based on the results of the analyses presented, several SLs were assessed for potential binding interactions with the serine-threonine protein kinase BRAF, a crucial target in melanoma therapy. These SLs were compared to the reference ligand Belvarafenib (V1Y), an approved synthetic small-molecule BRAF inhibitor.

The reference ligand V1Y exhibited the highest binding energy of **-12.8 kcal/mol**, which indicates stronger affinity for the BRAF protein. It formed an extensive network of interactions, including four conventional hydrogen bonds, a halogen interaction, a pi-cation interaction, and multiple hydrophobic interactions (pi-sigma, pi-sulphur, pi-pi stacking, pi-pi T-shaped, alkyl, and pi-alkyl). These interactions contribute to the binding of V1Y to BRAF.

Regarding the studied SLs, the binding energies ranged from **-9.1 kcal/mol** (lappadilactone, compound 1) to **-6.6 kcal/mol** (Reynosin, compound 7) which are lower than that of V1Y. However, some SLs exhibited promising binding interactions; Lappadilactone (compound 1) and Dehydrocostus lactone (compound 2) displayed relatively high binding energies of **-9.1 kcal/mol** and **-8.9 kcal/mol**, respectively (Figure 28), indicating favourable binding to BRAF. They formed conventional hydrogen bonds and hydrophobic interactions (alkyl and pi-alkyl) with key residues in the binding pocket. Isozaluzanin C (compound 3), Zaluzanin C (compound 4), Costunolide (compound 5), and α -cyclocostunolide (compound 9) exhibited binding energies ranging from **-8.4 kcal/mol** to **-8.2 kcal/mol**, these SLs formed hydrogen bonds (conventional and carbon-hydrogen) and hydrophobic interactions (alkyl and pi-alkyl) with residues like CYS532, ASP594, VAL471 and PHE595.

Arbusculin A (compound 6) and Santamarin (compound 8) had binding energies of **-7.4 kcal/mol** and **-8.0 kcal/mol**, respectively. Arbusculin A formed three conventional hydrogen bonds and two pi-alkyl interactions, while Santamarin showed a pi-sigma and an alkyl interaction. Reynosin (compound 7) displayed the lowest binding energy of **-6.6 kcal/mol** among the studied SLs, indicating a weaker affinity for BRAF. However, it formed four hydrogen bonds (three conventional and one carbon-hydrogen) and two alkyl interactions.

The SL-BRAF complexes shared the same binding pocket volumes except for Arbusculin A (compound 6) and Reynosin (compound 7). In addition, they shared common residues such as ILE463, GLY464, VAL471, ALA481, LYS483, GLU501, VAL504, LEU505, THR529, GLN530, TRP531, CYS532, PHE583, ASP594, PHE595 and THR599, indicating their importance in binding interactions.

overall, among the screened SLs, lappadilactone (compound 1) and Dehydrocostus lactone (compound 2) exhibited the most promising binding profiles, with relatively high binding energies and favourable interactions, including hydrogen bonds and hydrophobic contacts. These SLs could serve as potential lead compounds for further optimisation and development of BRAF inhibitors for melanoma therapy.

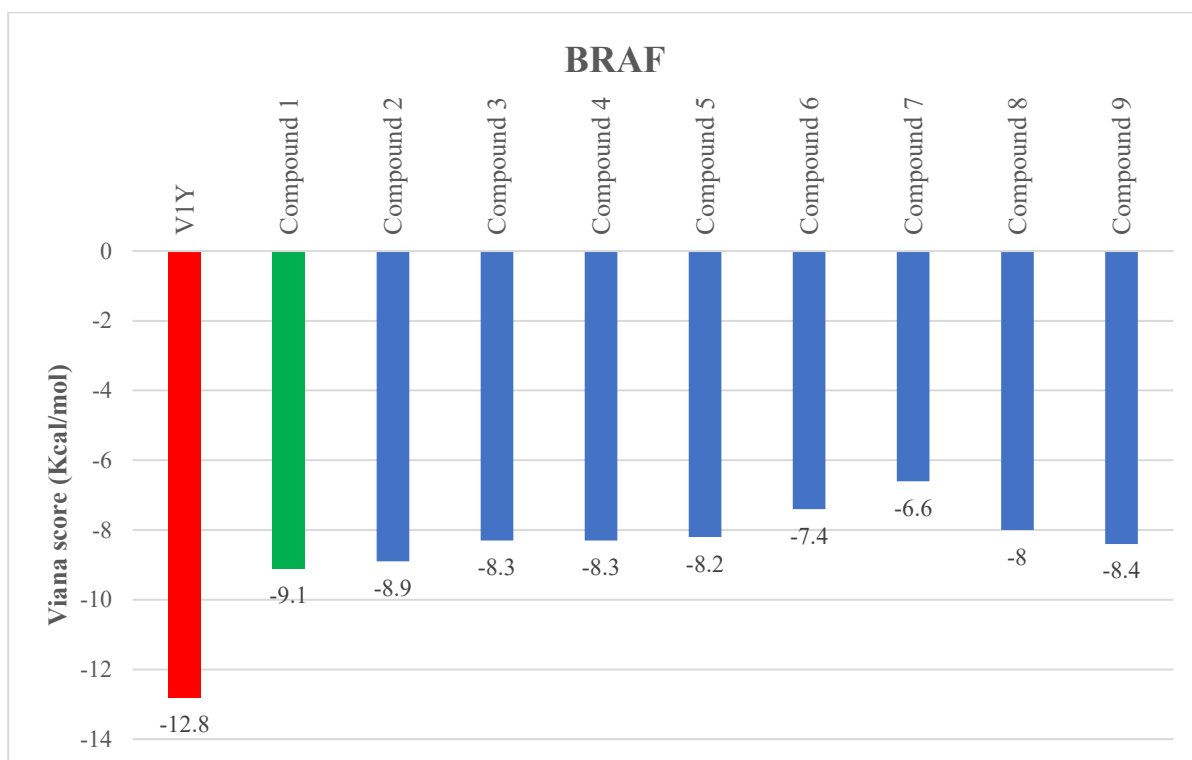


Figure 28. Binding energy of SLs-BRAF complexes

1.3 Interaction mode between SLs and ERK2

1.3.1 Study of the 8XE interactions with the protein ERK2 (Redocking the reference)

The molecular docking study and visual inspection highlight that the reference ligand 8XE in complex with the mitogen-activated protein kinase 1 ERK2 (PDB ID: 5NHJ) protein reveal the best binding mode exposes a predicted binding energy of **-8.8 kcal/mol**.

The binding pocket of the 8XE-ERK2 complex with calculated cavity volume of 1101 Å³ and predicted location centred at -13, 13, and 40 in terms of x, y and z coordinates respectively, includes the following residues: **ILE31**, GLY32, GLU33, GLY34, ALA35, TYR36, GLY37, MET38, **VAL39**, **ALA52**, **LYS54**, LYS55, **ILE56**, ARG67, GLU71, ILE84, GLN105, **ASP106**, **LEU107**, **MET108**, GLU109, THR110, **ASP111**, TYR113, LYS114, ASP149, LYS151, SER153, ASN154, LEU156, **CYS166**, ASP167, PHE168, GLY169, LEU170, VAL188 and THR190.

The complex exhibits a network of interactions. Specifically, six hydrogen bond interactions occur between the ligand 8XE and the ERK2 protein. Firstly, the NZ atom of the **LYS54** and **MET108** residues participates in conventional hydrogen bonds with an oxygen O and N3 atoms of 8XE at distances of 2.90 Å and 3.12 Å, respectively. Secondly, the N2 atom of 8XE engages in a conventional hydrogen bond with the backbone oxygen atom of **MET108** at a distance of 3.08 Å. Thirdly, a carbon-hydrogen bond emerges between the C5 atom of 8XE and the OD2 atom of **ASP106** at a distance of 3.38 Å. Fourthly, another carbon-hydrogen bond appears between the C3 atom of 8XE and the OD2 atom of **ASP111** at a distance of 3.49 Å. Finally, a pi-donor hydrogen bond coupled with a pi-sulphur interaction occurs between the SG atom of **CYS166** and the aromatic ring of 8XE at a distance of 3.89 Å.

Furthermore, several hydrophobic contacts exist between 8XE and the ERK2 protein. Three pi-sigma interactions manifest, involving the CG2 atoms of **ILE31** and **VAL39**, as well as the CD1 atom of **LEU156**, with distances ranging from 3.65 Å to 3.89 Å. Two alkyl hydrophobic interactions arise, with the carbon atom of 8XE interacting with the **ILE31** and **LEU107** residues at distances of 3.95 Å and 5.45 Å, respectively. Additionally, two pi-alkyl interactions form between the aromatic ring of 8XE and the **ILE31** and **ALA52** residues, with distances of 5.03 Å and 3.97 Å, respectively (Figure 29).

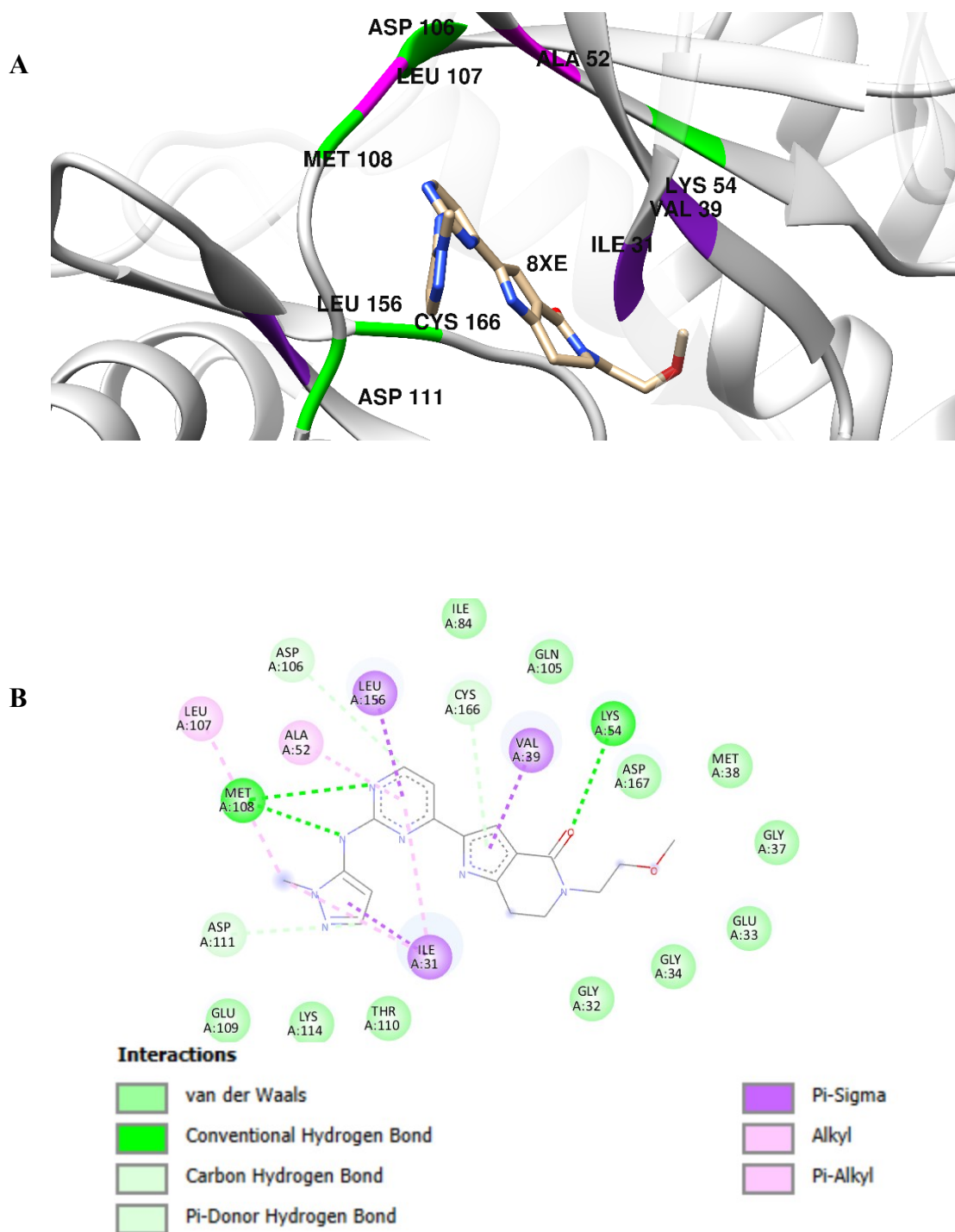


Figure 29. Interaction mode of 8XE and ERK2

A) Three-dimensional model; B) Two-dimensional model

1.3.2 Study of lappadilactone interactions with ERK2

The results of molecular docking and visual analysis show that the conformer of Lappadilactone binds to mitogen-activated protein kinase 1 ERK2 (PDB: 5NHJ) with the best predicted binding energy equal to **-9.5 kcal/mol**.

The pose interacts with the protein in a position surrounded by the following amino acid residues: TYR30, ILE31, GLY32, GLU33, GLY34, ALA35, TYR36, GLY37, MET38, **VAL39**, ALA52, LYS54, **ARG67**, GLU71, GLN105, ASP111, TYR113, LYS114, ASP149, **LYS151**, SER153, ASN154, LEU156, **CYS166**, ASP167, GLY169, LEU170, VAL188, ALA189, THR190, ARG191, TRP192 and TYR193, in a cavity characterised by a volume of 1101 Å³ and centre coordinates (x, y, z): -13, 13, 40.

The complex displays three conventional hydrogen bonds between Lappadilactone and 5NHJ: the **ARG67** residue forms the first connection between its NH₂ group as a donor and the oxygen atom (O) of Lappadilactone at a distance of 3.36 Å, the **LYS151** amino acid residue forms the second and third bonds between its NZ nitrogen atom and the oxygen atom of Lappadilactone at distances of 2.80 Å and 3.13 Å, respectively.

In addition to hydrogen bonds, the complex exhibits two hydrophobic bonds of the alkyl interactions type, including **VAL39** and **CYC166**, with distances of 4.68 Å and 5.34 Å, respectively. Increases the stability of the binary complex between Lappadilactone and ERK2 (Figure 30).

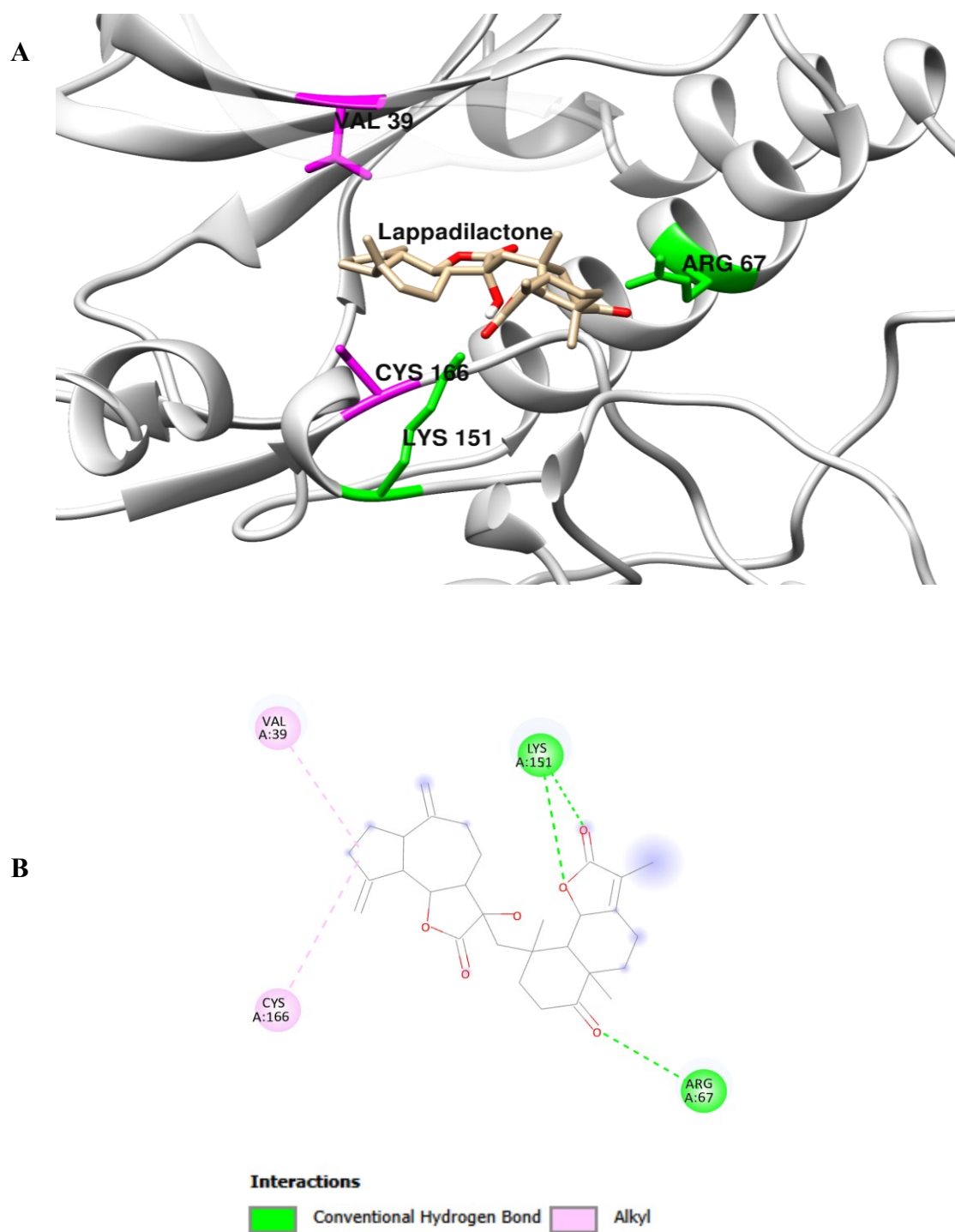


Figure 30. Interaction mode of Lappadilactone and ERK2

A) Three-dimensional model; B) Two-dimensional model

1.3.3 Study of Dehydrocostus lactone interactions with ERK2

The top-ranked binding mode of Dehydrocostus lactone with mitogen-activated protein kinase1 ERK2 shows a predicted binding energy of **-8.5 kcal/mol**.

According to the molecular docking study and visual analysis, the Dehydrocostus lactone binds to a pocket formed by the following residues: ILE31, GLY32, GLU33, GLY34, ALA35, TYR36, GLY37, MET38, **VAL39**, ALA52, **LYS54**, ARG67, GLU71, ILE84, GLN105, ASP106, LEU107, MET108, THR110, ASP111, ASP149, LYS151, SER153, ASN154, **LEU156**, **CYS166**, ASP167, GLY169, LEU170 and THR190 in a space of 1101 Å³ and centre at coordinates (x, y, z): -13, 13, 40.

Six alkyl hydrophobic interactions involve **VAL39** (two interactions), **LYS54**, **LEU156** and **CYS166** residues acting as donors to alkyl moiety with distances ranging from 4.19 Å to 5.23 Å (Figure 31).

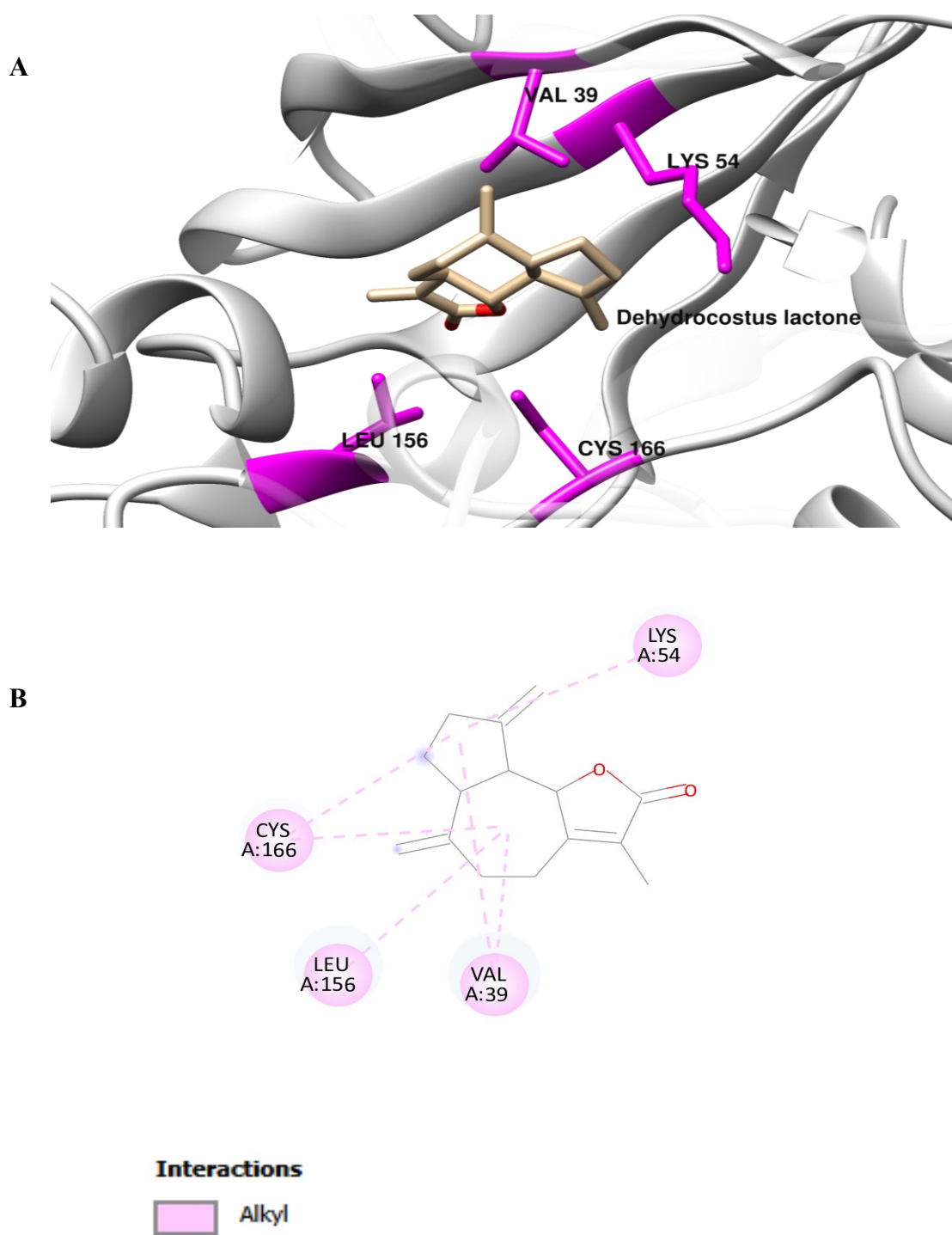


Figure 31. Interaction mode of Dehydrocostus lactone and ERK2

A) Three-dimensional model; B) Two-dimensional model

1.3.4 Study of Isozaluzanin C interactions with ERK2

The predicted binding energy associated with the most favourable binding pose emerges as **-7.8 kcal/mol**, for the Isozaluzanin C-ERK2 complex.

Isozaluzanin C resides within a binding pocket of the ERK2 protein composed of **TYR30**, **ILE31**, GLY32, GLU33, GLY34, ALA35, TYR36, GLY37, MET38, **VAL39**, CYS40, ALA52, **LYS54**, LYS55, ARG67, GLU71, ILE84, GLN105, ASP106, LEU107, MET108, GLU109, THR110, ASP111, ASP149, LYS151, SER153, ASN154, LEU156, **CYS166**, ASP167, PHE168, GLY169, LEU170, VAL188 and THR190. The calculated cavity volume is 1101 Å³, with the predicted centre located at (-13, 13, 40).

The complex (Figure 32) exhibits one conventional hydrogen bond interaction. **LYS54** acts as a hydrogen bond donor by its NZ atom to Isozaluzanin C's O3 atom at a distance of 2.95 Å.

Furthermore, the complex demonstrates four alkyl hydrophobic interactions contributing to its stability: contacts with **ILE31**, **VAL39**, **LEU156** and **CYS166** residues at distances of 5.49 Å, 4.03 Å, 5.49 Å and 4.74 Å, respectively.

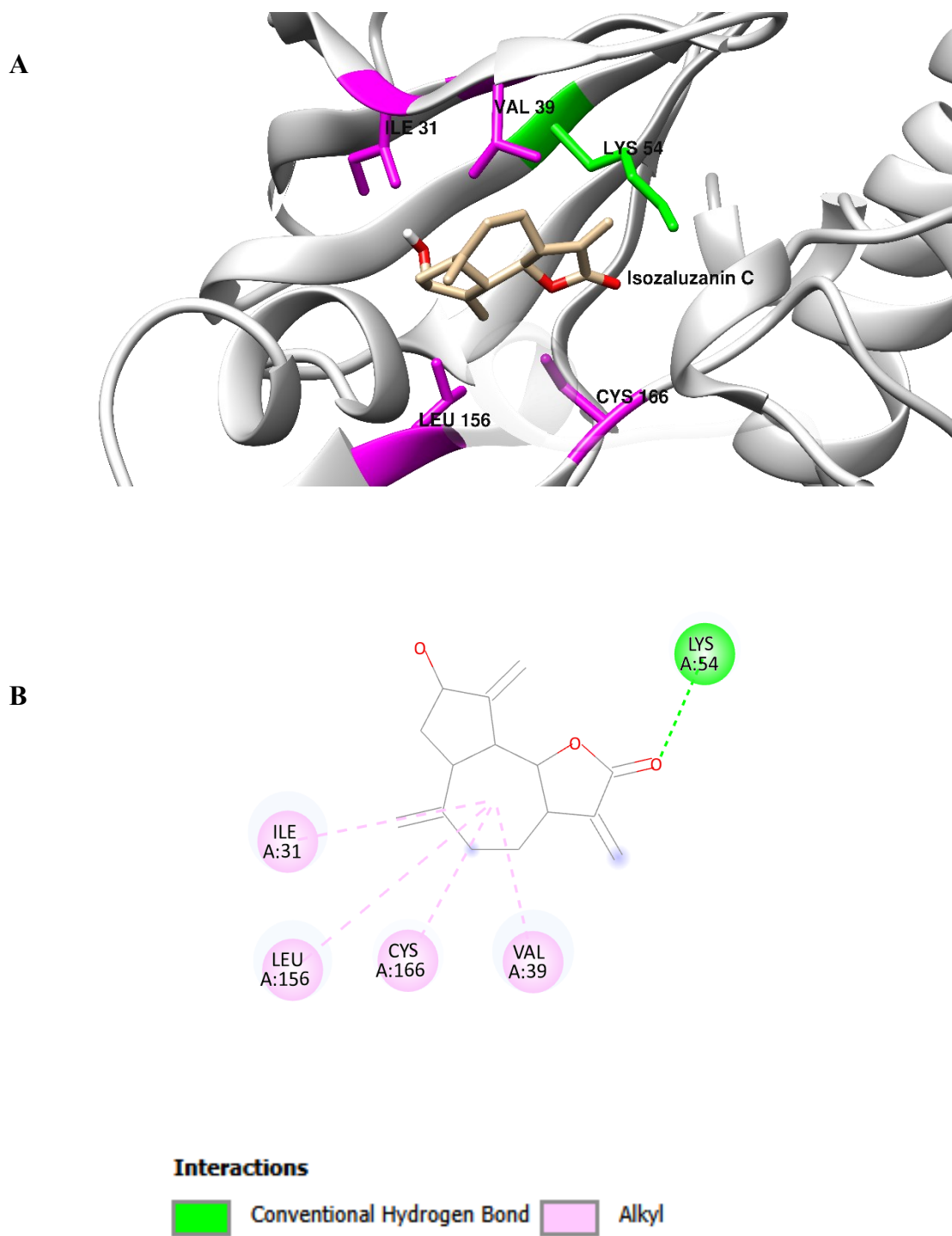


Figure 32. Interaction mode of Isozaluzanin C and ERK2

A) Three-dimensional model; B) Two-dimensional model

1.3.5 Study of Zaluzanin C interactions with ERK2

The Zaluzanin C-ERK2 complex analysis reveals a predicted binding energy value equal to **-7.8 kcal/mol** for a favourable binding pose.

The binding site of the Zaluzanin C-ERK2 complex is composed of the following key residues: TYR30, ILE31, GLY32, GLU33, GLY34, ALA35, TYR36, GLY37, MET38, **VAL39**, CYC40, ALA52, **LYS54**, LYS55, ARG67, GLU71, ILE84, GLN105, ASP106, LEU107, MET108, ASP111, TYR113, ASP149, LYS151, SER153, ASN154, **LEU156**, **CYS166**, ASP167, PHE168, LEU170 and THR190. Zaluzanin C occupies a binding pocket with a volume of 1101 Å³ and coordinates (x, y, z): -13, 13, 40.

A hydrogen bond is observed between Zaluzanin C and ERK2. **LYS54** engages in a conventional hydrogen bond with its NZ and the third oxygen atom of Zaluzanin C at a distance of 3.02 Å.

In addition, three alkyl hydrophobic interactions are observed between Zaluzanin C and the protein ERK2 residues: **VAL39**, **LEU156**, and **CYS166**, with distances of 4.09 Å, 5.48 Å and 4.74 Å, respectively (Figure 33).

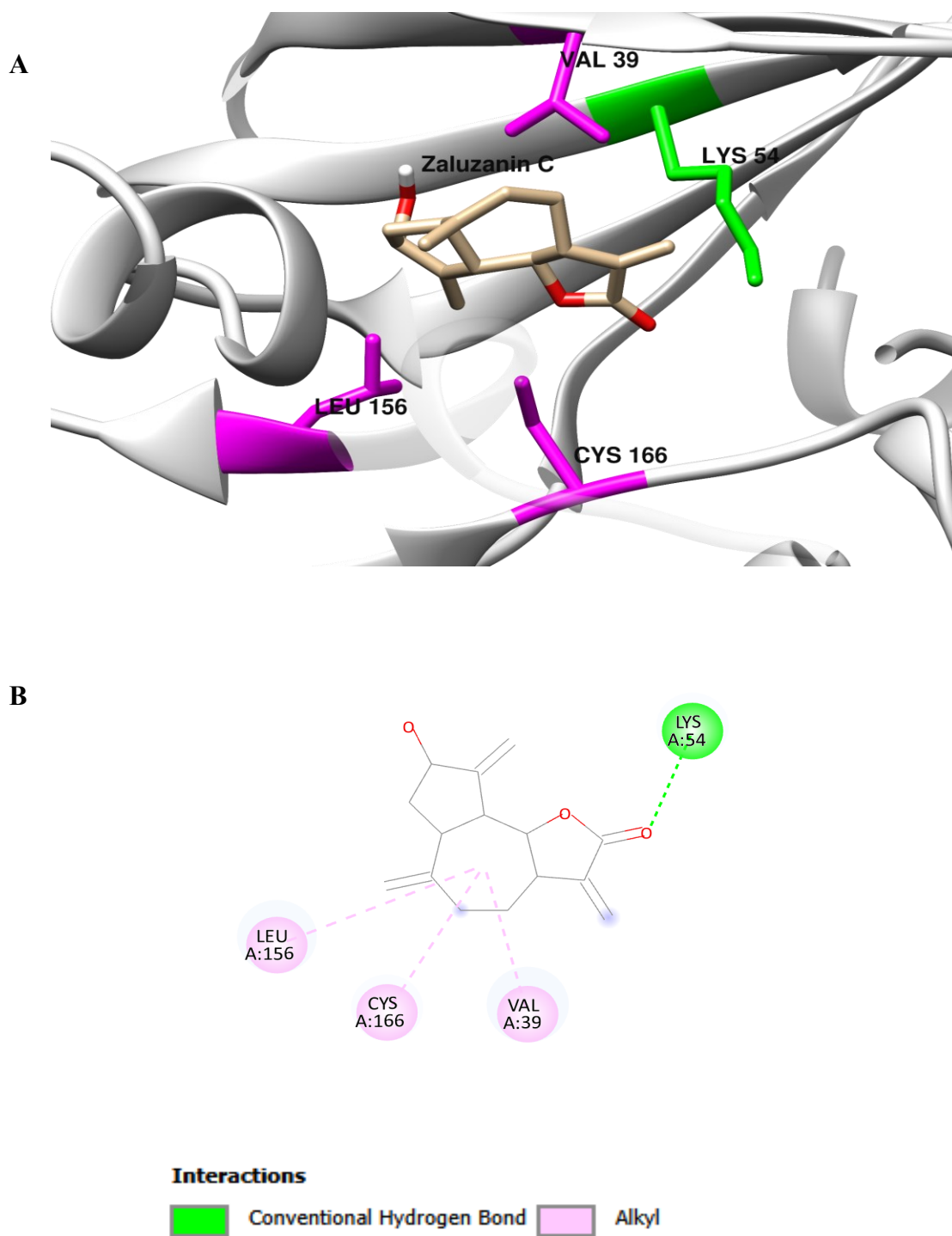


Figure 33. Interaction mode of Zaluzanin C and ERK2

A) Three-dimensional model; B) Two-dimensional model

1.3.6 Study of Costunolide interactions with ERK2

The Costunolide-ERK2 complex analysis reveals a predicted binding energy value equalling **-7.4 kcal/mol** for a favourable binding pose.

Costunolide binds in the ERK2 pocket, surrounded by the residues ILE31, GLY32, GLU33, GLY34, ALA35, TYR36, GLY37, MET38, VAL39, ALA52, LYS54, LYS55, ILE56, **ARG67**, GLU71, GLN105, ASP111, TYR113, ASP149, LYS151, SER153, ASN154, LEU156, CYS166, ASP167, GLY169, LEU170, VAL188 and THR190. The calculated pocket volume is 1101 Å³, with the predicted centre located at (-13, 13, 40).

The results reveal the formation of only one conventional hydrogen bond between Costunolide and ERK2, the **ARG67** residue participates in a hydrogen bond through its NH₂ group interacting with the O atom of Costunolide at a distance of 2.82 Å (Figure 34).

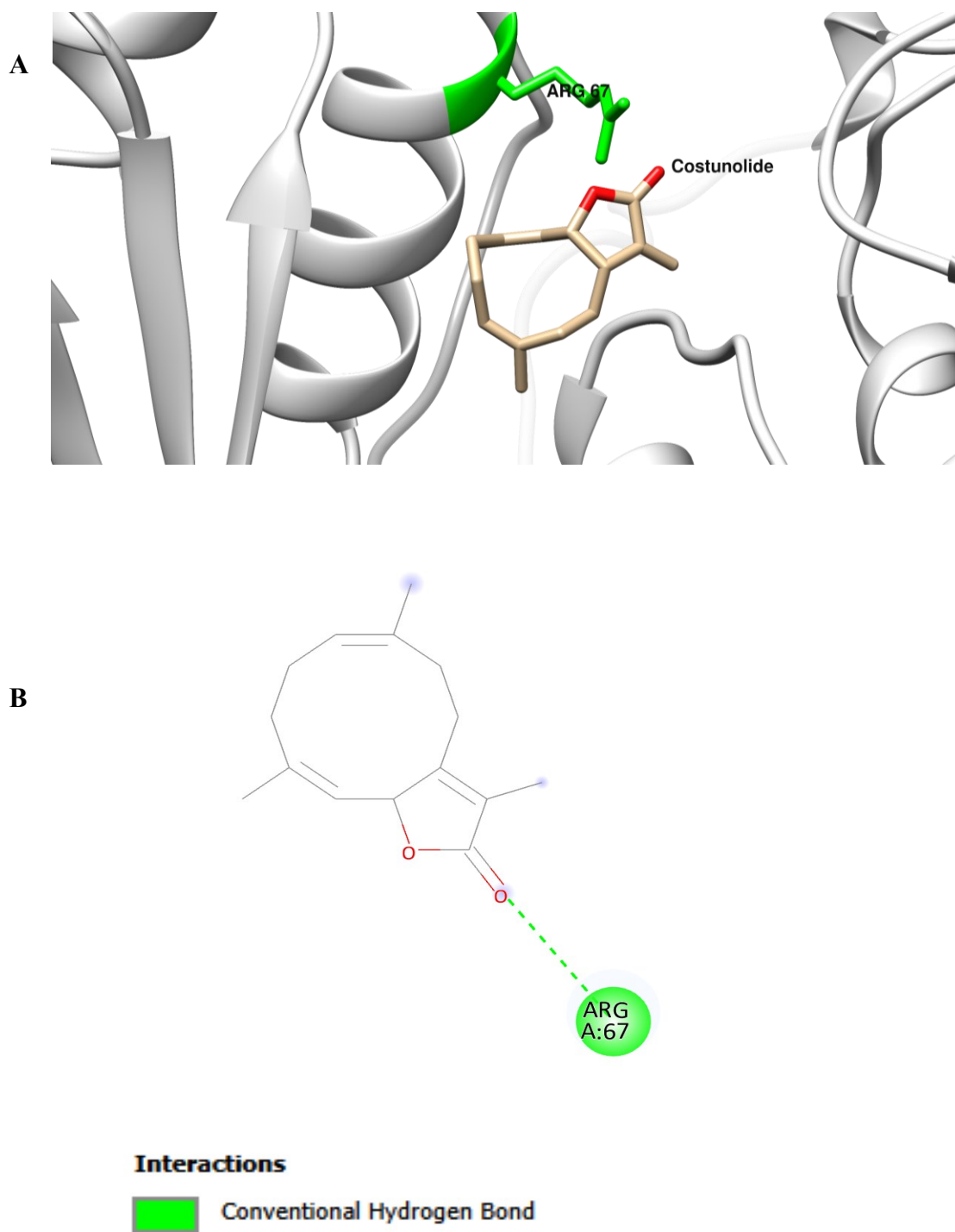


Figure 34. Interaction mode of Costunolide and ERK2

A) Three-dimensional model; B) Two-dimensional model

1.3.7 Study of Arbusculin A interactions with ERK2

The most favourable binding mode of the Arbusculin A-ERK2 complex shows a predicted binding energy value of **-7.1 kcal/mol**.

Arbusculin A docks into a cavity with a calculated volume of 1101 Å³ and coordinates (x, y, z): -13, 13, 40, surrounded by the following residues: ILE31, GLY32, GLU33, GLY34, ALA35, TYR36, GLY37, **VAL39**, **LYS54**, ARG67, GLU71, GLN105, ASP111, ASP149, LYS151, **SER153**, **ASN154**, LEU156, **CYS166**, ASP167, GLY169, LEU170, VAL188, ALA189 and THR190.

A hydrogen bonding network of three conventional hydrogen bond is observed between the Arbusculin A and the ERK2 protein, involving: the **LYS54** interacts with its NZ atom with O1 atom of Arbusculin A at a distance of 2.83 Å. The oxygen atom of the side chain (OG) of **SER153** forms a hydrogen bond with the third oxygen atom (O3) of Arbusculin A at a distance of 2.91 Å. The **ASN154** residue acts as a conventional hydrogen bond receptor through its backbone oxygen atom from the Arbusculin A H21 atom at a distance of 2.13 Å.

Additionally, the two alkyl hydrophobic interactions are presented between the Arbusculin A and the ERK2 protein residues: **VAL39** and **CYS166** at distances of 4.46 Å and 4.79 Å, respectively (Figure 35).

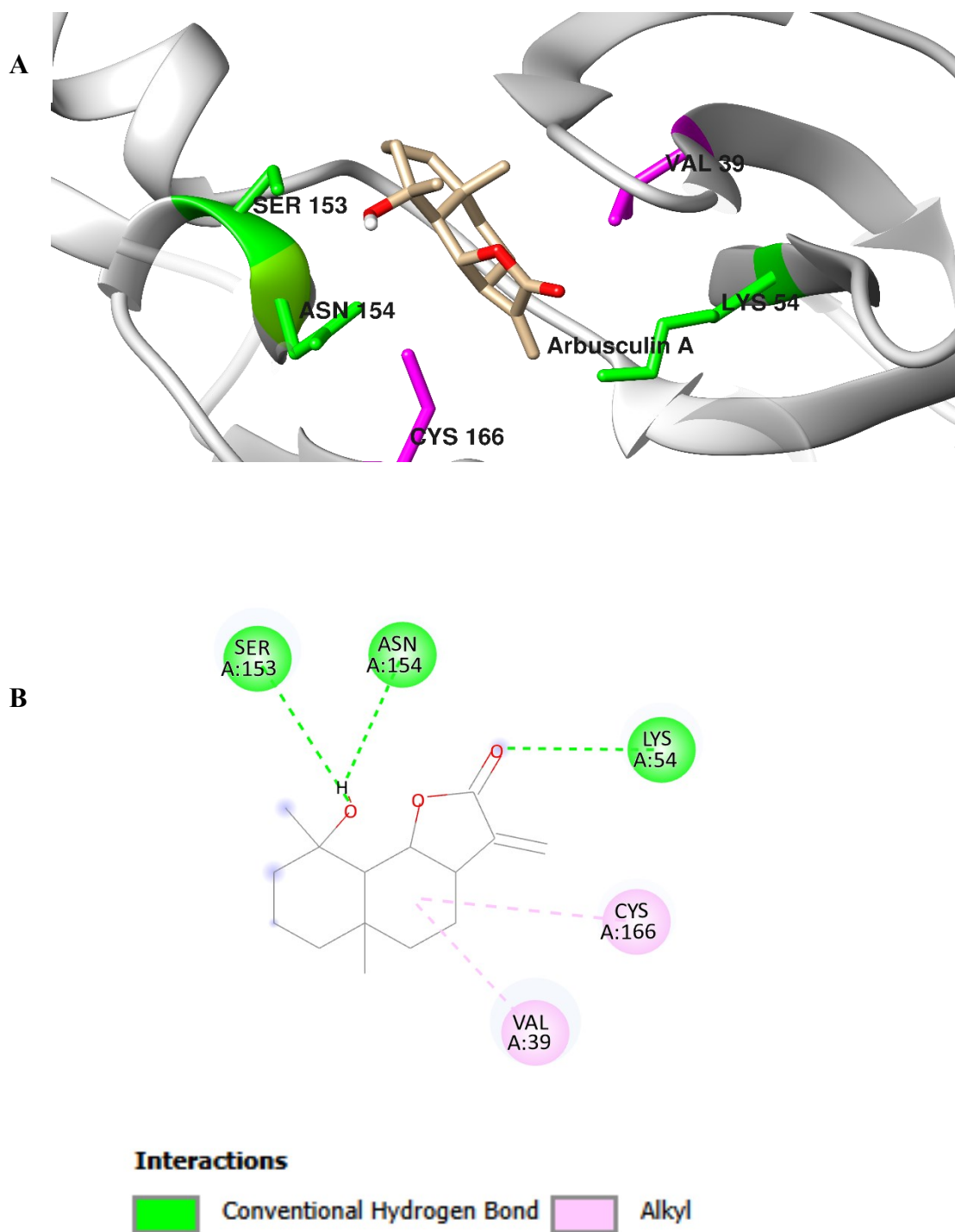


Figure 35. Interaction mode of Arbusculin A and ERK2

A) Three-dimensional model; B) Two-dimensional model

1.3.8 Study of Reynosin interactions with ERK2

The top-ranked binding mode of Reynosin binds to mitogen-activated protein kinase 1 ERK2 with a predicted binding energy of **-7.3 kcal/mol**.

The Reynosin occupies a binding pocket with a volume of 1101 Å³ with the predicted centre located at (-13, 13, 40). Including the subsequent amino acids: TYR30, ILE31, GLY32, GLU33, GLY34, **ALA35**, **TYR36**, **GLY37**, MET38, VAL39, LYS54, LYS55, ILE56, ARG67, GLU71, ASP111, ASP149, LYS151, SER153, ASN154, LEU156, CYS166, **ASP167**, GLY169, LEU170, VAL188 and THR190.

The binding of Reynosin to the ERK2 protein involves two hydrogen bond interactions. The **GLN37** residue acts as a conventional hydrogen bond donor for Reynosin at a distance of 2.88 Å. While the **ASP167** residue acts as receptor by its oxygen atom in a carbon hydrogen bond from the C6 atom of the ligand Reynosin at a distance of 3.34 Å.

In addition, one alkyl hydrophobic interaction is observed between Reynosin and the **TYR36** protein ERK2 residue at a distance of 5.36 Å. moreover, one unfavourable donor-donor interaction is occurred between the nitrogen N atom of **ALA35** residue and the H18 atom of Reynosin ligand at a distance of 2.39 Å (Figure 36).

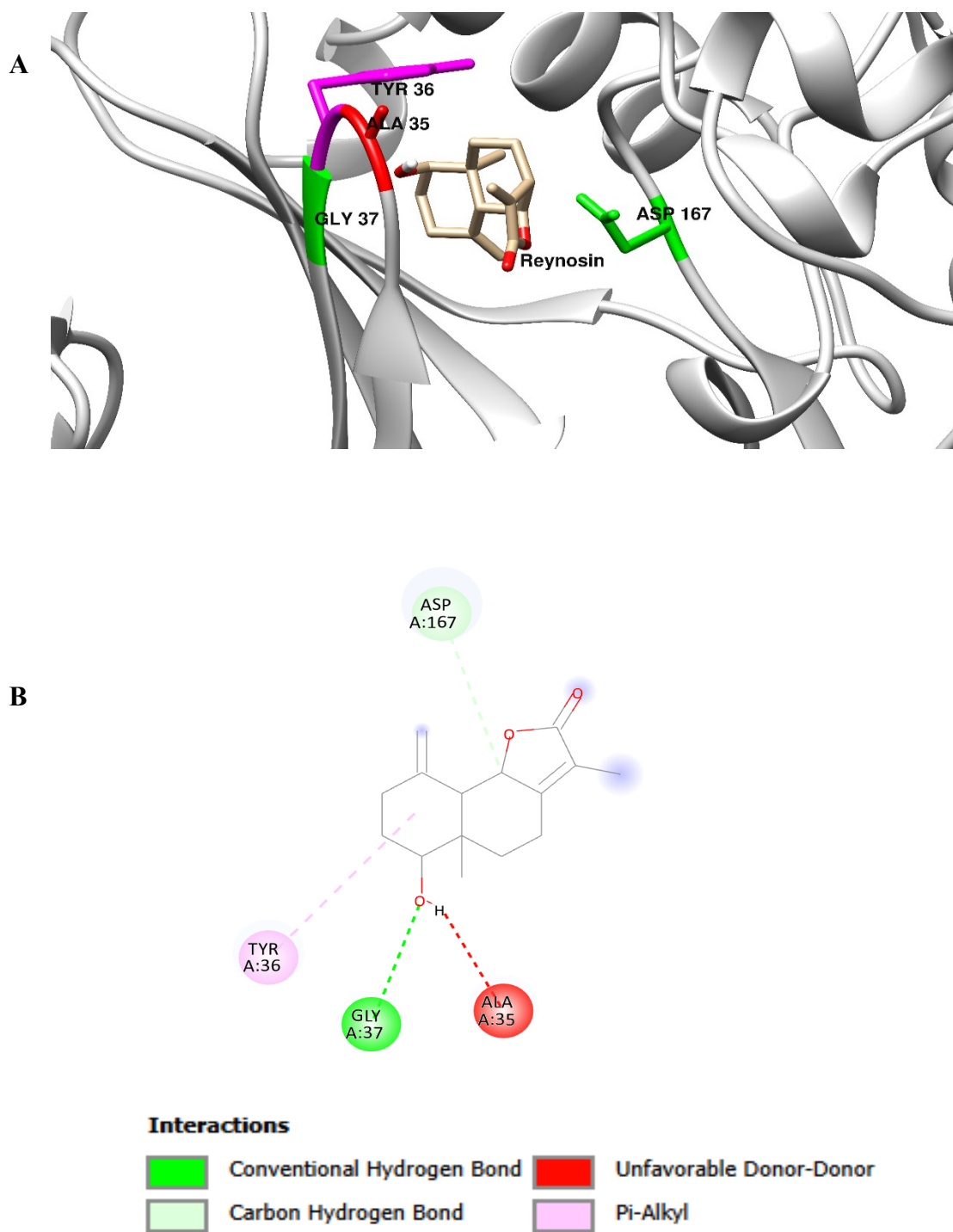


Figure 36. Interaction mode of Reynosin and ERK2

A) Three-dimensional model; B) Two-dimensional model

1.3.9 Study of Santamarin interactions with ERK2

The Santamarin-ERK2 complex exposes a predicted binding energy of **-6.8 kcal/mol**, in the best pose.

The binding pocket is composed of the following residues: TYR30, ILE31, GLY32, GLU33, GLY34, ALA35, TYR36, GLY37, MET38, **VAL39**, LYS54, LYS55, ILE56, ARG67, GLU71, GLN105, ASP111, ASP149, LYS151, **SER153**, ASN154, **LEU156**, **CYS166**, ASP167, GLY169, LEU170, VAL188, ALA189 and THR190. The calculated cavity volume is 1101 Å³, with the predicted centre located at coordinates (-13, 13, 40).

A conventional hydrogen bond is observed between the H12 atom of the ligand Santamarin and the oxygen atom of the **SER153** residue of the ERK2 protein, the distance between these two atoms is 3.0 Å.

Regarding the hydrophobic interactions, four alkyl interactions are identified. The first two alkyl interactions occurred between the **VAL39** residue and the Santamarin ligand, with distances of 4.28 Å and 4.85 Å, respectively. The third alkyl interaction is observed between the **CYS166** residue and Santamarin at a distance of 4.24 Å. Finally, the fourth alkyl interaction is present between the Santamarin and the **LEU156** residue at a distance of 4.80 Å (Figure 37).

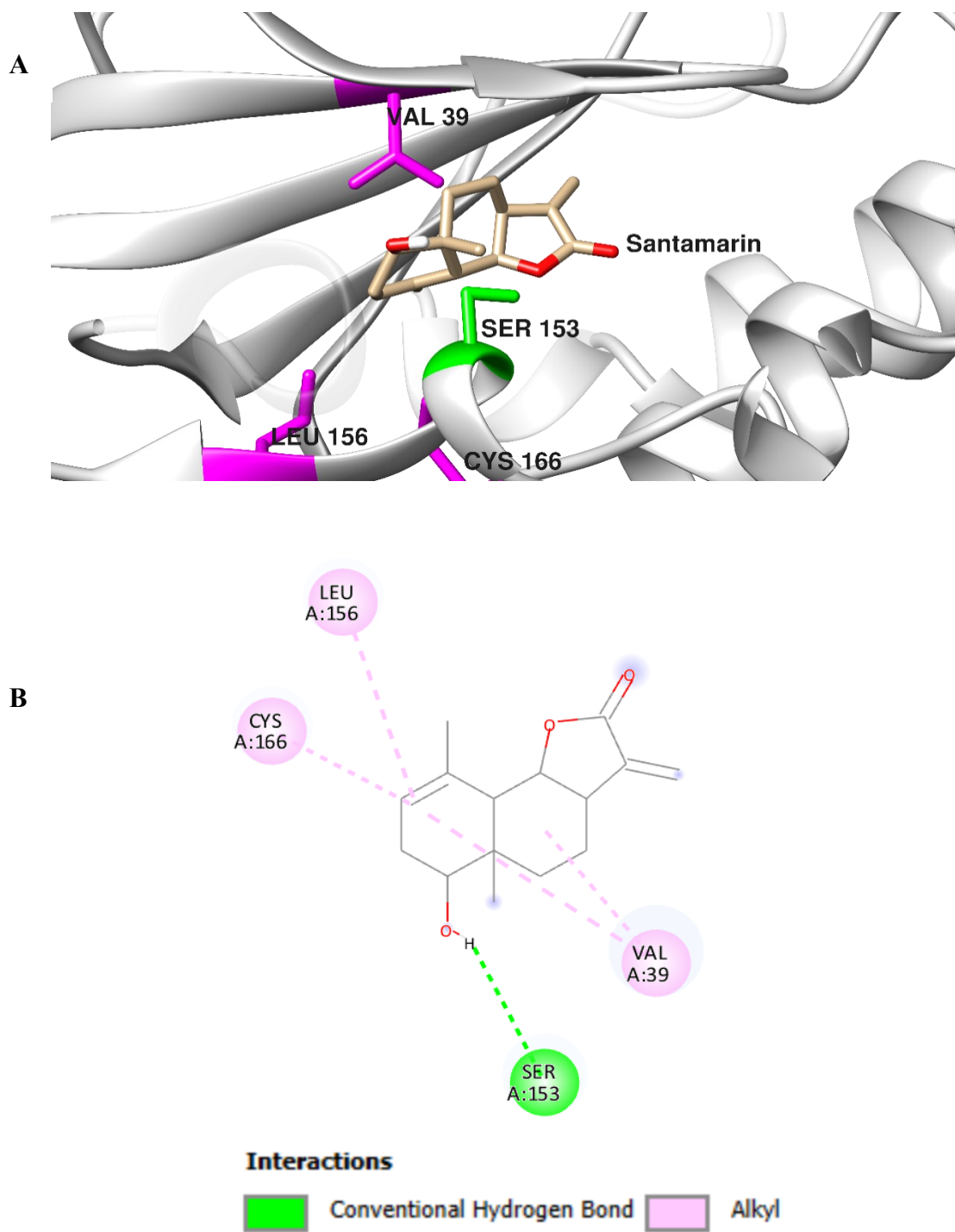


Figure 37. Interaction mode of Santamarin and ERK2

A) Three-dimensional model; B) Two-dimensional model

1.3.10 Study of α -cyclocostunolide interactions with ERK2

The α -cyclocostunolide-ERK2 complex analysis shows a predicted binding energy of **-6.8 kcal/mol** for the best binding mode.

Alpha-cyclocostunolide resides within a binding pocket composed of SER29, TYR30, ILE31, GLY32, GLU33, GLY34, GLY37, MET38, **VAL39**, SER41, ALA52, **LYS54**, GLU71, GLN105, ASP106, LEU107, MET108, GLU109, THR110, ASP111, LYS114, LYS151, SER153, ASN154, **LEU156**, **CYS166** and ASP167. The calculated cavity volume is 1101 Å³, with the predicted centre located at coordinates (-13, 13, 40).

The complex exhibits one conventional hydrogen bond interaction. **LYS54** acts as a hydrogen bond donor to α -cyclocostunolide at a distance of 2.80 Å.

Furthermore, the complex demonstrates four alkyl hydrophobic interactions contributing to its stability: contacts with **VAL39**, **LEU156** and **CYS166** residues at distances ranging from 4.28 Å to 5.47 Å (Figure 38).

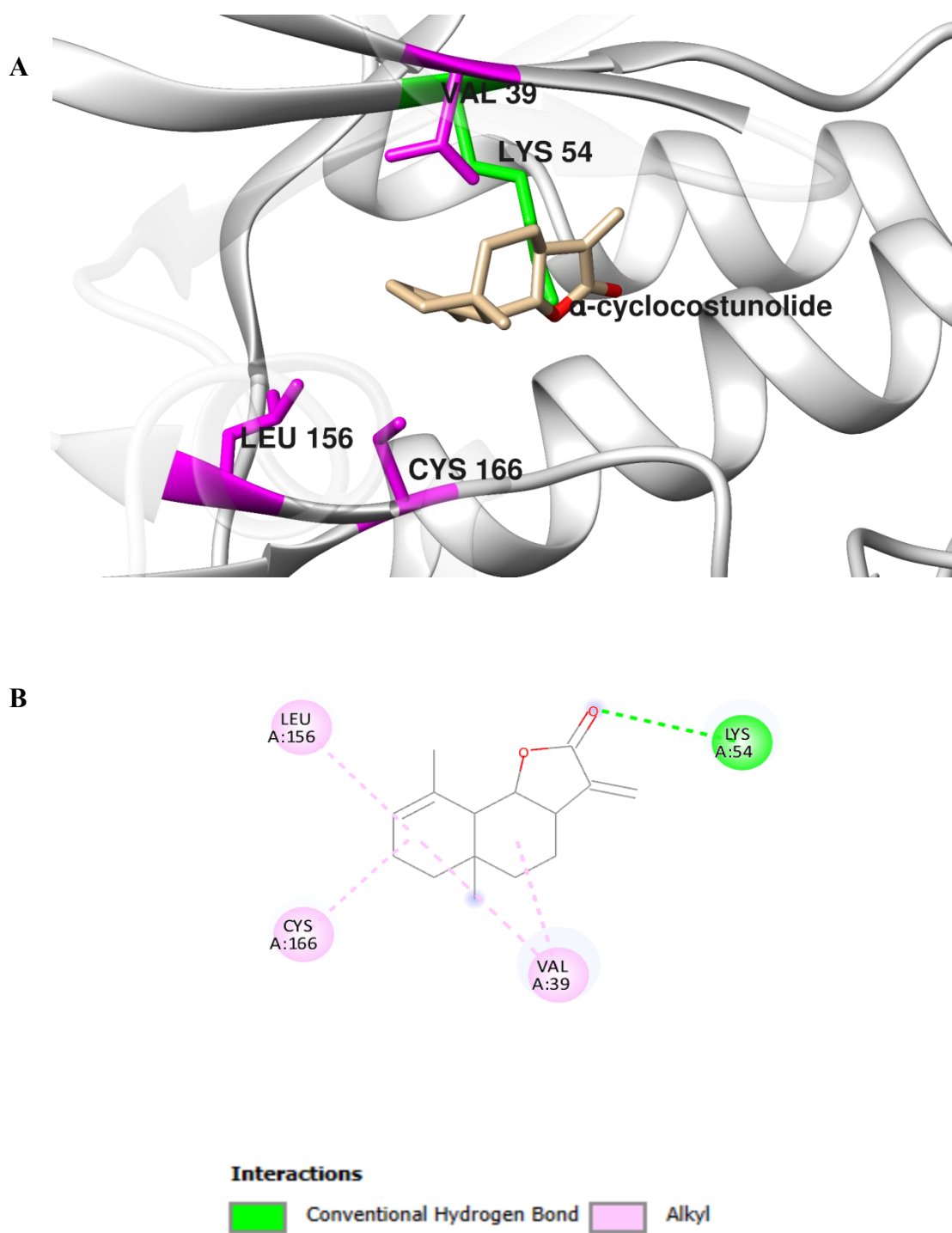


Figure 38. Interaction mode of α -cyclocostunolide and ERK2

A) Three-dimensional model; B) Two-dimensional model

The analysis of our molecular docking studies provides valuable insights into the binding interactions between the SLs and the mitogen-activated protein kinase1 protein ERK2, a crucial enzyme involved in various cellular processes, including cell proliferation, differentiation and survival. Among the nine screened compounds, Lappadilactone (compound 1) has the highest binding affinity with a predicted binding energy of **-9.5 kcal/mol**, even surpassing the reference ligand 8XE, a reversible covalent inhibitor with a binding energy of **-8.8 kcal/mol**. The superior binding affinity of Lappadilactone for the ERK2 protein is further supported by the presence of three conventional hydrogen bonds with the ARG67 and LYS151 residues and two hydrophobic alkyl interactions with the VAL39 and CYS166 residues. This combination of favourable binding energy and multiple stabilising interactions suggests that Lappadilactone may be a promising candidate for future optimisation as a potential natural-based therapeutic agent targeting the ERK2 protein. While the reversible covalent inhibitor compound 8XE has a slightly lower binding energy compared to Lappadilactone, it forms an extensive network of interactions, including six hydrogen bonds and seven hydrophobic contacts. These interactions involve residues such as LYS54, MET108, ASP106, ASP111, **CYS166**, ILE31, VAL39, ALA52 and LEU156, which contribute to the stability and specificity of the 8XE-ERK2 complex.

Dehydrocostus lactone (compound 2) has the second highest binding energy of **-8.5 kcal/mol**, despite lacking hydrogen bonding interactions, it forms six hydrophobic alkyl interactions with residues such as VAL39, LYS54, LEU156, and **CYS166**. Isozaluzanin C (compound 3), Zaluzanin C (compound 4), Costunolide (compound 5), Arbusculin A (compound 6), and Reynosin (compound 7) have lower binding energies ranging from **-7.1 kcal/mol** to **-7.8 kcal/mol** (Figure 39) and form a combination of hydrogen bonds and hydrophobic interactions, mainly involving residues such as VAL39, LYS54, LEU156 and **CYS166**. These compounds show moderate binding affinities but can serve as starting points for further structural optimization. In particular, Santamarin (compound 8) and α -cyclocostunolide (compound 9) have the lowest binding energy (**-6.8 kcal/mol**) among the SLs, but form a reasonable number of hydrophobic interactions, indicating potential for improvement through structural modifications.

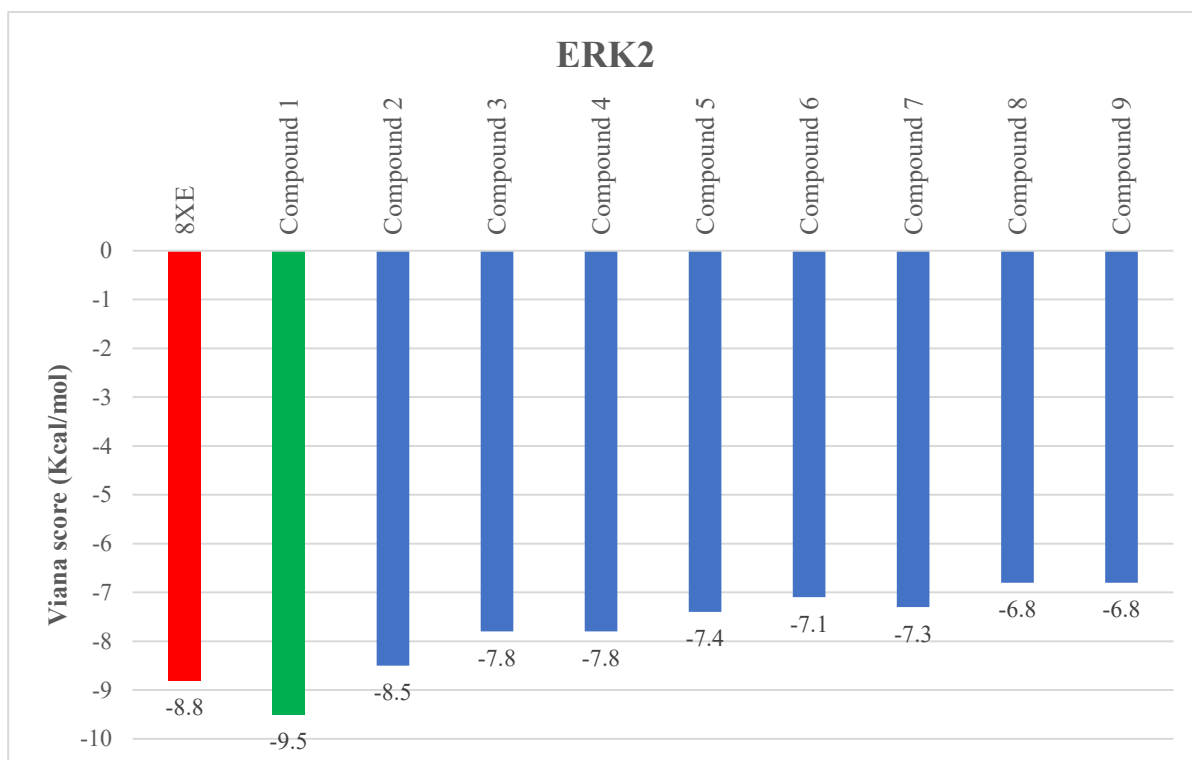


Figure 39. Binding energy of SLs-ERK2 complexes

2. ADME analysis

To predict the physicochemical and pharmacokinetic properties of the selected SLs, an ADME study was carried out using the SwissADME web-based server.

2.1 Physicochemical Properties

- **Molecular weights** range from 230.3 g/mol for Dehydrocostus lactone (compound 2) to 494.62 g/mol for Lappadilactone (compound 1). Compounds with a molecular weight of less than 500 g/mol are commonly associated with high oral bioavailability rates.
- **Lipophilicity (iLog P)** ranges from 2.24 for Zaluzanin C (compound 4) to 3.56 for Lappadilactone (compound 1). Lipophilicity is an important factor for membrane permeability and bioavailability. Compounds with moderate lipophilicity (iLog P between 2-5) are typically well absorbed, leading to high oral bioavailability.
- **Topological Polar Surface Area (TPSA)** values range from 26.3 Å² (compound 2, compound 5 and compound 9) to 89.9 Å² (compound 1). TPSA measures the polar surface area of a molecule and its capacity to traverse cell membranes. Molecules with lower TPSA values, typically below 140 Å², are considered to have greater membrane penetration properties compared to those with larger values, which indicate better oral availability (Table 3).

Table 3. *In silico* physicochemical properties of selected sesquiterpene lactones

Physicochemical properties	Compound 1	Compound 2	Compound 3	Compound 4	Compound 5	Compound 6	Compound 7	Compound 8	Compound 9
MW g/mol	494.62	230.3	246.3	246.3	232.32	250.33	248.32	248.32	232.32
(iLog P)	3.56	2.67	2.36	2.24	2.63	2.55	2.35	2.46	2.7
(TPSA) Å ²	89.9	26.3	46.53	46.53	26.3	46.53	46.53	46.53	26.3

2.2 Pharmacokinetic Properties

- **Gastrointestinal absorption** rates are high for all the compounds, making them ideal for oral medication use.

- **Blood-Brain Barrier (BBB) Permeability** is crucial for drugs that target the central nervous system; it is predicted to be lacking for Lappadilactone (compound 1), which will be a good choice to avoid the cytotoxic effects of excessive doses on the brain in the primary stages before the development of brain tumours. while the remaining compounds are predicted to have BBB permeability.
- **P-glycoprotein (P-gp) Substrate:** compound 1 is expected to be a P-gp substrate, while the other compounds are non-substrates. P-gp is an efflux transporter that can limit medication absorption and distribution, thus non-substrates are typically preferred.
- **Cytochrome P450 (CYP) Inhibition:** Most compounds are not predicted to inhibit the major CYP enzymes (CYP1A2, CYP2C19, CYP2C9, CYP2D6, and CYP3A4), with the exception of compound 2 and compound 9, which are projected to inhibit CYP2C19 and CYP2C9. Inhibiting CYP450, which is responsible for drug metabolism in the liver, can result in interactions with other drugs (Table 4).

Table 4. *In silico* pharmacokinetic properties of selected sesquiterpene lactones

Pharmacokinetic properties	Compound 1	Compound 2	Compound 3	Compound 4	Compound 5	Compound 6	Compound 7	Compound 8	Compound 9
gastrointestinal absorption	High	High	High	High	High	High	High	High	High
BBB permeability	No	Yes	Yes	Yes	Yes	Yes	Yes	Yes	Yes
(P-gp) Substrate	Yes	No	No	No	No	No	No	No	No
CYP1A2 inhibitor	No	No	No	No	No	No	No	No	No
CYP2C19 inhibitor	No	Yes	No	No	No	No	No	No	Yes
CYP2C9 inhibitor	Yes	Yes	No	No	No	No	No	No	Yes
CYP2D6 inhibitor	No	No	No	No	No	No	No	No	No
CYP3A4 inhibitor	No	No	No	No	No	No	No	No	No

2.3 Drug-likeness

- **Lipinski's Rule of Five:** All compounds are expected to follow Lipinski's Rule of Five, which outlines parameters for drug-like properties related to oral bioavailability.

- **Bioavailability score:** All compounds have a bioavailability score of 0.55, a measure of the probability of good oral bioavailability based on various physicochemical characteristics.
- **Synthetic accessibility** values range from 3.84 (compound 2) to 6.02 (compound 1), with higher values indicating more synthetic complexity. Most compounds have moderate synthetic accessibility, suggesting reasonable synthetic feasibility (Table 5).

Table 5. *In silico* drug-likeness properties of selected sesquiterpene lactones

Drug-likeness properties	Compound 1	Compound 2	Compound 3	Compound 4	Compound 5	Compound 6	Compound 7	Compound 8	Compound 9
Lipinski's Rule	Yes	Yes	Yes	Yes	Yes	Yes	Yes	Yes	Yes
bioavailability score	0.55	0.55	0.55	0.55	0.55	0.55	0.55	0.55	0.55
synthetic accessibility	6.02	3.84	4.15	4.15	4.29	4.04	4.06	4.31	4.04

Overall, the ADME profiles offer valuable insights into the physicochemical, pharmacokinetic, and drug-likeness properties of these SLs. The analysis helps in selecting and optimising promising candidates for further investigation as potential drug molecules. “The BOILED-Egg allows for evaluation of passive gastrointestinal absorption (HIA) and brain penetration (BBB) in function of the position of the molecules in the WLOGP-versus-TPSA referential” (Daina *et al.*, 2017) (Figure 40).

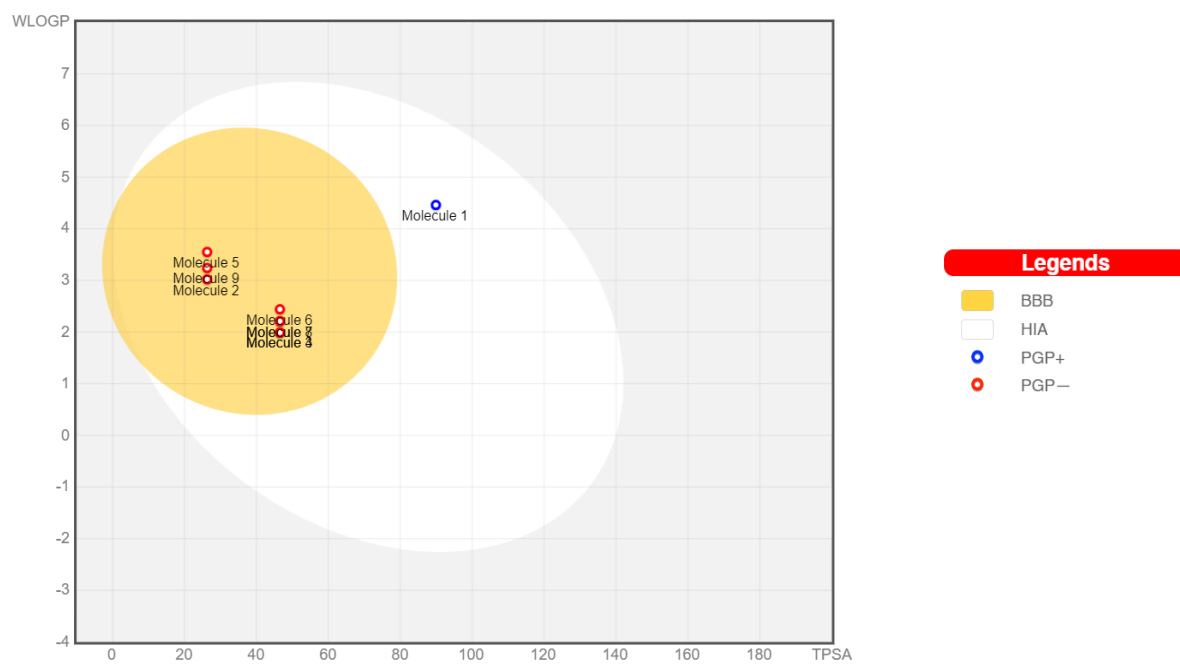


Figure 40. SwissADME BIOLED-Egg model for selected *Saussurea lappa* SLs within ADME parameters

3. General Discussion

The current study performed a molecular docking assessment of SLs from *Saussurea lappa*. The results show that these SLs could be useful as anti-melanoma drugs because they expressed interesting results targeting the key player pathway; MAPK signalling pathway proteins NRAS, BRAF, and ERK2. The discussion of binding energy analyses, interaction profiles, and ADME features provides a comprehensive understanding of the therapeutic potential and limitations of these natural-based agents.

We found that lappadilactone (compound 1) was the most promising SL because it had the strongest binding affinity with all our study targets (NRAS, BRAF, and ERK2). Dehydrocostus lactone (compound 2) which targets the BRAF and ERK2, followed closely behind. Both Isozaluzanin C and Zaluzanin C target NRAS.

ERK2 seems Lappadilactone best target, with a predicted binding energy of **-9.5 kcal/mol**, which is higher than that of the reference inhibitor 8XE. Hence, there are multiple stabilising interactions, including three conventional hydrogen bonds and two hydrophobic alkyl interactions involving the ARG67, LYS151, VAL39 and **CYS166** residues. ERK2, a critical signalling node in the MAPK pathway, regulates its output by activating its numerous substrates, both cytoplasmic and nuclear. Ward *et al.* (2017) revealed that the majority of melanoma tumours harbour mutations in the RAS (20%) or BRAF (60%) genes that acquired resistance to their inhibitors. Thus, the direct treatment of ERK2 could represent an additional therapeutic option.

The pocket of ERK2 in which all the nine SLs are interacted is proved by the study of Ogori *et al.* (2007) as the active site where the ATP binding site involves a covalent bond to Sc of ERK2 **CYS166**. All the compounds in our study except compound 7 and 8 demonstrated hydrophobic interactions with **CYS166**. Therefore, if the potential inhibitors can effectively bind or hold this residue, they may serve as effective inhibitors of ERK2.

At the BRAF target level, Isozaluzanin C exhibited the highest number of hydrogen bonds, suggesting enhanced stability and binding affinity due to the presence of a hydroxyl group. This observation confirms the findings of Cramer *et al.* (2019). The formation of hydrogen-bond networks by hydroxyl groups contributes to binding affinity. However, hydroxyl groups also carry a high desolvation penalty, which can reduce binding affinity. Still, because their

interactions are very directional, hydroxyl groups can only increase affinity when the ligand structure allows a perfect geometric match with the binding site. Sun *et al.* (2003) *in vitro* study looked at the structure-activity relationship and found that the α -methylene- γ -lactone moiety is needed for cytotoxicity and that activity is lower when a hydroxyl group is present.

Dehydrocostus lactone targets both BRAF and ERK2, allowing us to consider them as combinatorial therapies, addressing the challenges of single-agent therapies in advanced melanoma as Corrales *et al.* (2022) suggested.

The ADME profile is encouraging for all compounds reveals that they possess favourable physicochemical properties for oral administration, including moderate lipophilicity and low TPSA values and they are predicted to have a good gastrointestinal absorption. However, Lappadilactone is predicted to be a P-glycoprotein (P-gp) substrate, which could limit its absorption and distribution in the body. Moreover, Dehydrocostus lactone is predicted to be a CYP2C19 and CYP2C9 inhibitor which could lead to drug interactions if co-administered with other medications metabolised by this enzyme. Notably, Lappadilactone lacks blood-brain barrier (BBB) permeability, reducing the risk of overdose cytotoxic effects on the brain, while the other SLs are predicted to have BBB permeability. This characteristic is advantageous for melanoma treatments that require systemic distribution without affecting the central nervous system.

Conclusion

Conclusion

The present study has shed light on the promising therapeutic potential of sesquiterpene lactones (SLs) derived from *Saussurea lappa* as anti-melanoma agents. Through comprehensive molecular docking assessments and ADME profiling.

Previous research has shown that isolated SLs from *Saussurea lappa* have anti-cancer properties against specific human cancer cell lines. However, to the best of our knowledge, our present study is the first to investigate the potential of this plant as an anti-melanoma treatment. As a result, this study hypothesised that these compounds have the potential to prevent metastatic melanoma growth by specifically targeting the MAPK pathway. This would help overcome the resistance that has developed against BRAF and NRAS inhibitors.

The compounds Lappadilactone and Dehydrocostus lactone have been identified as the most promising options due to their significant binding affinities with key targets in the MAPK signalling pathway, such as NRAS, BRAF, and ERK2.

Lappadilactone was the best candidate because it had the best interactions with all the targets that were studied, including NRAS, BRAF, and especially ERK2, which is a key signalling node in the MAPK pathway. The predicted binding energy and several interactions inside its active site, such as hydrogen bonds and hydrophobic alkyl interactions, indicate its potential to effectively inhibit ERK2 activity. Dehydrocostus lactone targets both BRAF and ERK2, allowing us to consider them as combinatorial therapies, addressing the challenges of single-agent therapies in advanced melanoma.

The ADME analysis revealed that SLs have favourable physicochemical properties, moderate lipophilicity, and high predicted gastrointestinal absorption. This indicates that these SLs are suitable for oral administration. However, lappadilactone projected P-glycoprotein substrate status and Dehydrocostus lactone's possible CYP inhibition could affect absorption, distribution, and medication interactions, thus they must be addressed.

It is worth mentioning that Lappadilactone's inability to cross the blood-brain barrier is a positive trait, as it lowers the possibility of damaging effects on the central nervous system before melanoma metastasis reach the brain. Whether the other SLs can pass through the barrier, allowing for widespread distribution throughout the body for the treatment of metastatic melanoma.

These study results open up new possibilities for creating novel treatments for melanoma. These natural-based agents have the potential to directly target ERK2, providing an additional therapeutic option, especially in situations where resistance to current inhibitors has emerged.

Future research in computational methods should focus on studying the MEK protein and then using Molecular Dynamics simulations to evaluate the stability of the interactions. In addition, the focus should be on further optimising the identified SLs by introducing structural modifications to improve their pharmacokinetic properties and effectiveness. Moreover, it is important to carry out *in vitro* and *in vivo* studies to assess the effectiveness and safety of these compounds. Additionally, it would be beneficial to investigate their potential when used in relation to current treatments.

In conclusion, this study has revealed the possibility of SLs from *Saussurea lappa* acting as potential anti-melanoma agents. It emphasizes the importance of investigating natural sources to develop new therapeutic approaches for this aggressive form of cancer.

Bibliographical References

Bibliographical References

Alotaibi, A. A., Bepari, A., Assiri, R. A., Niazi, S. K., Nayaka, S., Rudrappa, M., Nagaraja, S. K., & Bhat, M. P. (2021). *Saussurea lappa* Exhibits Anti-Oncogenic Effect in Hepatocellular Carcinoma, HepG2 Cancer Cell Line by Bcl-2 Mediated Apoptotic Pathway and Mitochondrial Cytochrome C Release. *Current Issues in Molecular Biology*, *43*(2), 1114–1132. <https://doi.org/10.3390/cimb43020079>

Amaral, T., Sinnberg, T., Meier, F., Krepler, C., Levesque, M., Niessner, H., & Garbe, C. (2017a). MAPK pathway in melanoma part II—secondary and adaptive resistance mechanisms to BRAF inhibition. *European Journal of Cancer*, *73*, 93–101. <https://doi.org/10.1016/j.ejca.2016.12.012>

Amaral, T., Sinnberg, T., Meier, F., Krepler, C., Levesque, M., Niessner, H., & Garbe, C. (2017b). The mitogen-activated protein kinase pathway in melanoma part I - Activation and primary resistance mechanisms to BRAF inhibition. *European Journal of Cancer (Oxford, England: 1990)*, *73*, 85–92. <https://doi.org/10.1016/j.ejca.2016.12.010>

Arnold, M., Singh, D., Laversanne, M., Vignat, J., Vaccarella, S., Meheus, F., Cust, A. E., de Vries, E., Whiteman, D. C., & Bray, F. (2022). Global Burden of Cutaneous Melanoma in 2020 and Projections to 2040. *JAMA Dermatology*, *158*(5), 495–503. <https://doi.org/10.1001/jamadermatol.2022.0160>

Batool, M., Ahmad, B., & Choi, S. (2019). A Structure-Based Drug Discovery Paradigm. *International Journal of Molecular Sciences*, *20*(11), 2783. <https://doi.org/10.3390/ijms20112783>

Brás, T., Neves, L. A., Crespo, J. G., & Duarte, M. F. (2023). Advances in sesquiterpene lactones extraction. *TrAC Trends in Analytical Chemistry*, *158*, 116838. <https://doi.org/10.1016/j.trac.2022.116838>

Cazzato, G. (2023). Histopathological Diagnosis of Malignant Melanoma at the Dawn of 2023: Knowledge Gained and New Challenges. *Dermatopathology*, *10*(1), 91–92. <https://doi.org/10.3390/dermatopathology10010013>

- Chadwick, M., Trewin, H., Gawthrop, F., & Wagstaff, C. (2013).** Sesquiterpenoids Lactones: Benefits to Plants and People. *International Journal of Molecular Sciences*, *14*(6), 12780–12805. <https://doi.org/10.3390/ijms140612780>
- Chinembiri, T. N., du Plessis, L. H., Gerber, M., Hamman, J. H., & du Plessis, J. (2014).** Review of Natural Compounds for Potential Skin Cancer Treatment. *Molecules*, *19*(8), 11679–11721. <https://doi.org/10.3390/molecules190811679>
- Corrales, E., Levit-Zerdoun, E., Metzger, P., Mertes, R., Lehmann, A., Münch, J., Lemke, S., Kowar, S., & Boerries, M. (2022).** PI3K/AKT signaling allows for MAPK/ERK pathway independency mediating dedifferentiation-driven treatment resistance in melanoma. *Cell Communication and Signaling*, *20*(1), 187. <https://doi.org/10.1186/s12964-022-00989-y>
- Cramer, J., Sager, C. P., & Ernst, B. (2019).** Hydroxyl Groups in Synthetic and Natural-Product-Derived Therapeutics: A Perspective on a Common Functional Group. *Journal of Medicinal Chemistry*, *62*(20), 8915–8930. <https://doi.org/10.1021/acs.jmedchem.9b00179>
- Daina, A., Michielin, O., & Zoete, V. (2017).** SwissADME: A free web tool to evaluate pharmacokinetics, drug-likeness and medicinal chemistry friendliness of small molecules. *Scientific Reports*, *7*(1), 42717. <https://doi.org/10.1038/srep42717>
- Danao, K., Nandurkar, D., Rokde, V., Shivhare, R., & Mahajan, U. (2022).** Molecular Docking: Metamorphosis in Drug Discovery. In *Molecular Docking—Recent Advances*. IntechOpen. <https://doi.org/10.5772/intechopen.105972>
- Davis, L. E., Shalin, S. C., & Tackett, A. J. (2019).** Current state of melanoma diagnosis and treatment. *Cancer Biology & Therapy*, *20*(11), 1366–1379. <https://doi.org/10.1080/15384047.2019.1640032>
- Downward, J. (2003).** Targeting RAS signalling pathways in cancer therapy. *Nature Reviews Cancer*, *3*(1), 11–22. <https://doi.org/10.1038/nrc969>
- Evans, M. S., Madhunapantula, S. V., Robertson, G. P., & Drabick, J. J. (2013).** Current and Future Trials of Targeted Therapies in Cutaneous Melanoma. In W. S. El-Deiry (Ed.), *Impact of Genetic Targets on Cancer Therapy* (pp. 223–255). Springer. https://doi.org/10.1007/978-1-4614-6176-0_10

- Fermi, G., Perutz, M. F., Shaanan, B., & Fourme, R. (1984).** The crystal structure of human deoxyhaemoglobin at 1.74 Å resolution. *Journal of Molecular Biology*, 175(2), 159–174. [https://doi.org/10.1016/0022-2836\(84\)90472-8](https://doi.org/10.1016/0022-2836(84)90472-8)
- Ferrara, G., & Argenziano, G. (2021).** The WHO 2018 Classification of Cutaneous Melanocytic Neoplasms: Suggestions From Routine Practice. *Frontiers in Oncology*, 11, 675296. <https://doi.org/10.3389/fonc.2021.675296>
- Filimonov, D. A., Lagunin, A. A., Glorizova, T. A., Rudik, A. V., Druzhilovskii, D. S., Pogodin, P. V., & Poroikov, V. V. (2014).** Prediction of the Biological Activity Spectra of Organic Compounds Using the Pass Online Web Resource. *Chemistry of Heterocyclic Compounds*, 50(3), 444–457. <https://doi.org/10.1007/s10593-014-1496-1>
- Fristiohady, A., Asasutjarit, R., Purnama, L. O. M. J., Theeramunkong, S., Al-Ramadan, W., Haruna, L. A., Rahmatika, N. S., Baharum, S. N., & Sahidin, I. (2022).** Phytochemical Profile and Anticancer Activity from Medicinal Plants Against Melanoma Skin Cancer: A Review. *Indonesian Journal of Science and Technology*, 7(3), Article 3. <https://doi.org/10.17509/ijost.v7i3.51325>
- Guo, W., Wang, H., & Li, C. (2021).** Signal pathways of melanoma and targeted therapy. *Signal Transduction and Targeted Therapy*, 6(1), 1–39. <https://doi.org/10.1038/s41392-021-00827-6>
- Hassan, R., & Masoodi, M. H. (2020).** *Saussurea lappa*: A Comprehensive Review on its Pharmacological Activity and Phytochemistry. *Current Traditional Medicine*, 6(1), 13–23. <https://doi.org/10.2174/2215083805666190626144909>
- Isacescu, E., Chiroi, P., Zanoaga, O., Nutu, A., Budisan, L., Pirlog, R., Atanasov, A. G., & Berindan-Neagoe, I. (2023).** Melanoma Cellular Signaling Transduction Pathways Targeted by Polyphenols Action Mechanisms. *Antioxidants*, 12(2), 407. <https://doi.org/10.3390/antiox12020407>
- Ivanescu, B., Miron, A., & Corciova, A. (2015).** Sesquiterpene Lactones from Artemisia Genus: Biological Activities and Methods of Analysis. *Journal of Analytical Methods in Chemistry*, 2015, 1–21. <https://doi.org/10.1155/2015/247685>

- Kapetanovic, I. M. (2008).** Computer-aided drug discovery and development (CADDD): *In silico*-chemico-biological approach. *Chemico-Biological Interactions*, 171(2), 165–176. <https://doi.org/10.1016/j.cbi.2006.12.006>
- Khan, T., Ali, M., Khan, A., Nisar, P., Jan, S. A., Afridi, S., & Shinwari, Z. K. (2019).** Anticancer Plants: A Review of the Active Phytochemicals, Applications in Animal Models, and Regulatory Aspects. *Biomolecules*, 10(1), Article 1. <https://doi.org/10.3390/biom10010047>
- Liu, Y., & Sheikh, M. S. (2014).** Melanoma: Molecular Pathogenesis and Therapeutic Management. *Molecular and Cellular Pharmacology*, 6(3), 228.
- Liu, Y., Yang, X., Gan, J., Chen, S., Xiao, Z.-X., & Cao, Y. (2022).** CB-Dock2: Improved protein–ligand blind docking by integrating cavity detection, docking and homologous template fitting. *Nucleic Acids Research*, 50(W1), W159–W164. <https://doi.org/10.1093/nar/gkac394>
- Manimegalai, P., Selvam, K., Prakash, P., Kirubakaran, D., Shivakumar, M. S., & SenthilNathan, S. (2024).** *Pharmacological and Pharmacokinetic Studies of Hardwickia binata Roxb. Leaf Extract In Insilico and Invitro Models*. <https://doi.org/10.21203/rs.3.rs-1616288/v1>
- Mielczarek-Lewandowska, A., Hartman, M. L., & Czyz, M. (2020).** Inhibitors of HSP90 in melanoma. *Apoptosis*, 25(1–2), 12–28. <https://doi.org/10.1007/s10495-019-01577-1>
- Newman, D. J., & Cragg, G. M. (2020).** Natural Products as Sources of New Drugs over the Nearly Four Decades from 01/1981 to 09/2019. *Journal of Natural Products*, 83(3), 770–803. <https://doi.org/10.1021/acs.jnatprod.9b01285>
- Nirmalraj, S., Gayathiri, E., Sivamurugan, M., Manivasagaperumal, R., Jayanthi, J., Prakash, P., & Selvam, K. (2021).** Molecular docking based screening dynamics for plant based identified potential compounds of PDE12 inhibitors. *Current Research in Green and Sustainable Chemistry*, 4, 100122. <https://doi.org/10.1016/j.crgsc.2021.100122>
- Ochoa, D., Hercules, A., Carmona, M., Suveges, D., Baker, J., Malangone, C., Lopez, I., Miranda, A., Cruz-Castillo, C., Fumis, L., Bernal-Llinares, M., Tsukanov, K., Cornu, H., Tsigirigos, K., Razuvayevskaya, O., Buniello, A., Schwartzentruber, J., Karim, M., Ariano,**

B., Martinez Osorio R. E., Ferrer, J., Ge, X., Machlitt-Northen, S., Gonzalez-Uriarte, A., Saha, S., Tirunagari, S., Mehta, C., Maria Roldan-Romero, M., Horswell, S., Young, S., Ghossaini, M., Hulcoop, D. G., Dunham, I. & McDonagh, E. M. (2023). The next-generation Open Targets Platform: Reimagined, redesigned, rebuilt. *Nucleic Acids Research*, 51(D1), D1353–D1359. <https://doi.org/10.1093/nar/gkac1046>

Ohuri, M., Kinoshita, T., Yoshimura, S., Warizaya, M., Nakajima, H., & Miyake, H. (2007). Role of a cysteine residue in the active site of ERK and the MAPKK family. *Biochemical and Biophysical Research Communications*, 353(3), 633–637. <https://doi.org/10.1016/j.bbrc.2006.12.083>

Pinzi, L., & Rastelli, G. (2019). Molecular Docking: Shifting Paradigms in Drug Discovery. *International Journal of Molecular Sciences*, 20, 4331. <https://doi.org/10.3390/ijms20184331>

Prasetya, F. S., Destiarani, W., Prihastaningtyas, I. R. C., Agung, M. U. K., & Yusuf, M. (2023). Computational simulations of microalgae-derived bioactive compounds as a novel inhibitor against B-Raf V600E-driven melanoma. *Journal of Applied Pharmaceutical Science*, 13, (6), 068–086. <https://doi.org/10.7324/JAPS.2023.10012>

Punekar, S. R., Velcheti, V., Neel, B. G., & Wong, K.-K. (2022). The current state of the art and future trends in RAS-targeted cancer therapies. *Nature Reviews Clinical Oncology*, 19(10), 637–655. <https://doi.org/10.1038/s41571-022-00671-9>

Respondek, M., Beberok, A., Rzepka, Z., Rok, J., & Wrześniok, D. (2020). Mcl-1 Inhibitor Induces Cells Death in BRAF-Mutant Amelanotic Melanoma Trough GSH Depletion, DNA Damage and Cell Cycle Changes. *Pathology & Oncology Research*, 26(3), 1465–1474. <https://doi.org/10.1007/s12253-019-00715-z>

Shain, A. H., Yeh, I., Kovalyshyn, I., Sriharan, A., Talevich, E., Gagnon, A., Dummer, R., North, J., Pincus, L., Ruben, B., Rickaby, W., D'Arrigo, C., Robson, A., & Bastian, B. C. (2015). The Genetic Evolution of Melanoma from Precursor Lesions. *New England Journal of Medicine*, 373(20), 1926–1936. <https://doi.org/10.1056/NEJMoa1502583>

Sun, C.-M., Syu, W.-J., Don, M.-J., Lu, J.-J., & Lee, G.-H. (2003). Cytotoxic Sesquiterpene Lactones from the Root of *Saussurea lappa*. *Journal of Natural Products*, 66(9), 1175–1180. <https://doi.org/10.1021/np030147e>

Van Beusekom, B., Touw, W. G., Tatineni, M., Somani, S., Rajagopal, G., Luo, J., Gilliland, G. L., Perrakis, A., & Joosten, R. P. (2018). Homology-based hydrogen bond information improves crystallographic structures in the PDB. *Protein Science*, 27(3), 798–808. <https://doi.org/10.1002/pro.3353>

Velasquez-López, Y., Tejera, E., & Perez-Castillo, Y. (2022). Can docking scoring functions guarantee success in virtual screening? In *Annual Reports in Medicinal Chemistry*, 59, 1–41. Academic Press. <https://doi.org/10.1016/bs.armc.2022.08.008>

Vijayalakshmi, M., Umamaheswari, A., Agalya, B., Jegasubramaniam, S. N., & Prabu, S. L. (2022). Foresight on Phytoconstituents and Associated Pharmacological Activities of Traditional Medicinal Plant: *Saussurea costus* (Falc.) Lipschitz. *Current Pharmacology Reports*, 8(4), 281–289. <https://doi.org/10.1007/s40495-022-00287-8>

Whipple, C. A., Boni, A., Fisher, J. L., Hampton, T. H., Tsongalis, G. J., Mellinger, D. L., Yan, S., Tafe, L. J., Brinckerhoff, C. E., Turk, M. J., Mullins, D. W., Fadul, C. E., & Ernstoff, M. S. (2016). The mitogen-activated protein kinase pathway plays a critical role in regulating immunological properties of BRAF mutant cutaneous melanoma cells. *Melanoma Research*, 26(3), 223–235. <https://doi.org/10.1097/CMR.0000000000000244>

Yang, J., Splittgerber, R., Yull, F. E., Kantrow, S., Ayers, G. D., Karin, M., & Richmond, A. (2010). *Conditional ablation of Ikkb inhibits melanoma tumor development in mice*. American Society for Clinical Investigation. <https://doi.org/10.1172/JCI42358>

Zahara, K., Tabassum, S., Sabir, S., Arshad, M., Qureshi, R., Amjad, M. S., & Chaudhari, S. K. (2014). A review of therapeutic potential of *Saussurea lappa*-An endangered plant from Himalaya. *Asian Pacific Journal of Tropical Medicine*, 7, S60–S69. [https://doi.org/10.1016/S1995-7645\(14\)60204-2](https://doi.org/10.1016/S1995-7645(14)60204-2)

Webography

Melanoma Skin Cancer Statistics, (2023). Accessed on 28/04/2024. <https://www.cancer.org/cancer/types/melanoma-skin-cancer/about/key-statistics.html>

Sharma, A. (2020). Indian Costus Root – Kust e Talkh – Saussurea Lappa. *Trust The Herb*. Accessed on 20/06/2024. <https://trustherb.com/indian-costus-root-kust-e-talkh-saussurea-lappa/>

Annexes

Annexes

Annexe: Twenty amino acids table

3- letter code	One letter code	Amino acid
ALA	A	Alanine
ARG	R	Arginine
ASN	N	Asparagine
ASP	D	Aspartic acid
CYS	C	Cysteine
GLN	Q	Glutamine
GLU	E	Glutamic acid
GLY	G	Glycine
HIS	H	Histidine
ILE	I	Isoleucine
LEU	L	Leucine
LYS	K	Lysine
MET	M	Methionine
PHE	F	Phenylalanine
PRO	P	Proline
SER	S	Serine
THR	T	Threonine
TRP	W	Tryptophan
TYR	Y	Tyrosine
VAL	V	Valine

الجمهورية الجزائرية الديمقراطية الشعبية
République Algérienne Démocratique et Populaire
وزارة التعليم العالي والبحث العلمي
Ministère de l'Enseignement Supérieur Et de La Recherche Scientifique

Faculté des sciences de la nature et
de la vie et sciences de la terre

Département de Biologie

جامعة غرداية



Université de Ghardaïa



كلية علوم الطبيعة والحياة
وعلوم الأرض

قسم البيولوجيا

Ghardaïa le : 04/07/2024

Rapport : Correction du mémoire

Enseignant (e) (s) Chargé (e) de la correction :

Nom et prénom l'examineur et Signature	Nom et prénom de l'examineur 2 et Signature	Nom et prénom de président et Signature
BAKLI Mahfoud 	/	KEBILI Zohra 

Thème :

Molecular docking assessment of sesquiterpene lactones from *Saussurea lappa* as
potential anti-melanoma agents

Après les corrections apportées au mémoire, L'étudiante :

- HADDAD Sarra

Est autorisée à déposer le manuscrit au niveau du département.

Signature

الملخص

الميلانوما، نوع من أنواع سرطان الجلد القاتل والأكثر شيوعًا في جميع أنحاء العالم، والذي ينتج عن طفرات في الجينات المشفرة لبروتينات BRAF و NRAS المتضمنة في مسار MAPK، وهو مسار ناقل للإشارة الخلوية، رئيسي في تطور ونمو هذا النوع من السرطان بخلايا الميلانوسيت. على الرغم من أن العلاجات الكيميائية التي تستهدف تثبيط هذا المسار واعدة، إلا أن المقاومة لها غالبًا ما تتطور، مما يستلزم استكشاف عوامل جديدة.

استُخدمت طرق نمذجة تعتمد على الالتحام الجزيئي وتوقع خصائص ADME لدراسة تسع مركبات طبيعية، وهي لاكتونات سيسكيتيربينية، مشتقة من نبات سوسوريا لبا (*Saussurea lappa*)، لتحديد إمكاناتها كمثبطات لبروتينات NRAS و BRAF و ERK2 بمسار MAPK. أظهر لاباديلاكوتون أعلى ألفة ارتباط بطاقة ارتباط مساوية لـ -9.5 kcal/mol مع بروتين ERK2، متجاوزًا بذلك الجزيء المرجعي 8XE، ومشكلًا تفاعلات استقرار ارتباط من نوع الرابطة الهيدروجينية والكارهة للماء في حين أظهر ديهيدروكوستوس لكتون ارتباطًا أفضل ببروتين BRAF و ERK2 بطاقة ارتباط مساوية لـ -8.9 kcal/mol و -8.5 kcal/mol على الترتيب.

أظهرت نتائج توقعات ADME أن جميع المركبات التي تمت دراستها لها خصائص فيزيوكيميائية مواتية، معتدلة الألفة للدهون وامتصاصًا معويًا عاليًا. خلصت النتائج مجتمعةً إلى أن لاكتونات سيسكيتيربين من سوسوريا لبا، ولا سيما لاباديلاكوتون ولاكتون ديهيدروكوستوس لكتون، تمثل مثبطات طبيعية واعدة لمسار MAPK التي يمكن أن تشكل علاجات مستهدفة جديدة للميلانوما.

الكلمات الدالة: الميلانوما، مسار MAPK، الإلتحام الجزيئي، ADME، لاكتونات سيسكيتيربين، سوسوريا لبا.

Abstract

Melanoma, a deadly skin cancer, is increasing in global incidence. The MAPK pathway, frequently mutated in BRAF and NRAS genes, plays a central role in melanoma progression.

Although targeted therapies against this pathway have shown promise, resistance often emerges, which necessitates the exploration of novel agents.

The *in silico* molecular docking method and ADME prediction were used to test nine natural compounds, sesquiterpene lactones, from the medicinal plant *Saussurea lappa* for their potential as melanoma key pathway inhibitors (NRAS, BRAF, and ERK2).

Lappadilactone had the strongest binding affinity, especially to ERK2 equal to -9.5 kcal/mol , outperforming the reference ligand 8XE in binding energy. It formed stabilising interactions within the active site, such as hydrogen bonds and hydrophobic contacts. Dehydrocostus lactone demonstrated significant binding to both BRAF and ERK2 with binding energy of -8.9 kcal/mol and -8.5 kcal/mol , respectively.

ADME predictions showed that the compounds had favourable physicochemical properties, moderate lipophilicity, and high predicted gastrointestinal absorption.

These findings suggest that sesquiterpene lactones from *Saussurea lappa*, particularly Lappadilactone and Dehydrocostus lactone, represent promising natural-based MAPK pathway inhibitors with the potential to be novel targeted therapies against metastatic melanoma.

Keywords: melanoma, MAPK pathway, molecular docking, ADME, sesquiterpene lactones, *Saussurea lappa*.

Résumé

Le mélanome, un cancer de la peau mortel, est de plus en plus répandu dans le monde. La voie MAPK, fréquemment affectée par des mutations dans les gènes codant pour les protéines BRAF et NRAS, joue un rôle central dans la progression du mélanome.

Bien que les thérapies ciblant cette voie soient prometteuses, une résistance se développe souvent, nécessitant l'exploration de nouveaux agents.

Les méthodes *in silico* basées sur l'amarrage moléculaire et l'ADME ont été utilisées pour étudier neuf composés naturels, des lactones sesquiterpéniques, dérivés de la plante médicinale *Saussurea lappa*, afin de déterminer leur potentiel en tant qu'inhibiteurs des protéines NRAS, BRAF et ERK2, de la voie MAPK, une voie métabolique clé dans le mélanome.

Les résultats de Docking moléculaire obtenus ont montré que : parmi les molécules étudiées la Lappadilactone présentait l'affinité de liaison la plus élevée, en particulier avec la protéine ERK2 avec une énergie de liaison égale à -9.5 kcal/mol , surpassant le ligand de référence 8XE et formant des interactions stabilisantes de type liaison hydrogène et hydrophobe, alors que la Dehydrocostus lactone a montré une meilleure liaison vis-à-vis BRAF et ERK2 avec une énergie de liaison égale à -8.9 kcal/mol et -8.5 kcal/mol , respectivement.

ADME ont montré que tous les composés étudiés avaient des propriétés physicochimiques favorables, une lipophilie modérée et une absorption gastro-intestinale prédite élevée.

L'ensemble des résultats permet de conclure que les lactones sesquiterpéniques de *Saussurea lappa*, en particulier la Lappadilactone et la lactone Dehydrocostus, représentent des inhibiteurs naturels prometteurs de la voie MAPK qui pourraient constituer de nouvelles thérapies ciblées pour le mélanome métastatique.

Mots-clés : mélanome, voie MAPK, Docking moléculaire, ADME, lactones sesquiterpéniques, *Saussurea lappa*.